Exfoliation Mechanisms of 2D Materials and Their Applications

Md Akibul Islam[1,#], Peter Serles[1,#], Boran Kumral[1#], Pedro Guerra Demingos[2], Tanvir Qureshi[3,7], AshokKumar Meiyazhagan[4], Anand B. Puthirath[4], Mohammad Sayem Bin Abdullah[5], Syed Rafat Faysal[6], Pulickel M. Ajayan[4], Daman Panesar[3], Chandra Veer Singh[1,2], Tobin Filleter[1*]

[1] Department of Mechanical and Industrial Engineering, University of Toronto, Canada

[2] Department of Materials Science and Engineering, University of Toronto, Canada

[3] Department of Civil and Mineral Engineering, University of Toronto, Canada

[4] Department of Materials Science and NanoEngineering, Rice University, USA

[5] Department of Mechanical Engineering, University of Washington, WA 98195, USA

[6] Department of Mechanical Engineering, University of Alberta, Canada

[7] Department of Geography & Environmental Management, UWE Bristol, UK

[#]Equal contributor

*Email: T. Filleter: Filleter@mie.utoronto.ca

Index

Keywords: Exfoliation Mechanisms, 2D materials, Cleavage, Ball Milling, Electrochemical, Shear, Ultrasonication

Abstract

Due to the strong in-plane but weak out-of-plane bonding, it is relatively easy to separate nanosheets of two-dimensional (2D) materials from their respective bulk crystals. This exfoliation of 2D materials can yield large 2D nanosheets, hundreds of microns wide, that can be as thin as one or a few atomic layers thick. However, the underlying physical mechanisms unique to each exfoliation technique can produce a wide distribution of defects, yields, functionalization, lateral sizes, and thicknesses which can be appropriate for specific end applications. The five most commonly used exfoliation techniques include micromechanical cleavage, ultrasonication, shear exfoliation, ball milling, and electrochemical exfoliation. In this review, we present an overview of the field of 2D material exfoliation and the underlying physical mechanisms with emphasis on progress over the last decade. The beneficial characteristics and shortcomings of each exfoliation process are discussed in the context of their functional properties to guide the selection of the best technique for a given application. Furthermore, an analysis of standard applications of exfoliated 2D nanosheets is presented including their use in energy storage, electronics, lubrication, composite, and structural applications. By providing detailed insights into the underlying exfoliation mechanisms along with the advantages and disadvantages of each technique, this review intends to guide the reader toward the appropriate batch-scale exfoliation techniques for a wide variety of industrial applications.

1. Introduction

Since the first report of mechanical exfoliation of monolayer graphene in 2005[1], hundreds of two-dimensional (2D) materials, which are crystalline solids of one or few-atomic thicknesses, have been synthesized using various exfoliation and deposition techniques. These 2D materials have attracted significant attention due to their unprecedented mechanical strength[2–4], electrical and thermal conductivities[5], extremely high surface area-to-volume ratio[6], and quantum mechanical effects[7]. Despite numerous unique properties, wafer-scale applications of 2D materials have been limited due to the lack of scalable synthesis or fabrication processes. Bottom-up processes such as chemical vapor deposition (CVD)[8–11] and physical vapor deposition (PVD)[12–14] can deposit few-layer and low defect density 2D materials on the desired substrate but are costly and time-consuming so face significant challenges in commercial scale applications. Fortunately, most applications do not require monolayer precision for 2D material thicknesses, including reinforcements for composites[15–17], solid lubrication[18,19], conductive inks[20–22], purification and filtering[23–25], drug delivery[26,27], biomarkers[28], coatings[29,30], or supercapacitors[31–33]. Exfoliation processes such as micromechanical cleavage, ball milling, and electrochemical intercalation (Figure 1) can produce few-layer or even monolayer 2D materials that are hundreds of microns wide and, for certain techniques, in bulk quantities. Meanwhile shear flow and ultrasonication exfoliation techniques tend to produce laterally smaller 2D materials sheets but in greater quantities and as a continuous process. These different exfoliation techniques present a wide variance in processing time, yield, and material quality which makes it essential to choose the proper process for a given application, material, or resulting quality. There exists a series of excellent reviews on specific exfoliation processes[34–36], however, the present work aims to present

a comprehensive comparison between the various exfoliation techniques including discussions on the underlying mechanisms, material quality (e.g. density of defects), yield, and respective end-use applications to aid the reader in selecting the most appropriate synthesis method.

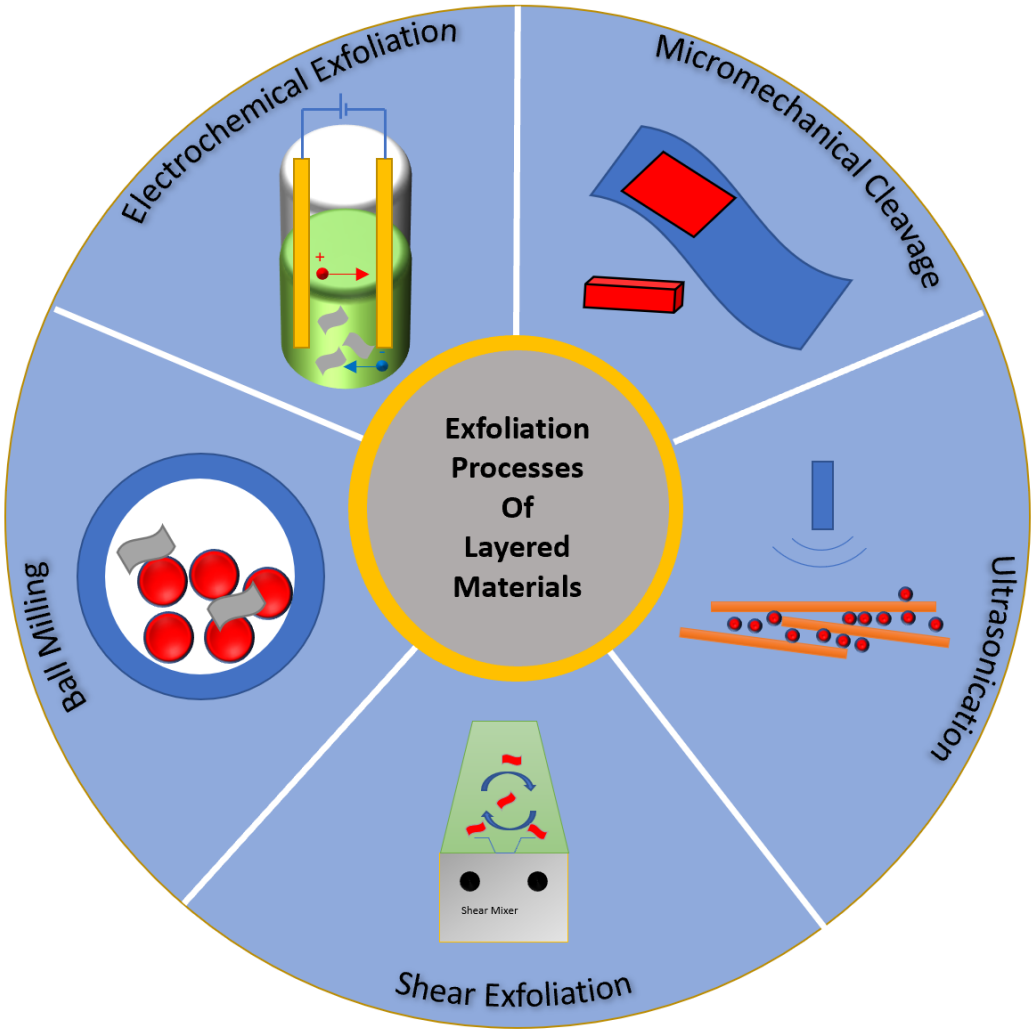

Figure 1. **The five most common exfoliation processes.** 2D materials are most commonly exfoliated using micromechanical cleavage, ball milling, ultrasonication, shear exfoliation, or electrochemical exfoliation which employ a combination of mechanical forces and chemical process to separate layers of 2D materials.

2. Two-Dimensional Materials

Within most layered materials such as graphene, molybdenum disulfide (MoS_2), or hexagonal boron nitride (hBN), weak van der Waals bonds act to hold the layers together in the (001) direction, while covalent bonds act within the layers in the (100) and (010) directions. The van der Waals bonds have a weaker bond strength (0.4-4 kJ/mol) accompanied by a longer bond length (0.3-0.6 nm), whereas covalent bonds possess a stronger bond strength (for example, 345 kJ/mol for C-C bonds) accompanied by a much shorter bond length (~0.154 nm for C-C). Therefore, it is

easy to separate these layers in the (001) plane by mechanical, chemical, or electrochemical techniques by overcoming the weak van der Waals forces. By exfoliating the bulk material into individual sheets of nanometer thickness, a wide variety of unique material properties are enabled that are not present in their bulk form. For example, the surface area-to-volume ratio is dramatically increased by exfoliation thereby enhancing the reactivity and catalytic capability of these materials[37]. Additionally, in a bulk crystal, the nature of the electronic wave function is three-dimensional while electrons are limited to planar dimensions when the material is confined to 2D. The confinement results in a 2D electron wave function that modifies the band structure of the material[38,39]. Furthermore, the vibration of surface atoms is not restricted in the out of plane direction, leading to the appearance of forbidden phonon modes and surface properties[40]. 2D materials thereby exhibit uniquely enhanced physical, electrical, and chemical properties compared to their bulk counterparts.

The first-ever atomically thin material exfoliated from its bulk counterpart was graphene[41]. Its excellent electron mobility was first predicted back in 1940 and was realized when Geim and Novosolov isolated monolayer graphene by exfoliation in 2005[42]. They reported carrier mobility at >200,000 $cm^2\ V^{-1}\ s^{-1}$ with an electron density of $2 \times 10^{11}\ cm^{-2}$, making it one of the highest values ever reported[43]. Additionally, graphene exhibits a unique ambipolar electric field effect where room temperature electron or hole concentrations can be tuned by changing the applied gate voltage[41]. The unique electrical properties of graphene enabled the development of ultrafast integrated circuits, with single device speeds up to 100 GHz having been demonstrated[44]. Graphene also has a very high surface area-to-volume ratio, making it an ideal material for applications such as high-efficiency batteries and supercapacitors in which high electrical conductivity and a large contact area are required. In addition to its excellent electrical properties, graphene also exhibits distinctive mechanical properties; the Young modulus of graphene was reported to be >1 TPa with an intrinsic strength of 100 GPa, making this the highest known Young's modulus in any material[4,45–47].

In addition to graphene, there is an enormous range of 2D materials, as over 1500 different materials have been identified or isolated to date[48]. Some common examples include hexagonal boron nitride (*h*BN), molybdenum disulfide (MoS_2), tungsten disulfide (WS_2), and phosphorene (Figure 2). Due to the similarity in the hexagonal crystal structure and its white powder bulk form, boron nitride is often referred to as "white graphene" (Figure 2A). Its stacking structure is highly stable and allows *h*BN to maintain its structure up to 1000°C in air or 2850°C in an inert environment[49,50]. *h*BN shows high in-plane thermal conductivity up to 390 W/m-K, which makes it an excellent material for thermally conductive polymers[51], ceramic composites[52], UV emitters[53], and thermal radiators[54]. However, despite having a similar structure to graphene, *h*BN has a wide bandgap (E_g) of 5.9 eV[55], making it an electrically insulating material, whereas graphene is electrically conducting. Additionally, monolayer *h*BN has been reported to exhibit an ultrahigh Young's modulus of 0.75-0.865 TPa[56] which is comparable to the Young's modulus of monolayer graphene (~1 TPa).

Transition metal dichalcogenides (TMDs) are another common type of 2D material which are predominantly semiconductors of the form MX_2, where M is a transition metal atom, and X is a chalcogenide atom. TMD single layers consist of a metal atom sandwiched between two chalcogen atoms with covalent bonding. Figure 2B shows the structure of Mo atoms (blue) sandwiched

between two S atoms (yellow) in single-layer MoS_2. TMDs exhibit tunable electronic band structures, which creates opportunities in fabricating miniaturized field-effect transistors (FETs), which form the basic building block of modern electronics[57]. MoS_2 has a layer-dependent bandgap with a crossover from indirect (1.2 eV) for monolayer thickness to direct (1.9 eV) in the bulk material[58–60]. It also shows relatively high mobility for transistor applications (~200 $cm^2V^{-1}s^{-1}$) plus a high on/off ratio (~10^8) at room temperature, making MoS_2 an excellent semiconductor material[61–64]. MoS_2 also exhibits favorable mechanical properties, such as a high Young's modulus of 170-370 GPa which is comparable to steel and an in-plane breaking strength of ~23 GPa, making it a good candidate for mechanical applications[3].

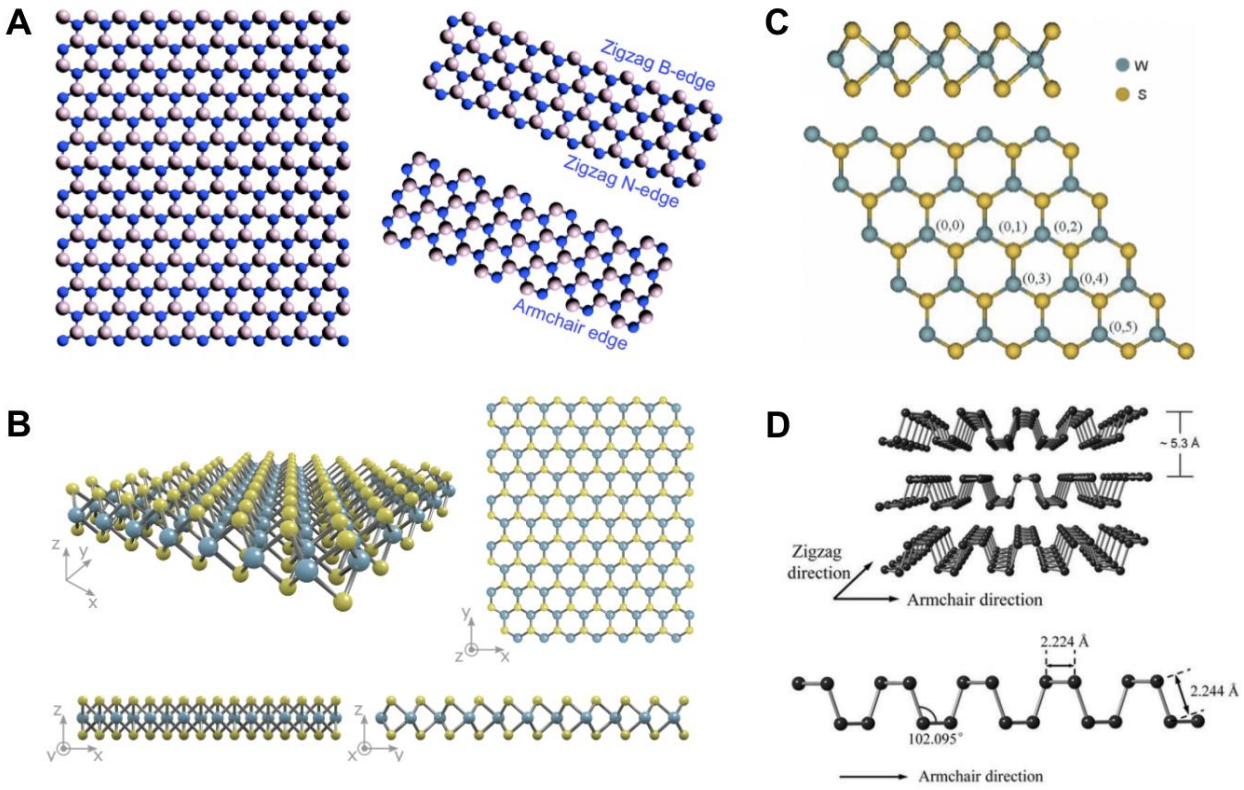

Figure 2. Common atomic structures of 2D exfoliated materials. A) A planar monolayer boron nitride nanosheet (BNNS) and nanoribbons terminated at different edge structures[65], B) A schematic representation of a monolayer of MoS_2, C) A schematic of a monolayer of WS_2 where one W atom is sandwiched between two S atoms[66], D) Few layers (top) and monolayers (bottom) of black phosphorus[67]. A) Reproduced with permission from ***Chem. Soc. Rev.***, 2014,**43**, 934-959. Copyright 2014 Royal Society of Chemistry. D) Reproduced with permission from ***Mater. Horiz.***, 2017,**4**, 800-816. Copyright 2017 Royal Society of Chemistry.

Another well-known TMD is tungsten disulfide (WS_2), which consists of a prismatic structure similar to MoS_2 (Figure 2C)[68]. Simulations of WS_2 have estimated the bandgap of bilayer WS_2 to be 1.42 eV (indirect), monolayer WS_2 to be 1.91 eV (direct)[69], and the Young's modulus to be ~15 GPa[69,70]. Finally, phosphorene is a direct bandgap semiconductor 2D material of its own structural classification (Figure 2D). The bandgap of phosphorene varies from 0.3 eV in bulk black

phosphorous to ~2 eV in single-layer phosphorene[71]. Interestingly, phosphorene is significantly anisotropic in-plane, unlike most 2D materials, with a conductivity 50% lower in the zigzag direction than in the armchair direction due to its unique structure[72]. To date, over 1500 2D materials have been identified which enables an enormous library of 2D material properties and combinations for a wide selection of given applications. For further reading on the properties of 2D materials, the readers are directed toward several excellent reviews on the subject[55,73,74]. However, while the intrinsic material properties are crucial for a given application, selecting the proper exfoliation process to produce the desired material quality, dimensions, and yield is equally critical.

3. Exfoliation Techniques

3.1 Mechanics of Exfoliation

The process of overcoming interlayer bonds to cleave thin layers of 2D materials is a complex balance of forces that depends on a number of parameters. Prior to discussing the various exfoliation techniques, we consider the governing mechanisms which regulate the exfoliation process. The feasibility of exfoliation depends primarily on the interlayer strength of the material. The van der Waals interaction energy between two surfaces per unit area is given by[75]:

$$W = -\frac{A}{12\pi D^2} \tag{3.1.1}$$

where D is the distance between the two surfaces, and A is the Hamaker constant, defined as $A = \pi^2 C_{vdW}\rho_1\rho_2$, where C_{vdW} measures the van der Waals force between the two materials, and ρ_i is their atomic density. Hence, the effective van der Waals force between the two surfaces per unit area, F_{ad}, is given by[75]:

$$F_{ad} = -\frac{\partial W}{\partial D} = -\frac{A}{6\pi D^3} \tag{3.1.2}$$

However, although the cohesion energy between two layers is uniquely defined by their interactions at equilibrium interlayer distance, the cohesion force depends on the exfoliation pathway (the exact way the two layers are pulled apart). For instance, Equation 3.1.3 models the force acting on the layers as they are separated while remaining parallel to each other and perpendicular to the separation distance D. In the case of the upper layer being peeled away from the lower one along a distance d, the peeling force (per unit area), F_{peel}, is[75]:

$$F_{peel} = \frac{A}{12\pi D^2 d} = F_{ad}\frac{D}{2d} \tag{3.1.3}$$

Since the typical interlayer distance D is much smaller than any in-plane length d, the peeling force F_{peel} is considerably lower than the adhesion force F_{ad}[75]. This is what makes exfoliation possible.

Since exfoliation energy cannot be directly determined via experiments, Density Functional Theory (DFT) has been a powerful tool to investigate exfoliation, as it can be used to calculate cohesion and adhesion energies[76–78]. Consequently, this approach has been used to calculate the exfoliation energy for several 2D materials such as graphene and graphene oxide (GO)[79], TMDs[80],

borophene[81], phosphorene[82], *h*BN[83], MXenes[84], among many others. A comparative study found exfoliation energies of 18.5 and 22.7 meV/Å^2 for graphene and MoS_2, respectively, pointing out the role of polarized bonds in increasing interlayer strength[83]. Since a threshold of 20.0 meV/Å^2 is typically adopted for easy exfoliation, these results also reflect the difficulty of exfoliating TMDs. Another work screened multiple materials, finding that exfoliation energy decreases with charge separation, which induces greater Coulombic repulsion between layers[80]. Surface coverage also plays a key role, e.g. MXenes ending in OH groups can form H-bonds, exhibiting cleavage energy twice as high as F and O coverages[84]. The exfoliation energy computed with DFT is widely used as an indication for the feasibility of experimental isolation of new 2D materials[85,86].

Machine Learning (ML) approaches have also recently been explored for the prediction of exfoliation properties, since ML is less computationally expensive than DFT while allowing for good transferability with experimental properties. Wan et al.[87] trained several ML tools with the 2DMatPedia database[88], which contains DFT-calculated exfoliation energy for over 4000 2D materials. The authors found that exfoliation energy increases with the number of valence electrons per atom, which allows stronger bonding between layers. Similarly, Siriwardane et al.[89] used 7000 layered ternary compounds from the Materials Project database[90] to train multiple ML models. They found that formation energy (a measure of thermodynamic stability) and exfoliation energy tend to follow the same trend, pointing out that stable bulk phases are harder to exfoliate. However, the results indicate that cleavage of Ga- and In-based MAB phases should be possible (M=metal, A=group III-A elements). Finally, Saito et al.[91] recently used a deep learning method to identify the thickness of atomic layer flakes from optical microscopy images. Their artificial neural network was able to differentiate mono- from bi-layer graphene and MoS_2 with up to 80% success, which highlights the possibility of replacing part of manual work with AI systems for 2D materials production.

Overall, several approaches can be used to model exfoliation, from fundamental physical-chemical theory to simulation techniques and machine learning tools. The five following sections dive deeper into each of the main exfoliation techniques, which are studied with models that are specific to each case. Additionally, Table 1 presents an index summary of the five exfoliation techniques including material yields, advantages, and disadvantages to help direct the reader towards the appropriate techniques. Table S1 (Supplementary Information) further presents a summary of applications employing exfoliated 2D materials used in energy & storage, mechanics & design, polymer composite, and cement composite applications.

3.2 Micromechanical Cleavage

The first exfoliation of 2D atomic layers from bulk crystals was performed using the "Scotch Tape" method[41]. In this process, a graphite flake is placed on a piece of tape, stuck against itself, and then peeled repeatedly. The graphite flakes become thinner on each subsequent peel and then the tape is pressed on a substrate to leave behind an assortment of 2D material thicknesses (Figure 3A-C). The first-ever isolation of a single layer of 2D material was similarly reported by Novoselov et al. in 2005[1] by mechanical exfoliation, also referred to as micromechanical cleavage. In their study, a fresh surface of a graphite was rubbed against another surface, which left a variety of flakes on it and was later determined by transmission electron microscopy (TEM) and atomic force microscopy (AFM) to contain monolayers.

One challenge with the scotch tape method is that due to the repeated mechanical stresses by folding the tape multiple times, the 2D material flakes can break apart which results in low yield and low lateral dimension 2D sheets[92]. To increase the yield of this process, the interaction between the monolayer 2D material and the underlying substrate is enhanced by exposing the substrate to oxygen plasma to remove any organic absorbates on the surface[93]. After that, the scotch tape with the thinned graphite flakes is placed on the substrate and heated at 100°C for 2 to 5 mins. This annealing process vents the trapped gas between the interface of the 2D material and the substrate, thus ensuring a more uniform interaction between the substrate and the 2D layers. This produces larger sheets of monolayer 2D materials without mechanical deformations such as buckles or wrinkles.

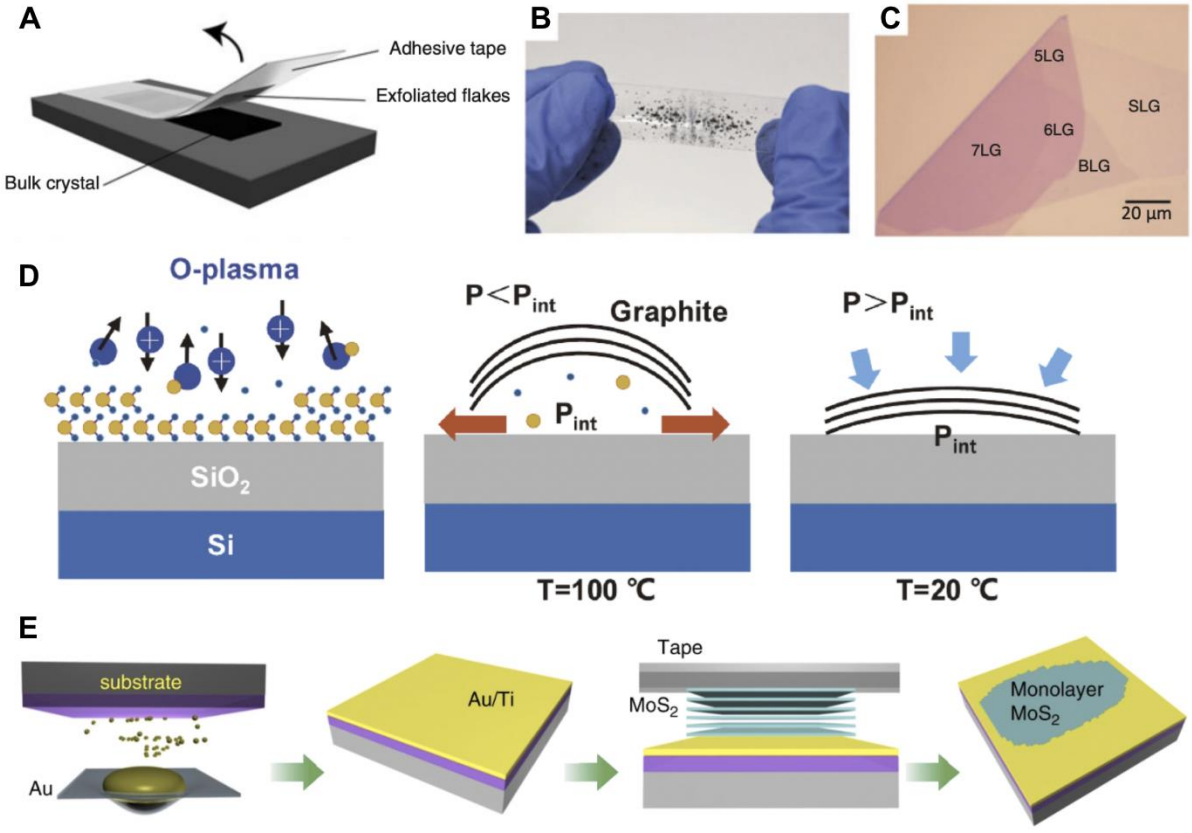

Figure 3. Micromechanical cleavage techniques using scotch tape. A) A schematic representation of the micromechanical cleavage method for exfoliating 2D material. B) Partially exfoliated graphene on scotch tape[94]. C) Optical microscope image of an exfoliated single layer, bilayer, and multilayer graphene flakes[95]. D) Schematic representation of performing oxygen plasma treatment to remove organic residues from the substrate, annealing the substrate containing graphite on adhesive tape to enhance the adhesion between the substrate and the boundary graphite layers, and cooling the substrate to reduce the pressure at the interface between graphite and the substrate[93]. E) Schematic of the metal-assisted exfoliation process of 2D monolayers[96]. C) Reproduced with permission from ***ACS Nano*** 2015, 9, 11, 10612–10620. Copyright 2015 American Chemical Society. D) Reproduced with permission from ***ACS Nano*** 2013, 7, 11, 10344–10353.Cpoyright 2013 American Chemical Society. E) Reproduced with permission from ***Nature Communications*** 11, Article number: 2453 (2020)

The first isolation and experimental study on thin sheets of *h*BN was reported by Pacilé et al. by micromechanical cleavage where layers of *h*BN were peeled off using adhesive tape attached to a SiO_2 substrate. The thinnest regions of exfoliated *h*BN was 3.5 nm or ~10 layers thick[97]. Although the synthesis of monolayer graphene is relatively straightforward and consistent using micromechanical cleavage, it is not the case for the isolation of most other 2D materials. For example, even though *h*BN includes weak van der Waals bonds, there is a robust lip-lip interaction between the basal planes of BN. As AA´ is the preferred stacking order in exfoliated *h*BN, favorable electrostatic or polar-polar interactions lead to B atoms eclipsing N atoms on the adjacent layers. These unique lip-lip interactions between different layers of BN nanosheets are stronger than the interlayer bonding of the layers in graphene[98]. Additionally, the lack of availability of large, ordered microcrystals of *h*BN also contributes to this problem. Despite these challenges, single layer *h*BN was recently reported to be exfoliated using the scotch tape method, with the thickness of a single layer of boron nitride reported as 0.48 nm[56]. It should be noted that the yield remains very low, which is not scalable for most applications.

Micromechanical cleavage faces challenges for the isolation of many layered 2D materials, such as TMDs, due to the low adhesion energy between the substrate and the 2D material. This poses a significant challenge in exfoliating these layered materials for practical applications. To address this, Huang *et al.* reported a metal-assisted exfoliation method (Figure 3E)[96]. For TMDs, the group 16 (VIA) chalcogen atoms (S, Se, Te) show a high affinity with gold so the substrate is coated with a thin layer of gold to exfoliate large areas of 2D TMD sheets with high yield[99]. This process produces the layered material firmly adhered to an engineering-relevant substrate without any alteration in its chemical or mechanical properties while facilitating the separation of monolayer and few-layer thicknesses. Late et al.[64] first reported the mechanical exfoliation of single layer MoS_2 achieving a thickness of 0.7 nm, while other TMDs, such as $MoSe_2$, WSe_2, WS_2, or $NbSe_2$, have also been reported to be mechanically exfoliated to a few layers[100,101]. Recently, a fully automated micromechanical exfoliation system for MoS_2 and molybdenum ditelluride ($MoTe_2$) was designed by DiCamillo et al[102] where adhesive tapes were applied using a non-movable base and movable tool of a rheometer. A program was set to apply force and rotate the rheometer tool thus creating a shear cleavage force between bulk MoS_2 or $MoTe_2$ and the substrate which facilitates the exfoliation process.

The fundamental mechanisms which enable micromechanical cleavage are extremely complex to model and calculate as it is a multifaceted dynamic system. For example, micromechanical exfoliation does not remove a single layer from the bulk, but a multilayer slab, which makes it very challenging for DFT simulations. However, Sinclair *et al.*[103] developed a Monte Carlo mathematical model to predict repeated graphite exfoliation. Exfoliating *n* times, the model predicts how many steps are necessary before a single layer is produced. The matrix $\boldsymbol{B}$ is built to group the transition probabilities among transient states and a vector $\boldsymbol{b}$ is modeled to group the probabilities from any state to the adsorbing one. The resulting probability density function *g(c)* is[103]:

$$g(c) = \alpha \boldsymbol{B}^{n-1} \boldsymbol{b} \tag{3.2.1}$$

Starting with 30,000 layers (~10 μm thickness) and using $\alpha = 0.01$, the expected number of steps for reaching monolayer graphene is 11 when each cleavage happens at a random location. However, the authors used Molecular Dynamics simulations (MD) to show that polymer-based mechanical exfoliation favors cleavage near the surface. When the probabilities are changed to follow this finding, the number of steps needed to reach monolayer graphene is only 4, pointing out the importance of engineering the exfoliation method for optimal performance.

In addition to multilayer peeling, micromechanical cleavage may involve fracture. To understand this scenario, a few different approaches have been used. Yang and Vijayanand introduced a continuum model for the peeling process of graphene[104] which combined von Karman's plate theory, elastic fracture mechanics, and a cohesive spring model for interlayer delamination. As exfoliation happens, intermediate layers are partly attached to the upper stack and partly to the lower substrate, which sets the stage for delamination fracture. The main crack opening profile is governed by[104]:

$$w = w_{long} + w_{short} = \sqrt{\frac{\Gamma_{long}}{2D_m}}y^2 + 2\sqrt{\frac{\Gamma_{short}S'_{11}e}{\pi}}\sqrt{y} \tag{3.2.2}$$

Where w is the total deflection resulting from the applied force, with a long- and a short-range contribution; Γ is the cleavage toughness for each type of fracture (the long-range term coinciding with the interlayer cohesive energy); S'_{11} and e are derived from the elastic constant matrix of the material as defined elsewhere[105]; and D_m is the film flexural rigidity, which depends on the in-plane Young's modulus E_m and Poisson's ratio of the 2D material v_m as[104]:

$$D_m = \frac{E_m h^3}{12(1-v_m^2)} \tag{3.2.3}$$

Graphene delamination was described by an interlayer potential that yields tangential traction (p_α) as a function of energy density (γ_t), C-C bond length (d, or d_0 for optimal distance), and tangential displacement between layers (r_α, measured from the ground state stacking), where α, m and l are integers that count the dimensions of the system, following the definitions introduced by Yang[106]:

$$p_\alpha^{m,l} = \frac{\pi\gamma_t(r_\alpha^{m,l}-r_\alpha)}{2d_0 d^{m,l}}\sin\frac{\pi d^{m,l}}{d_0} \tag{3.2.4}$$

Finally, a cohesive model was used for tearing initiated crack growth. The total energy release (Γ) depends on the length of the layer (l), and the x- and z-components of the cohesive force at the tearing crack line (ku and kw, respectively, where k is a spring constant, and u and w are the displacement components)[104]:

$$\Gamma = -4\int_0^l ku\frac{\partial u}{\partial y}dy - 4\int_0^l kw\frac{\partial w}{\partial y}dy \tag{3.2.5}$$

A finite difference method was used to simulate the system. The graphene layer undergoes in-plane stretching and shearing, as well as out-of-plane bending, which can only be captured with von Karman's nonlinear plate theory. As a result, the layer is torn mainly by stretching, not by

tearing within the fracture zone. In addition, the distance between the tearing crack tip and the main cleavage crack front is predicted to be approximately 45 nm.

While DFT can only model simplified systems, as discussed in the previous section and illustrated in Figure 4A, classical MD can simulate more complex processes. For example, Jayasena and Sinclair independently simulated graphene exfoliation by polymer 'sticky tapes' (PMMA and PDMS) (Figure 4B)[103,107]. Even when pulling the polymer orthogonally, a mixed mechanism was observed for graphene exfoliation, with normal and shear components, which characterizes peeling. Other mechanical exfoliation mechanisms have also been studied with MD, such as the wedge-based method (Figure 4C)[108] or contact with an atomic force microscope tip (Figure 4D)[109]. The atomic force microscope tip was modeled using van der Waals forces with a Lennard-Jones potential; by bringing the surfaces together and then separating them, the authors observed micromechanical cleavage in which the top graphene layer was separated from the lower ones. Thanks to the usage of a reactive force field, breakage of C-C bonds was observed at high separation rates and increased van der Waals forces, leading to the formation of a graphene nanoflake.

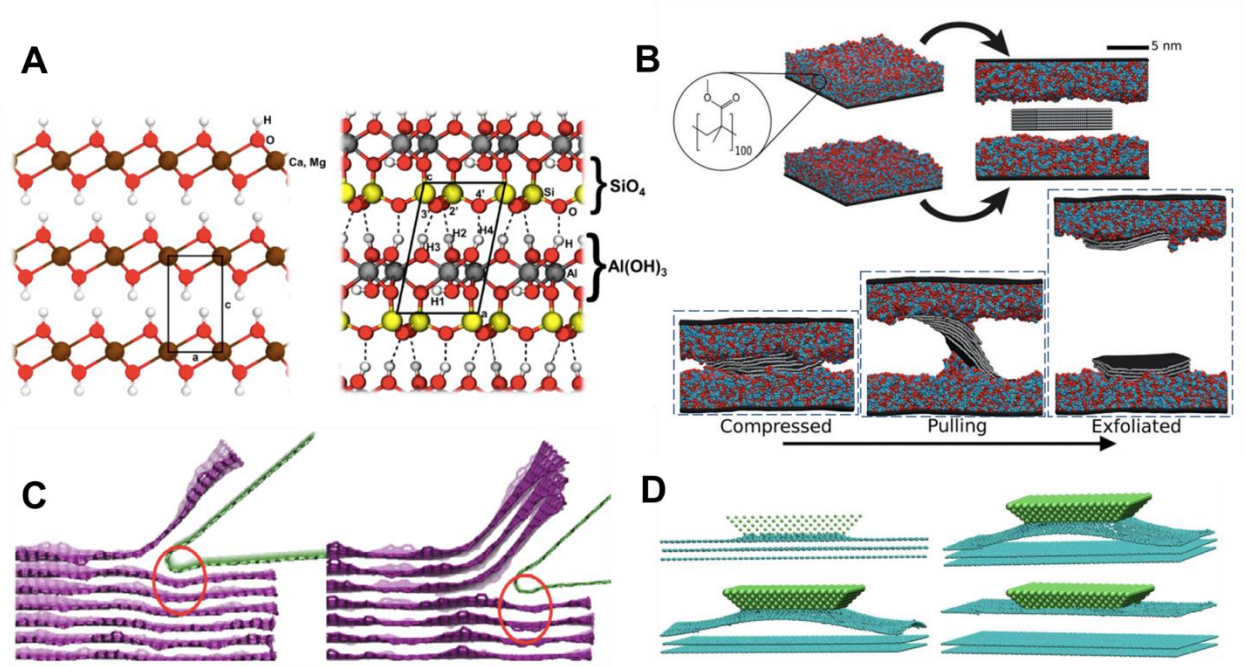

Figure 4. Atomistic simulations of mechanical exfoliation methods. A) DFT-calculated structure and H-bond formation in layered materials[76]. B) MD simulation of the polymer 'sticky tape' exfoliation of graphene[103]. C) MD simulation of the wedge-based mechanical exfoliation of graphene[108]. D) MD simulation of indentation of graphene, capturing layer cleavage[109]. A) Reproduced with permission from ***J. Chem. Theory Comput.*** 2020, 16, 8, 5244–5252. Copyright 2020 American Chemical Society. B) Reproduced with permission from ***Phys. Chem. Chem. Phys.***, 2019,**21**, 5716-5722. Copyright 2019 Royal Society of Chemistry. D) Reproduced with permission from ***Carbon*** 48 (2010) 1234-1243. Copyright 2009 Elsevier Ltd.

Although micromechanical cleavage is a well-known technique capable of producing 2D materials with high crystallinity and was used to exfoliate graphene for the first time, this method remains mostly relevant for laboratory-scale studies due to low throughput and consistency. In this regard, micromechanical cleavage has been most successfully used to investigate the benchmark properties of high quality 2D materials for many fundamental studies. For example, in 2008 the Young's modulus and intrinsic strength of defect-free exfoliated monolayer graphene was measured by Lee et al.[4] to be 1.0 TPa and 130 GPa, respectively, making it one of the strongest materials available. This mechanical cleavage method has also been used to exfoliate pristine 2D sheets of MoS_2[3,110], hBN[56], and graphene oxide[111] proving their exceptional mechanical strength and fracture behavior. The ultrahigh strength and stiffness values of these 2D materials are attributed to the pristine nature of 2D materials when produced by exfoliation, including a structure free of point defects and without out-of-plane bonding (i.e., only covalent sp^2 bonding in graphene sheets)[4,112].

Interestingly, despite exhibiting nearly exhibiting identical structures, the Young's modulus and fracture strength of micromechanically exfoliated graphene has been demonstrated to decrease with increasing layer thickness, but that of *h*BN was found to be independent of the layer number up to 9 layers (Figure 5 A&B)[56]. This can be attributed to the increased lip-lip interaction in *h*BN which makes the interlayer coupling more pronounced. Exfoliated 2D materials have also shown exceptional properties in several unique dynamic loading applications. The lifetime of micromechanical exfoliated graphene under cyclic fatigue loading exhibited the longest fatigue life of any known material, reaching over one billion cycles at loads greater than 50% of its fracture strength[113]. Additionally, exfoliated graphene displayed remarkable ballistic shielding properties due to its high in-plane strength and kinetic energy absorption at supersonic speeds (Figure 5C). At comparable densities, the specific penetration energy of multilayer exfoliated graphene was 2-3x higher than that of other materials, such as Kevlar and steel.

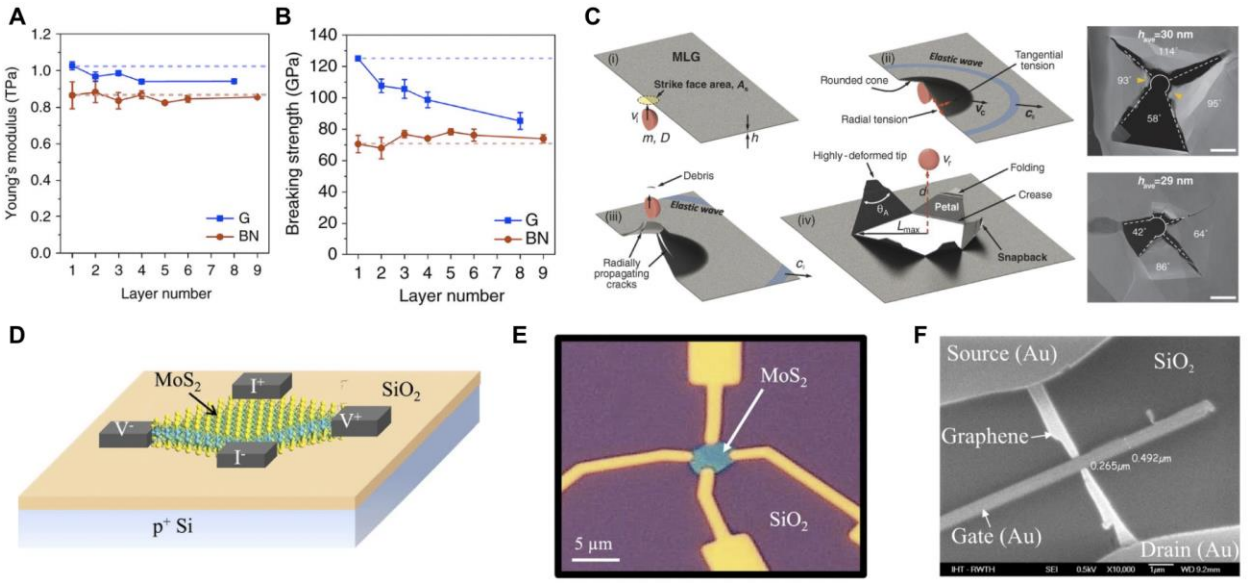

Figure 5. Mechanics & FET Fundamental Demonstrations of 2D materials. A&B) Young's modulus and breaking strength of mechanically exfoliated graphene and *h*BN nanosheets with varying layer numbers.[56] C) Supersonic impact energy absorption of exfoliated graphene showing a schematic of the process and postmortem images.[114] D) Schematic and E) optical micrograph of an exfoliated MoS2-based FET.[115] F) SEM image of the first reported graphene FET fabricated using exfoliated graphene.[116] A&B) Reproduced with permission from ***Nature Communications*** **volume 8**, Article number: 15815 (2017). C) Reproduced with permission from ***Science,*** 28 Nov 2014, Vol 346 Issue 6213, pp 1092-1096. Copyright 2014 Science. D&E) Reproduced with permission from ***npj 2D Materials and Applications*** 1, Article number:34 (2017)

Due to the pristine nature of mechanically exfoliated 2D materials, they have also been widely used to fabricate ultrathin field effect transistors (FETs). FETs use an electric field to control current flow from the source to the drain with a control electrode forming the gate and make up the basic component of logic devices (Figure 5D-F). The potential exhibited by exfoliated graphene for FETs are driven by the excellent electron mobility due to its near defect-free nature, which is reported to be as high as 2 x 10^5 cm^2 V^{-1} s^{-1} at room temperature[5]. In contrast, there is a significant difference in the electron mobility of exfoliated graphene compared to graphene synthesized using other methods, such as CVD[117], which shows electron mobility of only 12,000 cm^2 V^{-1} s^{-1} [118]. Bandgap materials such as 2D MoS_2 have also been successfully used to develop FETs as semiconducting phases[115,116].

Micromechanical exfoliation was the first technique to isolate 2D materials from their bulk forms owing to the ease of mechanically overcoming the van der Waals forces in the material to split apart the layers. This technique can repeatably produce 2D materials with minimal defects and large lateral sizes, making it ideal for identifying and evaluating the fundamental properties of the materials and creating proof-of-concept designs such as 2D material FETs. However, as mechanically separating layers of 2D materials is a tedious process with low throughput, this technique has been largely limited to bench-scale applications.

3.3 Ball Milling

While adhesive tape-based micromechanical exfoliation was the first to demonstrate successful isolation of 2D materials, ball milling employs a similar mechanical exfoliation technique but is more suitable for batch scalability. Conventionally, ball milling is used for fragmentation and mixing metallic powder to fabricate alloys but recently, researchers have employed this method to exfoliate layered 2D materials in bulk quantities. As the balls roll and bounce in the mill along with the 2D material, they exhibit shear, rolling, and impact forces on the 2D material which can overcome the van der Waals bonding and separate 2D layers. For example, Lee et al.[119] demonstrated a technique to ball mill *h*BN in the presence of sodium hydroxide (NaOH), as seen in Figure 6A. Synergistic shear and hydroxylation enables cutting into the *h*BN plane, which induces minimal structural damage (Figure 7A) while yielding a high percentage of flakes up to 1.5 µm in width with a yield of 18%. However, ball milling alone is very aggressive and has been shown to induce basal plane and edge defects in layered materials (Figure 6 B&C)[120]. This is because two significant mechanisms are in play during the ball mill exfoliation process; shear forces by rolling of the balls allow for large area exfoliation of 2D materials, while the impact forces of bouncing balls break the agglomerated particles into smaller ones. The impact forces can additionally fragment the 2D sheets, which can lower yield, reduce lateral size, and induce defects in the exfoliated sheets[92]. Despite this disadvantage, ball milling produces a significantly higher

yield of layered materials compared to other 2D material synthesis techniques and is easily scalable to industrial volumes.

Ball milling is a widely employed technique used to exfoliate a variety of 2D materials including MoS_2[121,122], graphene[123], SnS_2/graphene hybrid nanosheets[124], MoS_2/rGO sandwiches[125], and *h*BN[126]. These high-yield processes have successfully produced exfoliated 2D materials for use in lubrication oil[127], electrochemical energy storage[125], conductive polymers[128], and Li-ion batteries[124]. Part of this success can be attributed to milling-generated defects, which are actually beneficial in engineering the properties of 2D materials for applications such as energy storage where the defects provide more active adsorption sites, allow faster diffusion, and enhance storage capacity[129]. One major consideration for ball milling is that different milling parameters are vital in determining product quality and yield. Deepika et al.[127] systemically studied milling parameters such as milling speed, ball-to-powder ratio, and ball size to optimize the system for the highest efficiency and product yield. Smaller balls (0.1-0.2 mm), intermediate speeds of approximately 800 rpm, and a ball-to-powder ratio of 10:1 exfoliated layered BNNSs most efficiently. Under this optimum condition, they reported a yield as high as 13.8%, and the BNNSs were 0.5-1.5 μm in diameter and a few nanometers thick.

Plasma- and hydrothermal-assisted ball milling are two enhanced forms of ball milling that have received considerable attention for commercial applications. Lin et al.[130] reported the exfoliation of few-layer graphene using plasma-assisted ball milling to avoid the formation of amorphous carbon during the exfoliation from bulk graphite. The generated plasma keeps the bulk powder in a high-stress state, ensuring crystallinity throughout exfoliation. Additionally, Xia et al. used a hydrothermal-assisted ball milling process to produce SnS_2/graphene composite nanosheets that showed excellent rate capability and cycling stability of LL-SnS_2 electrodes for lithium-ion batteries[124]. One gram of SnS_2, 0.2g of graphite, and 20 mL anhydrous ethanol were mixed in a planetary ball mill to produce the composite exfoliated graphene structure that was used as an anode material.

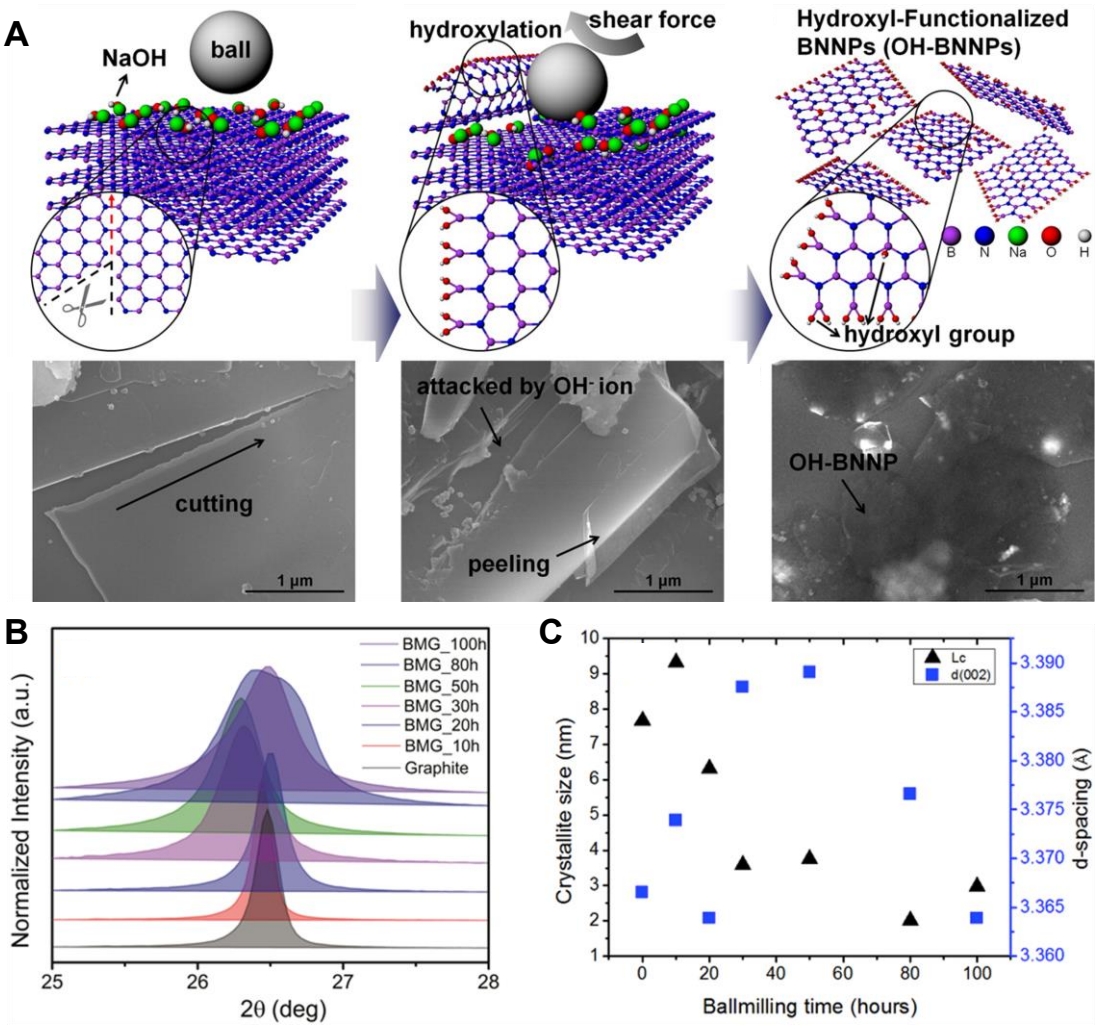

Figure 6. Ball milling exfoliation mechanisms of 2D materials. A) Schematic diagram and corresponding SEM images of the exfoliation mechanism of *h*BN.[119] B) XRD and C) variation of interplanar spacing with milling time of ball-milled graphene.[120] A) Reproduced with permission from ***Nano Lett.*** 2015, 15, 2, 1238–1244. Copyright 2015 American Chemical Society. B&C) Reproduced with permission from ***Scientific Reports*** 8, Article number 15773 (2018)

Since ball milling was historically used for size reduction in many types of processes, several attempts were made to model its underlying mechanisms[131]. A key aspect of ball milling is the energy provided to the material by the balls. For instance, Burgio's model[132] calculates the transferred energy by a single ball in a single impact (ΔE_b), which depends on the density of the milling material (ρ_b), the ball diameter (d_b), the speed of the ball mill main disk (W_d), the vial diameter (D_v), the main disk diameter (D_d), and the transmission ratio between the main disk and the vial (R_T)[132]:

$$\Delta E_b = \left(-\frac{\pi \rho_b d_b^3 W_d^2}{24}\right)\left(\frac{D_v - d_b + R_T^2 D_d}{R_T^2}\right)\left(\frac{D_v - d_b}{R_T}\right) \quad (3.3.1)$$

Equation 3.3.1 features different geometrical parameters of the mill. As a result, the energy ΔE_b depends on the free space within the vial. A factor ϕ_b was proposed to describe the degree of filling, allowing for the accumulated energy (ΔE_{ac}) to be more accurately modeled as a function of time (t), using a constant that captures the elasticity of the collisions (K), as shown in Equation 3.3.2. For a given experimental setup, all the variables in brackets have constant values, which allows simplification to an expression whose terms can be controlled experimentally. By using this modeling, Ghayour found that increasing the number of balls has minimum impact on transferred energy due to a decrease in their kinetic energy and mobility[133]. Martinez-Garcia used this approach to model the mechanosynthesis of hexagonal Re_2C, finding that there exists a minimum transferred energy necessary to trigger the process equivalent to overcoming the interlayer binding energy[134].

$$\Delta E_{ac} = \left[\left(-\frac{\pi\phi_b K N_b d_b^3}{24}\right)\left(1-\frac{1}{R_T}\right)\left(\frac{D_v - d_b + R_T^2 D_d}{R_T^2}\right)\left(\frac{D_v - d_b}{R_T}\right)\right]\frac{\rho_b W_d^3 t}{m_s} \quad (3.3.2)$$

MD can also be used to simulate the micromechanics of the ball milling process[135,136], although, to our knowledge, this approach has not been used to model the mechanics of exfoliation in particular. Hara, for instance, used MD to study the milling-induced allotropic transformation of cobalt, by compressing a nanoparticle at different angles between two walls[136]. This methodology could be extended to investigate exfoliation, since both compressive and shear forces are generated. Indirect approaches, on the other hand, have been applied to investigate the processes during exfoliation. For instance, Arao investigated salt-assisted ball milling for graphene production and used MD to show that salt adsorption takes place on active carbon at graphitic sheets[137].

Ball milling also offers a unique ability among synthesis methods in the one-step manufacturing of composite or functionalized structures. For example, TMD/graphene nanocomposites have recently attracted researchers' attention for their potential application as electrode materials. Using MoS_2 and graphene oxide as bulk precursors, large-scale MoS_2/reduced GO electrode composites were prepared from a one-step solvent-free ball milling process without postprocessing requirements[125]. Interestingly, a planetary ball milling process with ammonia borane has been used to exfoliate fluorinated graphene sheets from bulk graphite fluoride[138]. Fluorographene is challenging to exfoliate but the strong dipole interactions between NH_3BH_3 and FG along with the shear forces by ball milling produced high quality nanosheets that were 1-6 nm thick with a lateral size of 0.3-1 µm. Additionally, *h*BN is often sought as a filler for polymer composites due to its excellent thermal conductivity, however, due to the inert nature and strong ionic bonds of *h*BN, exfoliation and functionalization are very challenging[139]. Yu et al.[128] addressed this through co-ball milling of polymer and *h*BN in solution as an effective one-step synthesis process for producing polymer-functionalized few-layer boron nitride for cellulose composites with high thermal conductivity.

Polymer-2D material composites represent one of the most common methods to exploit the enhanced properties of exfoliated 2D materials for macroscale applications. While polymers are typically very inexpensive to produce, they lack electrical or thermal conductivity as well as high strength and stiffness which are some of the predominant benefits of 2D materials. By dispersing exfoliated 2D materials throughout the polymer matrix, often during the polymer mixing and molding process, the composite can exhibit enhanced properties from the nanoscale material at a

level of macroscale applicability. Scalability is one of the most important parameters as polymer composites require significant volumes of 2D materials. Additionally, in many cases, tens of layers are preferable to few-layer 2D materials which makes ball milling an ideal synthesis method for preparing polymer composites as shown for *h*BN[128], MoS_2[122], graphene[130], reduced GO[140], and other 2D materials. This process is demonstrated in Figure 7A wherein the graphene is exfoliated and dispersed into the epoxy solution throughout a 30h ball milling process before being cured into the final composite shape[141].

As 2D materials present strengths and stiffnesses that are typically many orders of magnitude greater than polymers, the mechanical properties of polymers can be greatly enhanced by composite synthesis. For example, dispersion of exfoliated graphene in polyurethane has demonstrated increases in the strength and stiffness by over two orders of magnitude at a mass fraction of 55%[142]. Similarly, the Young's modulus has been found to increase by 60% at 20 wt.% exfoliated graphene,[143] and the tensile strength of various polymers has been found to increase by 12-90% with the addition of exfoliated MoS_2[144]. The potential of polymer reinforcement can also be clearly noted for several cases involving low concentrations of reinforcement. At low loading volumes, the Young's modulus of graphene/epoxy composites are nearly doubled at 0.1 wt.% graphene (Figure 7B)[141]. Shen et al.[145] produced PEO composites with eight different 2D materials at 0.5 wt.% and found the strength and stiffness to be reliant on the exfoliation capacity of the respective 2D material and the morphology of the composite (Figure 7C). *h*BN-reinforced PVA showed a linear increase in the strength and stiffness with the volume fraction up to a 40% increase at 0.3 vol.% *h*BN[146]. Graphene reinforcement of PVA has also shown strength increases of greater than 90% for volume fractions below 0.4 vol.%[147]. This demonstrates the potential for exfoliated 2D material additives to significantly enhance polymers' properties without greatly increasing the cost or altering the composition. Additionally, exfoliation techniques such as ball milling of 2D materials is especially beneficial for mechanical reinforcement as larger particles, which are facile to produce at scalable quantities by ball milling and other exfoliation processes, produce greater strengthening effects due to greater volumes of interconnected material[148].

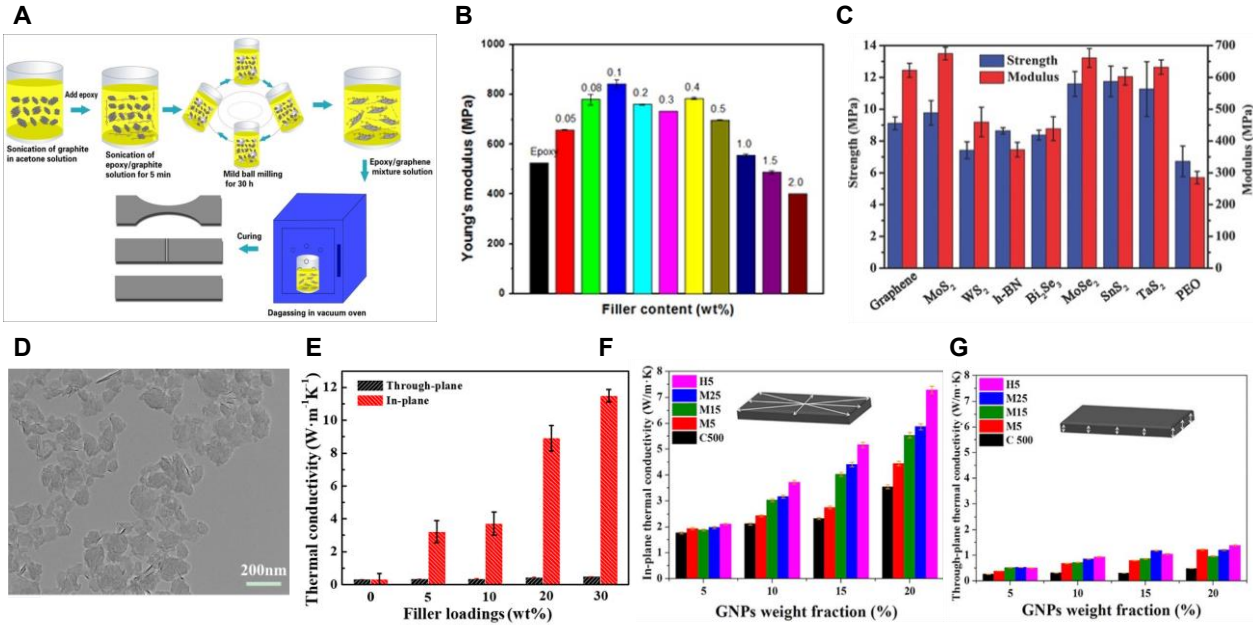

Figure 7. Polymer composites with exfoliated 2D materials. A) Schematic illustration of epoxy-graphene composite prepared by one-step ball milling. B) Young's modulus of epoxy composites with ball milling exfoliated graphene fillers[141]. C) Tensile strength and modulus of PEO composite materials with eight different types of exfoliated 2D materials[145]. D) TEM image of the hexagonal boron nitride nanosheets produced by ball milling[149]. E) Thermal conductivity of poly (vinyl alcohol)/boron nitride nanosheets (PVA/BNNSs) composites through-plane and in-plane with different BNNSs additions[149]. F&G) In-plane and through-plane thermal conductivity of composites filled with GNPs of various layer sizes and thicknesses[150]. A&B) Reproduced with permission from ***Polymer Composites***, volume 37, Issue 4, Pages 1190-1197 (2016). Copyright 2016 John Wiley & Sons, Inc. C) Reproduced with permission from ***Small***, volume 12, Issue 20, Pages 2741-2749 (2016). Copyright 2016 John Wiley & Sons, Inc. D&E) Reproduced with permission from ***Polymer Composites***, volume 43, Issue 2, Pages 946-954 (2022). Copyright 2022 John Wiley & Sons, Inc. F&G) Reproduced with permission from ***Scientific Reports*** 6, Article number: 26825 (2016)

The other significant drawback with polymer materials is that pure polymers are electrically and thermally insulating in almost all cases. However, similar to the effective mechanical reinforcement achieved in 2D material-polymer composites, composites of exfoliated 2D materials in polymers have yielded electrically conductive composites that have found applications in electromagnetic shielding [151,152] anti-static components,[153] and strain sensors[154,155]. Predominantly exfoliated graphene has been used as the filler in these composite matrices due to its high conductivity, however, TMDs, including exfoliated MoS_2[156] and WS_2[157] are also common for applications that require semiconducting properties. Similarly, the thermal conductivity of polymers can be significantly enhanced with the addition of 2D materials. Most prominently, this presents new applications in thermal dissipation for small-scale electronic systems with demonstrated applicability by exfoliated graphene,[158,159], MoS_2[160], and *h*BN[149] (Figure 7 D&E).

One drawback of 2D material-polymer composites is the significant heterogeneity in the out-of-plane direction due to fillers' alignment and planar orientation during molding. Kim et al.[150] found that the thermal conductivity of exfoliated graphene nanoplatelet composites differed by close to an order of magnitude between the in-plane and through-plane directions (Figure 7F&G). Similarly, Sullivan et al.[161] noted that the electrical conductivity of exfoliated graphene nanoplatelet composites differs by two orders of magnitude in the through-plane direction compared to the in-plane direction. This can serve as an engineered parameter to produce orientation-dependent conductivity for shielding applications of polymer composites.

The mechanical exfoliation of 2D materials by ball milling is a batch-scalable process that has demonstrated extremely high yields of many types of 2D materials. However, the aggressive nature of the technique leads to high defect densities and smaller lateral sizes, which is restrictive for some of the end applications of these materials. As a result, one of the best applications for ball-milled 2D materials is the production of polymer composites, including mechanical reinforcement and thermal and electrical conductivity enhancement for multifunctional applications[162].

3.4 Ultrasonication

While micromechanical cleavage and ball milling induce exfoliation by physically separating layers, many materials can be solution-processed and exfoliated through the relatively gentler process of ultrasonication. During ultrasonication, a solution containing dispersed bulk materials is exposed to a transducer that emits ultrasonic waves throughout the material. These ultrasonic

waves generate vast swarms of unstable cavitation bubbles that, upon their inward collapse, emit high temperature, pressure, and velocity jets of liquid in the local environment. This creates a hydrodynamic shear force that leads to deagglomeration of the bulk materials and is strong enough to overcome the weak van der Waals forces between layers to exfoliate relatively small 2D layers from the bulk material[163,164]. 2D materials exfoliated via ultrasonication tend to have lateral sizes of a few micrometers, and with thicknesses no more than a few layers[165]. Yields of ~1 wt% are routinely achievable, which can be improved to 7-12 wt% with further processing[164]. This process is shown as a schematic in Figure 8A[166], while Figure 8B shows a high-speed image sequence of ultrasonic exfoliation of a graphene flake[167].

Liquid-phase exfoliation is a chemical process assisted by mechanical mechanisms, and vice-versa. Therefore, the choice of medium for ultrasonication is a governing parameter and different solvents can help achieve different production objectives[165,168,169]. A study of over 40 different solvents identified surface tension as one of the most important solvent parameters and characterized solubility parameters for highly efficient exfoliation[170]. A common mechanism in which a solvent assists the exfoliation process is through interfacial tension by reduction of the potential energy within layers to overcome van der Waals forces of the layered material. The greater the difference between the surface tension of the solvent and the 2D material, the greater heterogeneity of the exfoliated sheets. Solvents with surface tensions close to that of the 2D material, such as ortho-dichlorobenzene in the case of graphene, have shown to produce relatively large and highly homogenous dispersions without a noticeable Raman D band indicating low defect concentration[171]. Arifutzzaman et al.[172] exfoliated graphene using sonication in N-methyl-2-pyrrolidone (NMP) and N,N-dimethylformaldehyde (DMF) which showed that the defect population of graphene exfoliated in NMP was significantly lower than that in DMF due to the lower energy cost for creating new surface areas in NMP, which is a result of similar surface energies.

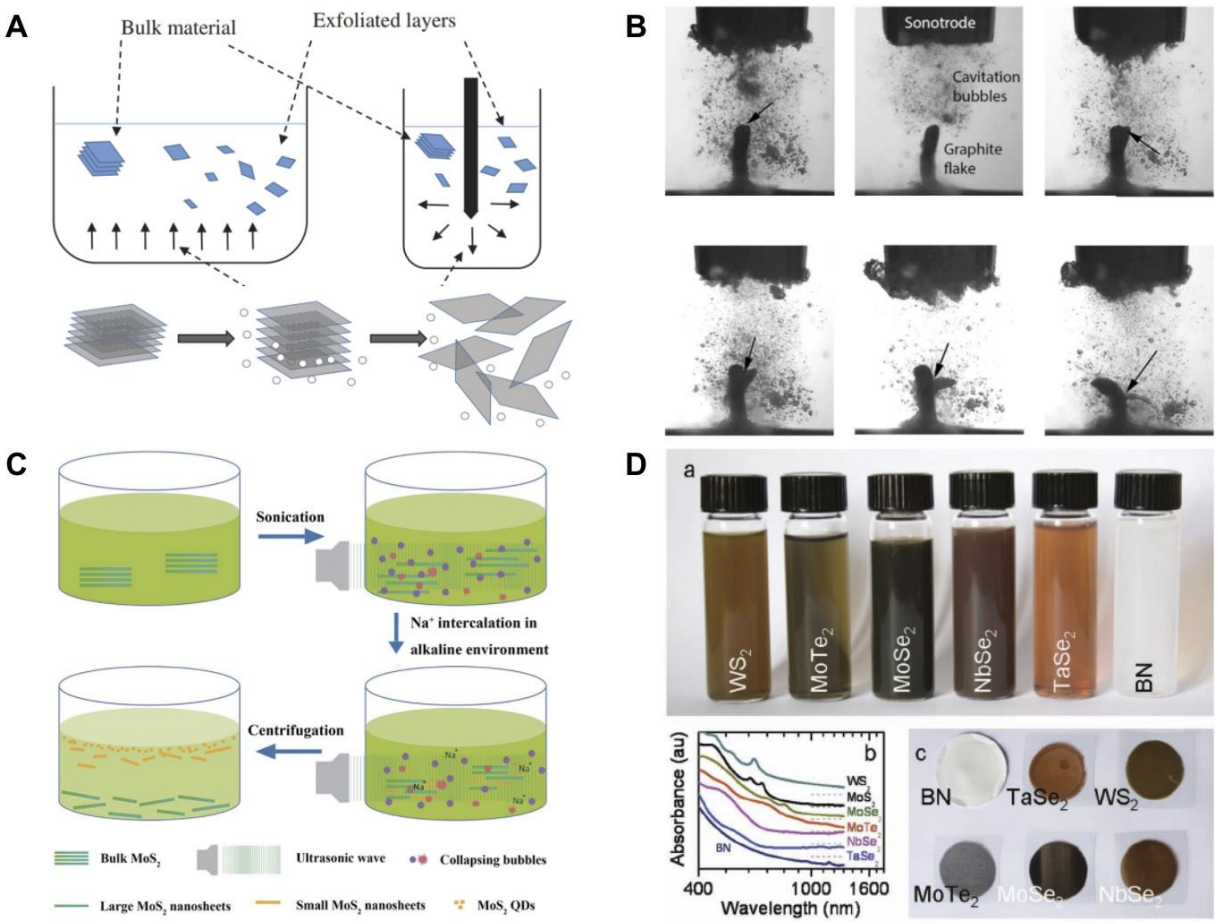

Figure 8. Liquid sonication exfoliation mechanisms of 2D materials A) A schematic of liquid sonication demonstrating how bulk material is fragmented into 2D nanosheets using ultrasonication[166], B) High-speed sequence of frames illustrating the ultrasonication exfoliation of a graphene flake[167], C) Schematic of surfactant-assisted ultrasonic exfoliation of graphene nanosheets[173], D) Ultrasonicated WS_2, $MoTe_2$, $MoSe_2$, $NbSe_2$ $TaSe_2$ and *h*BN stabilized in water using sodium cholate[174] A) Reproduced with permission from ***Nanophotonics*** Volume 9, Issue 8, Page: 2169-2189 (2019). B) Reproduced with permission from ***Carbon***, Volume 168, Pages 737-747 (2020). C) Reproduced with permission from ***Langmuir*** 2012, 28, 40, 14110-14113 (2012). Copyright 2012 American Chemical Society. D) Reproduced with permission from ***Advanced Materials***, Volume 23, Issue 34, Pages 3944-3948 (2011). Copyright 2011 John Wiley & Sons, Inc.

Additionally, several additive compounds can assist the ultrasonication mechanism. Stabilizers such as surfactants, polymers, pyrene derivatives, and supercritical fluid solvents have been employed to improve the efficiency and reduce the toxicity of liquid-phase exfoliation[175–177]. Surfactants, ionic or non-ionic, can charge individual flakes to cause electrostatic repulsion between them to aid the exfoliation process[177,178]. Also, surfactants lower the liquid-vapor interfacial energy, promoting greater cavitation events by sonication. This improves the yield without needing to increase the sonication power, as the cavitation bubbles only need to be powerful enough to overcome the weak van der Waals forces and prevents material degradation as the strong in-plane covalent bonding is largely preserved without the introduction of defects[167,173]. Furthermore, the surfactant absorbs onto the exfoliated sheets, creating an additional repulsive force that prevents the reaggregation of the sheets post-sonication[174]. Similarly, adding alkali metal ions such as Na^+ during the sonication

process can lead to ion intercalation between the 2D sheets. This intercalation further weakens the van der Waals forces, thus improving the 2D material yield of the supernatant, as represented in Figure 8C[179,180]. Various polymers such as polyvinyl chloride (PVC), poly (methylmethacrylate) (PMMA), and polyvinylpyrrolidone (PVP) have been employed and introduced into the sonication medium[181,182]. It has been revealed that through steric stabilization, polymers are effective in preventing aggregation of exfoliated sheets in solvents[183]. Additionally, polymers can mediate the surface energy mismatch between solvents and layered materials. Ethyl cellulose was mixed with ethanol to exfoliate graphene to address the surface energy mismatch between ethanol and graphene, demonstrating that polymeric stabilizers can also allow for exfoliation in non-traditional solvents[183]. Pyrene stabilizers have been demonstrated to be highly effective stabilizers for high-yield exfoliation of monolayer graphene with exfoliated sheets showing high levels of purity[184–186]. The interaction between π orbitals of pyrenes and graphene reduces the surface energy of the dispersion increasing purity[165,185]. Supercritical fluids have also been employed in liquid-phase exfoliation[187,188] as they have densities like liquids and diffusion and solubility characteristics like gases. Therefore, they can easily diffuse between layered materials and assist in exfoliation.

The evolution of particle size distribution during ultrasonication can be calculated with an equation for the mass fraction (m_i, i being the size class) as a function of time (t), as originally used to model ball milling[189,190]. The process depends on the selection function (S_i), which is the rate constant for particles to be broken to smaller sizes; and the breakage distribution function ($b_{i,j}$), which is the mass fraction of particles broken (from j to i)[189,190]:

$$\frac{dm(t)}{dt} = -S_i m_i(t) + \sum_{j=1}^{i-1} S_j b_{i,j} m_j(t) \tag{3.4.1}$$

This function can be written in a cumulative form. In this case, the cumulative size distribution function ($R_i(t) = \sum_{j=1}^{i} m_j(t)$ for particles of size greater than i) depends on the cumulative breakage function ($B_{i,j} = \sum_{k=i+1}^{n} b_{k,j}$ for the probability for fragments from particles j to have a size less than i)[189,190]:

$$\frac{dR_i(t)}{dt} = -S_i R_i(t) + \sum_{j=1}^{i-1} R_j(t)\left[S_{j+1} B_{i,j+1} - S_j B_{i,j}\right] \tag{3.4.2}$$

These formulations are useful since the parameters S_i and $B_{i,j}$ can be estimated experimentally from particle size distribution, by solving the equations above. For instance, Kapur[191] proposed an approximate solution where $f(t)$ is the residual ratio that represents the fraction of particles that have not been broken yet[191]:

$$f(t) = \frac{R_i(t)}{R_i(0)} = exp\left[\sum_{k=1}^{p} K_i^{(k)} \frac{t^k}{k!}\right] \approx exp\,(K_i^{(1)} t) \tag{3.4.3}$$

In Equation 3.4.3, the approximation can be used for short exfoliation times. This expression can then be used to estimate the operation parameters. Li et al.[192] applied this methodology to the liquid-phase exfoliation of GO, finding that its breakage happens mainly due to sheet fracture (rather than abrasion), which governs its lateral size.

A similar approach to model the kinetics of exfoliation is to use an approach akin to polymer decomposition[193]. In this case, the concentration of the *i*-layered material $[P_i]$ is a function of a kinetic constant *k*, as shown in Equation 3.4.4. This model shows that, at long periods of time, monolayers dominate over thicker slabs, which can help target a specific thickness distribution by engineering process parameters such as operation time [194].

$$\frac{d[P_i]}{dt} = \sum_{j=i+1}^{p} k[P_j] - \sum_{j=1}^{i-1} k[P_i] \tag{3.4.4}$$

Since ultrasonication exfoliates by cavitation, modeling pressure distribution in the liquid system can provide great mechanistic insight. This can be done by solving the linear steady-state wave equation by FEM, which considers the coupling between the acoustic field of the solution and the vibration of the surrounding vessel. The model includes acoustic pressure (*P*), density (ρ), and the speed of sound (*c*), as shown in Equation 3.4.5[194]:

$$\frac{1}{\rho}\nabla^2 P - \frac{1}{\rho c^2}\frac{\partial^2 P}{\partial t^2} = 0 \tag{3.4.5}$$

If the sonication system uses a transducer that works at constant frequency *f*, then pressure is simply a time harmonic $P(r,t) = p(r)e^{i\omega t}$, where $\omega = 2\pi f$ and $p(r)$ is the pressure amplitude. The space-dependent wave equation then becomes[194]:

$$\frac{1}{\rho}\nabla^2 p + \frac{\omega^2}{\rho c^2} p = 0 \tag{3.4.6}$$

The numerical solution of this equation can be obtained with FEM. Yi et al.[194] found that changing cavitation in the synthesis vessel can critically affect exfoliation, with injected power being nearly proportional to cavitation volume and therefore sample volume, and pressure amplitude and cavitation intensity having effects on graphene yield as well.

Using a different strategy to investigate vibration, Pupysheva et al.[195] performed MD simulations to study the exfoliation mechanism of graphene under ultrasonication with and without a surfactant. A classical force field was used to estimate the soft and hard modes of vibration of graphene, corresponding to parallel and perpendicular displacements between successive layers, respectively. The obtained data was fit to harmonic curves for the estimation of the effective force constant (*k*), which in turn was used to calculate the resonance frequency (*f*) from the reduced mass (μ), as shown in Equation 3.4.7. They found that parallel exfoliation along the zigzag edge is the most likely, and that adsorbed surfactants have no major impact on resonance frequencies, which suggests that they facilitate exfoliation only by preventing exposed layers to regroup[195].

$$f = \frac{1}{2\pi}\sqrt{\frac{k}{\mu}} \tag{3.4.7}$$

Unlike other cleavage techniques, liquid-phase exfoliation has been widely explored by MD. Since these simulations can capture dispersive, polar and hydrogen-bonding interactions at the solvent-nanomaterial interface, they can be used to evaluate how efficient a liquid is at exfoliating and specially at dispersing the material[196]. For instance, Shih et al.[193] studied graphene in different

polar solvents, calculating the Potential of Mean Force (PMF) between parallel sheets to estimate their stability in a dispersion. The authors investigated the atomic mechanism of confinement and desorption of solvent molecules from interlayer space, as well as the kinetics of graphene aggregation. To achieve this, they developed a kinetic theory of colloid aggregation that can be used to predict the lifetime and time-dependent layer distribution of graphene in different solvents. Starting from only monolayers in the dispersion, the concentration of *i*-layer graphene sheets (N_i) depends on a kinetic constant (k)[193]:

$$N_i(t) = N_{i0}\left(\frac{1}{1+N_{i0}kt}\right)^2\left(\frac{N_{i0}kt}{1+N_{i0}kt}\right)^{i-1} \quad (3.4.8)$$

And k can be calculated from the diffusivity of monolayer graphene (D), the closest interlayer distance ($r_0 \approx 3.5$Å), the PMF per unit area between parallel sheets (Φ), the average collision area (A_C), the temperature (T), and Boltzmann's constant (k_B), as shown in Equation 3.4.9. In this model, Φ can be extracted from MD simulations, and A_C is the only adjustable parameter[193].

$$k = \frac{8\pi D}{\int_{r_0}^{\infty}\frac{exp\,(\Phi A_C/k_BT)}{r^2}dr} \quad (3.4.9)$$

Furthermore, MD has been used to unveil the mechanism of liquid-phase exfoliation of several other 2D materials. For instance, it showed that intercalated polar solvents are strongly adsorbed on *h*BN surfaces, forming quasi-stable states that reduce interlayer binding[197], that polar solvents also favor exposed edges in MoS_2, promoting exfoliation and hindering aggregation[198], and that the efficiency of phosphorene exfoliation is enhanced when solvent molecules can reach planarity and therefore "sharpen" the molecular wedge that separates layers[196]. DFT too can shine light on the energy variations due to molecule or ion intercalation. For example, it showed that the intercalation of many solvent molecules within graphene is energetically favorable[199].

Smith et al.[174] demonstrated the exfoliation of monolayers and a few layers of a wide variety of TMDs and *h*BN using low-power bath sonication stabilized in water with sodium cholate (Figure 8D). Following ultrasonication, the solutions containing nanosheets are typically centrifuged to separate the exfoliated nanosheets from the unexfoliated bulk material and dried to a powder as shown in Figure 8D. Since many TMDs are degraded in the presence of air, ultrasonic exfoliation in a liquid medium (i.e., alkali-stabilized water, isopropanol, cyclohexanone, dimethylsulfoxide, N-methyl-pyrrolidinone, dimethylacetamide, etc.) promises larger scalability for layered TMDs. The process is widely applicable as most layered materials have binding energies appropriate for bath sonication with appropriate liquid mediums. Graphene dispersions, for example, were prepared using NMP as a solvent by Hernandez et al.[164] to minimize the energy mismatch between the exfoliated material and solvent for efficient low defect exfoliation.

Numerous reports on the exfoliation of graphene by sonication are available,[136,161,162,200,201,] and many TMDs have also been widely exfoliated by sonication for their potential applications in semiconducting devices[202–204]. Umar et al. demonstrated the exfoliation of *h*BN in polyvinyl alcohol (PVA), producing exfoliated nanosheets of ~3 layers on average[146]. In addition to these standard materials, other unique 2D materials, such as phosphorene,[205] molybdenum trioxide (MoO_3),[173] and ultrathin $WO_3{\cdot}2H_2O$,[206] have been reported. $WO_3{\cdot}2H_2O$ was exfoliated by bath

sonication for application in memory devices by Liang et al. [206], producing nanosheets of 2-3 nm thickness. It should also be noted that the amplitude of the sonicator and the sonication time significantly affects the quality of the 2D flakes. Baig et al.[207] found that the defect density in exfoliated graphene increased with both amplitude and sonication time. With the increase in sonication time from 10 min to 120 min, the Raman I_D/I_G ratio increased from 0.07 to 0.182, which corresponded to a 61% increase in the defect content at 120 mins compared to 10 mins. Similarly, an increase in sonicator amplitude from 60 to 100% corresponded with a significant introduction of defects in exfoliated graphene. Interestingly, Tyurnina et al.[208] employed a dual-frequency ultrasonication technique with concurrent 1174 kHz and 20 kHz waves to exfoliate graphene in water which created a wider population and size distribution of cavitation bubbles. As a result, they demonstrated a high yield of mono to tri-layer graphene flakes with widths exceeding 1 μm^2. The mechanism of cavitation towards exfoliation of graphene was examined in detail by Morton et al.[209] who determined the shockwaves to emit a pressure magnitude up to 5 MPa and liquid jets on the order of 80 m/s. They further noted that stable cavitation resulting in bubble oscillations produced a higher yield with reduced defects as the repeated gentle forces slowly separate graphene layers.

As ultrasonication is a solution-based exfoliation technique, it has become the most common exfoliation technique for preparing 2D-material lubricant fluids. This is due to the dual process of 2D material dispersion and exfoliation during sonication, which can be directly performed in the base lubricant in a one-step process.[210–212] Exfoliated 2D materials can significantly reduce the friction and wear rates of the contact when trapped between the sliding faces due to their van der Waals forces between the layers, which creates a low coefficient of friction due to shear energy dissipation.[213] The majority of exfoliated 2D materials have been used as lubricants, including graphene, GO, MoS_2, *h*BN, WS_2, and many others.[213] As ultrasonication produces a dispersion of few-layer exfoliated 2D materials in an aqueous solution, this allows for a facile one-step approach for the production of 2D material-dispersed lubricants such as MoS_2 and WS_2 in mineral oils,[214,215] graphene in SAE 15 W-40[216], or hBN, graphene, and MoS_2 in water-based lubricants.[210,211,217]

The affinity of graphene to water makes it an ideal additive to water-based lubricants; the exfoliation of graphene and GO in DI water has demonstrated a reduction in the coefficient of friction by a factor of 6 and 2, respectively, in a steel-steel contact[210]. *h*BN has also been used extensively as an additive to water-based lubricants with concentrations as low as 0.01 wt.% exfoliated *h*BN in water reducing the friction and wear behavior by up to 20%[217]. Conversely, TMDs degrade in water and are commonly used in oil-based lubricants; 0.5 wt.% chemically exfoliated MoS_2 in oil-based lubricants can reduce the total wear by 40-50% and the friction by up to 15-20%[214]. Meanwhile 1.0 wt.% exfoliated WS_2 dispersed in oil has shown a reduction in wear by 43% and friction by up to 39%[215].

As additives in bulk lubricants, nanomaterials must be effectively dispersed in the solution to be trapped within the tribological running surfaces for effective lubrication. However, dispersion can be a challenge for 2D materials due to the aggregation and viscosity of lubricant oil. In such cases, functionalization can improve the dispersion and lubricating properties of exfoliated 2D materials. For example, surface functionalization using thiol molecules has been employed in situ during the ultrasonic exfoliation process to prevent aggregation of MoS_2 sheets in the final lubricant composition. 0.1 wt.% of this functionalized MoS_2 in a water-based lubricant was enough to reduce the friction by 50% and the wear volume by 70%[211]. MD simulations suggest that the enhancement

of 2D materials dispersion due to functionalization is related to increased attraction between the material and the solvent, which agglomerates near the layers and improves repulsion between the sheets[218]. Functionalization can also enhance lubrication directly. For instance, DFT calculations show that graphene functionalization reduces friction by decreasing the energy corrugation at the interface due to the repulsion between similarly charged atoms[219]. However, charge displacement doesn't always enhance lubrication, as oxidation of MoS_2 increases friction due to a less uniform charge distribution and interlayer bonding[220]. Additionally, the size of 2D material particles after exfoliation influences the friction and wear behavior. Exfoliated *h*BN particles showed optimal wear reduction properties at an average size of 70 nm in SAE 40 W-15 oil,[221] while reduction of the MoS_2 particle size from 2 μm to 180 nm by extended ultrasonication reduced the friction coefficient and wear rates by a factor of more than 2[222].

As macroscopic lubricants require significant volumes of material to be dispersed throughout liquid media, and as 2D materials require multilayer thicknesses to provide van der Waals shear effectively, ultrasonication is an ideal exfoliation method for preparing 2D material lubricants. Ultrasonication has been demonstrated to be effective for exfoliating a wide variety of 2D materials thereby offering promise for many commercial tribological applications that may require different tribochemical conditions. Through the exfoliation of these materials directly in the lubricant medium, ultrasonication provides a simple one-step scalable method for producing 2D material lubricants.

3.5 Shear Exfoliation

An alternative method for solution exfoliation of 2D materials, which is also highly scalable, is high shear mixing. This technique involves exfoliating nanoparticle agglomerates in a solution by the viscous forces that flow through a narrow channel with very high velocity. The viscous forces in the channel cause the solvent to exert high shear forces across the 2D particles which, when combined with the weakening of van der Waals forces by the solvent solution, break the van der Waals bonds producing thinner sheets[223]. Additionally, the shear forces in the solvent mechanically enhance the degree of intercalation for molecules between 2D layers which further decreases van der Waals forces in a synergistic effect[224,225]. This results in 2D sheets with a low defect content as the forces required are much weaker than other exfoliation methods[225]. Nonetheless, this process requires a balance of forces to ensure efficient exfoliation without breaking the exfoliated 2D sheets.

Paton et al.[200] first demonstrated a rotary mixing process where a critical shear rate of ~10^4 s^{-1} was necessary for the shear exfoliation of graphene in NMP. The rotor-stator gap was maintained on the order of 100 μm to create high shear rates in the narrow channel. However, due to the breaking of the nanosheets, high defect contents were recorded in 2D graphene exfoliated at high rotor speed. To address this issue, Liu *et al.* used a high shear mixer to exfoliate relatively low-defect density graphene nanosheets[226]. The shear mixer consisted of a high-speed rotor and a stator (Figure 9A) where the rotor's blades spin at high speed, expelling the solvents into the surrounding space and resulting in high-speed fluid flows in the tight space between the stator and rotor. The fluid's velocity gradient generates an enormous shear force across the 2D material which separates the weakly bonded 2D nanosheets from the bulk material. Moreover, jet cavitation due to the high-

pressure difference and collision between the particles also facilitates the exfoliation of layered materials (Figure 9A).

The mechanics behind this process are of utmost importance, as the critical shear rate of the solvent plays a significant role in determining the quality of the exfoliated nanosheets. The critical shear rate ($\dot{\gamma}$) depends on several factors, including the fluid density (ρ) and viscosity (μ), the bulk particle's mechanical properties (length *L*, width *W*, Young's modulus *E*, bending rigidity *D*, the total number of layers *N*, flaw size *a*), interfacial adhesion energy between the sheets (Γ), and area of contact. The relation between the critical shear rate and the adhesion energy between the 2D sheets in bulk particles is shown in Equation 3.5.1[227].

$$\frac{\gamma \mu \dot{a} a^3}{D} \sim \left(\frac{\Gamma a^2}{D}\right)^{\xi} \tag{3.5.1}$$

It can be noted that an increase in flaw size will make the material weaker, and thus shear rate ($\dot{\gamma}$) must decrease with increasing flaw size (*a)* to preserve the material integrity. Conversely, any increase in adhesion energy must be matched with an increased shear rate to avoid agglomeration. For large aspect ratio particles suspended in a solution, it can be assumed that the particles are aligned with the fluid flow. The instantaneous equilibrium between the external work, the change in adhesion energy, and the change in bending energy for an inextensible sheet can be used to compute the critical value for exfoliation. The critical shear rate can thus be explained as a function of *a*, *D* and μ which takes the form[227]:

$$a^{-1/2}\sqrt{\mu \dot{\gamma} D} + \Gamma = 2\mu \dot{\gamma} a \tag{3.5.2}$$

And this equation can be rewritten in terms of the nondimensional shear rate and nondimensional adhesion energy[227]:

$$\frac{\Gamma a^2}{2D} = \frac{\gamma \mu \dot{a} a^3}{D} - \frac{1}{2}\sqrt{\frac{\gamma \mu \dot{a} a^3}{D}} \tag{3.5.3}$$

Botto et al.[227] reported that the bending rigidity of the of the 2D sheets have little contribution on the exfoliation efficiency for strongly stressed nanosheets so Equation 3.5.2 can be simplified as[227]:

$$\dot{\gamma} \approx \frac{\Gamma}{2\mu a} \tag{3.5.4}$$

For mildly stressed sheets, the contribution of bending rigidity is significant so the critical shear rate for peeling of one layer of 2D material from bulk crystal is expressed as Equation 3.5.5[227].

$$\frac{\gamma \mu \dot{a} a^3}{D} = \frac{\Gamma a^2}{2D}\left(1 + \frac{1}{4\left(\frac{\Gamma a^2}{D}\right)} + \frac{\sqrt{1+\frac{8\Gamma a^2}{D}}}{\frac{4\Gamma a^2}{D}}\right) \tag{3.5.5}$$

In a more recent paper, Botto's team used numerical solutions of the Stokes equations to predict a realistic hydrodynamic load distribution[228]. By combining the results with an analytical model, they proposed that the critical shear rate also depends on q_0, which characterizes the loading, and χ, which represents the ratio between crack length (a) and cohesion length ($\lambda^4 = 4D/k_e$), as given by $\chi = k_e a^4/4D$. The expression for the critical shear rate is thus[228]:

$$\frac{\gamma\dot{\mu}a^3}{D} = \frac{2\sqrt{2}}{q_0}\left(\frac{\Gamma a^2}{D}\right)^{1/2}\left(\frac{\chi}{1+\chi}\right)^{3/2} \tag{3.5.6}$$

Extending this mechanism of shear induced exfoliation, Paton et al.[229] demonstrated the production of few-layer graphene using microfluidizers. A pneumatic or hydraulic powered piston pumps fluid down a microchannel in a microfluidizer, producing considerable pressure at a very high fluid speed. This results in a high shear rate which is applied uniformly to the sample. Natural graphite was dispersed in deionized water containing surfactants (sodium cholate), and a pressure of 209 MPa was maintained in the microfluidizer. The final concentration reported was 0.31 g/L, which corresponds to a 3% yield, with the overall production rate reported to be 72 mg/hr. Most flakes were relatively thin (~10-12 layers) and a small percentage of flakes contained an average of 2 layers. Tran et al.[230] demonstrated shear exfoliation of graphene using Taylor-Couette flow, which consists of a viscous fluid confined in the gap of two rotating cylinders. In this case, the authors used an outer cylinder with a diameter of 57 mm and an inner cylinder with a diameter of 52 mm. The liquid in the 2.5 mm gap between the cylinders created enough shear force to exfoliate graphene with a reported yield of approximately 5%, and most of the flakes showed a thickness less than or equal to 3 nm. This technique was noted to induce few defects with the Raman $\Delta(I_D/I_G)$ of the exfoliated graphene reported as 0.14. However, one issue with rotary shear exfoliation is the lack of scalability and economic feasibility. As such, scalable techniques such as non-rotary shear and high-speed liquid flow through a narrow channel have become preferable and noted to generate a sufficient shear rate to exfoliate of graphene[200].

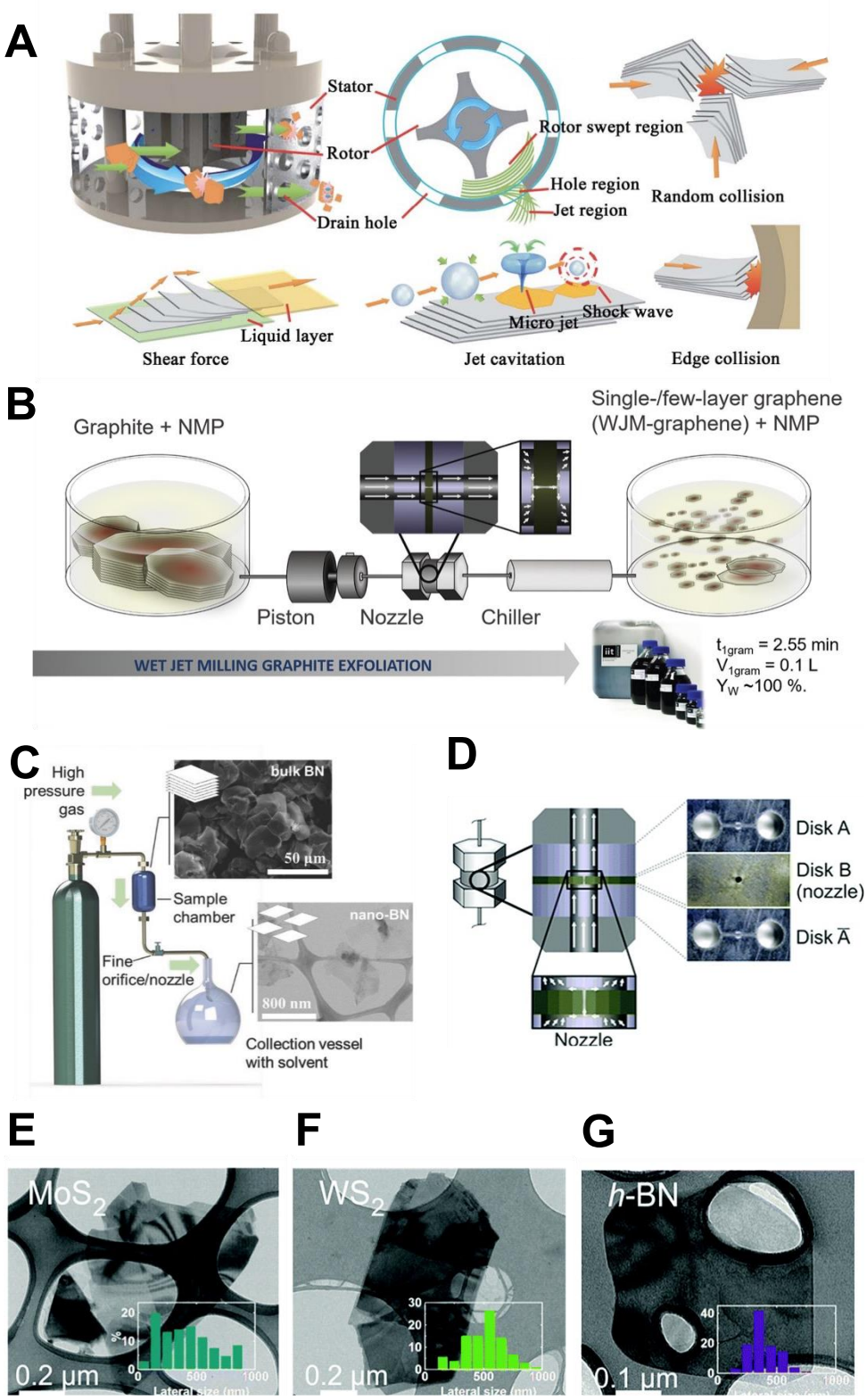

Figure 9. **Shear exfoliation mechanisms of 2D materials**. Shear exfoliation technique. A) Schematic of a high shear mixer and mechanisms facilitating exfoliation of layer materials in shear mixture[226]. B) Schematic of the compressible flow exfoliation (CFE) process[231]. C) Schematic representation of the exfoliation of few-layer graphene from bulk graphite using the wet jet milling method[123], D) Cross-section

of the shear processor nozzle[232], E-G) MoS_2, WS_2, and *h*BN produced by wet jet milling[232]. B) Reproduced with permission from *Advanced Materials*, Volume 30, Issue 30, 1800200 (2018). Copyright 2018 John Wiley & Sons, Inc. C) Reproduced with permission from *Advanced Functional Materials*, Volume 29, Issue 14, 1807659 (2019). Copyright 2019 John Wiley & Sons, Inc.

A recent technique in exfoliating layered materials using shear force has been demonstrated by Rizvi et al. using a compressible flow exfoliation (CFE) process (Figure 9B) [231]. This technique uses a high-pressure compressible gas rather than a liquid to produce a yield as high as 10%. A unique advantage also arises from decoupling the exfoliation step from the dispersion step by making the process solvent independent. Unlike ultrasonication, CFE introduces minimal defects in the exfoliated layered materials due to the rapid movement of the bulk material through ultrasonic shock waves (~0.2 seconds) in the gaseous medium compared to liquid-based shear exfoliation.

Other unconventional approaches have also been pursued in shear exfoliation; Varrla et al.[233] exfoliated graphene from graphite using only household detergent and a kitchen blender. Most of the exfoliated flakes were ten layers or less and had $\Delta(I_D/I_G)$ values from 0.2-0.5 with a process yield of 1%. The same approach was also applied to several exfoliated TMDs, including MoS_2 with a thickness of ~2-12 layers[204] and a concentration as high as ~0.5 mg/mL, corresponding to a yield of 1% from the bulk material and an optimized production rate of ~60 mg/hour. Gravity-based exfoliation was described by Yin et al.[234] for MoS_2 nanosheets which employed a combination of shear and collision forces generated in the gap between the stator and rotor of a shear homogenizer to produce the exfoliation. Almost 84% of the nanosheets were reported to be less than five layers thick, with 22% of the flakes as bilayers and ~40% of the flakes as trilayers. Another interesting approach was demonstrated by Chen et al. using a vortex fluidic device (VFD) to exfoliate graphene and BNNSs[235]. Exfoliation occurs in the thin film of the VFD, which contains a rapidly rotating 45° inclined glass tube. Due to the interplay between centrifugal force and gravitational force, efficient exfoliation occurs. They reported a yield of ~1% for graphene monolayer and ~5% for a monolayer of BNNSs. Large-scale production of luminescent quantum dots of exfoliated TMDs has also been reported using a high shear mixer[236] wherein the MoS_2 or WS_2 crystals were mixed with DMF, and homogenization of the mixture took place in a high shear mixer. After running the mixture for 1 hour at 5000 rpm, the dots formed from the bulk crystals with a lateral length of ~5 nm and a thickness of 3-5 layers.

Wet jet milling is another solution-based shear exfoliation technique (Figure 9 C&D) that has been reported in recent years as a scalable and continuous method to exfoliate few-layer 2D materials. Bellani et al.[123] reported a three-pass wet jet milling technique to produce 20 g/h single- or few-layer graphene for supercapacitor materials. This process uses a high pressurized (180-250 MPa) jet stream that is produced by a hydraulic piston to force the solvent and layered crystal mixture through perforated disks with 0.1-0.3 mm nozzle diameters[232]. This creates a high shear flow that homogenizes and exfoliates the layered materials by taking advantage of the fluid shear forces in the processor. Castillo et al. also reported a similar wet jet milling method to produce very thin (~1.5 nm) graphene dispersions. Almost half of the flakes produced were between 1.5 and 5 nm in thickness, and the production rate was reported to be 2.35 L/h[232]. Examples of low-defect 2D materials produced by wet-jet milling and CFE are shown in Figure 9 E-G[200,232].

One of the most common applications of shear exfoliation, as a rigorous solution-based technique that also effectively disperses the material within the matrix, is in the formation of cement composites with graphitic materials. Cement, the binder and predominant source of strength in concrete, forms an effective composite material by exfoliating graphene and its derivative materials into the matrix to improve the overall macroscopic properties. While concrete performs excellently in compression, it fails easily in tension or shear, where the high mechanical strength and specific surface area of graphene materials make them exceptional additives[237–239]. Typically, bulk quantities (kilograms) of graphite materials are required for cement-based composites[140,239,240], and shear exfoliation-based methods can produce large amounts of exfoliated 2D materials with high yields compared to other bottom-up methods. Additionally, shear exfoliation methods allow for combined exfoliation and mixing of cement composites and are less complicated and time-consuming than other synthesis methods.

The mixing of graphene-cement composites is principally conducted in two stages: (i) dispersion and exfoliation of graphene materials in water and (ii) mixing of graphene supernatant with dry cement and aggregates[239–243]. The effective dispersion and exfoliation of graphene derivatives are concurrent when preparing the supernatant and have been demonstrated to be highly effective through continuous high-speed shear mixing[240,244–246]. One challenge, however, is that pristine graphene is hydrophobic and challenging to disperse in water. This has resulted in the adoption of functionalized graphene such as GO, which is hydrophilic and highly dispersible in water for graphene-cement composites[240,243,247]. However, even with appropriate dispersion in water, the dispersion of graphene and its derivatives is challenging in a highly alkaline cement paste matrix saturated with ions such as Ca^{2+}, K^{+}, Na^{+}, and OH^{-} [246,248,249]. As such, shear mixing is often combined with chemical exfoliation by surfactants, particularly perchloroethylene (PCE), to prepare cement-based composites. PCE improves the dispersion and exfoliation of GO in an aqueous solution due to two major effects: (i) stronger hydrogen bonding and (ii) steric repulsion between GO and PCE[250]. The steric stabilization effect and self-agglomeration of GO-PCE suspensions are schematically presented in Figure 10A. The mixing sequence of graphene derivatives, surfactants, water, cement, and aggregate also plays a vital role in the exfoliation and dispersion of graphene derivatives in aqueous solutions. Figure 10B presents a series of GO dispersion in four mixing sequences (Samples 1-4) among PCE, cement, and GO in water from a study by Lu et al.[250].

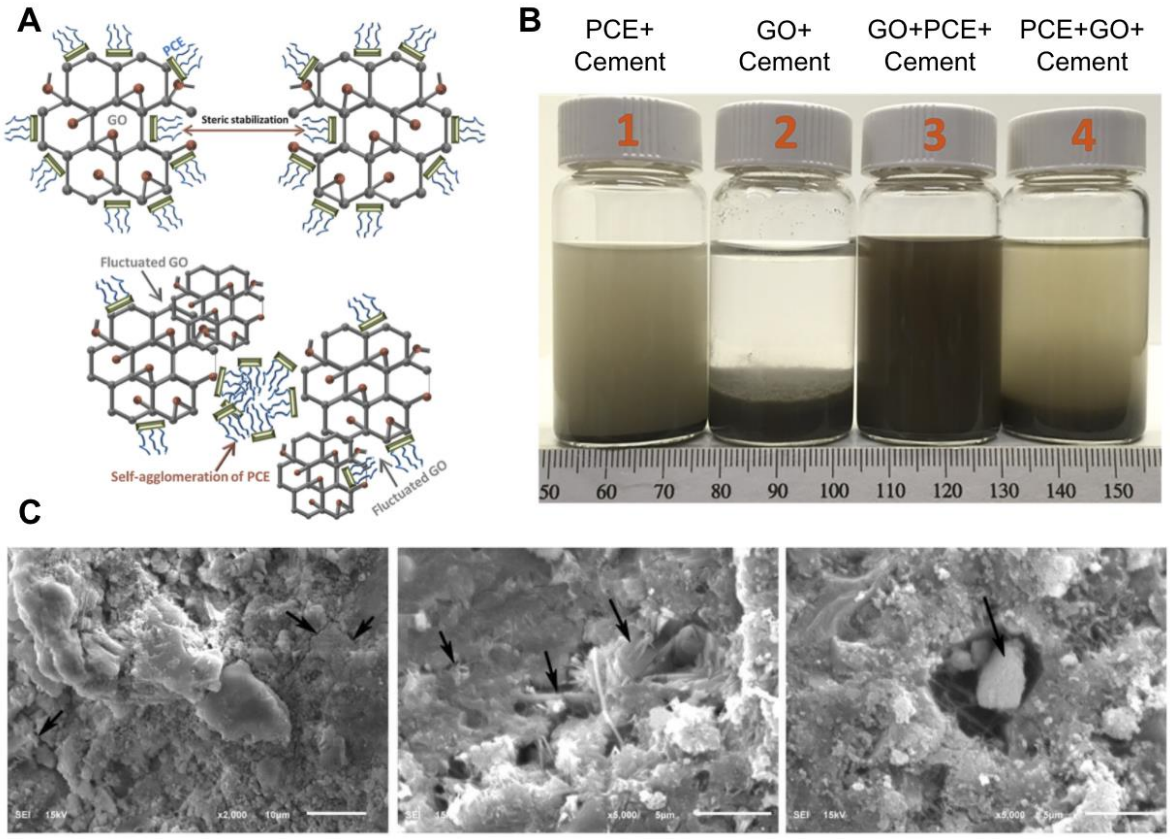

Figure 10. **Graphitic materials in reinforced cement composites.** A) Schematic of steric stabilization by PCE for GO dispersion in water and cementitious solution[250], B) GO, PCE, and cement three-phase suspensions with different mixing orders[250], C) SEM images of crack bridging and pore filling by GO in a GO-cement paste composite[247]. A&B) Reproduced with permission from ***Materials & Design,*** Volume 127, Pages 154-161 (2017). Copyrights 2017 Elsevier Ltd. C) Reproduced with permission from ***Composites Part B: Engineering,*** Volume 159, Pages 248-258 (2019). Copyrights 2019 Elsevier Ltd.

Exfoliated 2D materials can significantly improve the mechanical properties of cement in different loading modes by acting as high strength and stiffness aggregate particles in the mixture. For graphene derivatives, this enhancement occurs due to two primary mechanisms in cement-based composites: enhancing the mechanical properties by biphasic reinforcement and modifying the microstructural properties. For example, the oxygen-containing functional groups of GO facilitate its efficient dispersion during shear exfoliation, enhance cement hydration, and reinforce the composite microstructure, which demonstrate increases in the compressive and flexural strength by 28% and 80%[240] or 21% and 26%[251] in two different studies compared to the standard cement mix. Exfoliated graphene materials also considerably modify the microstructural properties in the composite by influencing the exothermic reaction between cement and water during the cement hydration process, which alters the composite microstructure at the nano- and microscales[240]. Three typical examples of GO-cement composite microstructures are presented in Figure 10C[247]. The exfoliated 2D planes of GO and the different functional groups, such as carboxylic acid groups, encourage the precipitation of $CaOH_2$ and C-S-H gel and bond with those hydration products within the cement composite matrix[252–256]. These factors effectively reinforce the cement-based composite matrix and fill pores, densifying the microstructure. Indeed, MD simulations have

shown that GO acts as a nucleation site for C-S-H gel hydration, thanks to H-bond formation between OH groups and water molecules, producing a hydrophilic interface[257,258]. They also pointed out that strengthening in these composites happens mainly by H-bonds and covalent-ionic bonds (O-Ca-O or O-Al-O) involving OH groups[258].

Shear exfoliation is a truly continuous process where the constant flow of material through the rotor or nozzle can produce bulk quantities of material in a liquid solution, making it an ideal synthesis method for applications requiring significant amounts of material when specific defect concentrations and monolayer precision are not required. Several different techniques can be used to produce continuous shear forces within the supernatant solution, including compressible flow exfoliation and wet-jet milling. As shear exfoliation provides a scalable, facile, and concurrent method for synthesizing 2D material in a liquid medium, cement composites are quickly produced in a two-step process, enhancing the dispersion, mixing, and curing processes. As the most used material globally, cement reinforcement and enhancement are of utmost concern for structural applications, and cement-2D material composites have demonstrated vastly enhanced structural properties.

3.6 Electrochemical Exfoliation

Electrochemical exfoliation is a scalable method capable of producing a large quantity of 2D nanosheets in a liquid solution (electrolyte) using an electrical current either by cathodic reduction or anodic oxidation. The electrical current introduces ions within the electrolyte that are attracted to the bulk 2D material and intercalate between layers. This intercalation thereby weakens van der Waals bonds and separates layers through a one-step rate-controlled exfoliation process. Electrochemical exfoliation methods are relatively simple to design, assemble, and operate under ambient conditions. In 2014, Liu *et al.* first demonstrated a mechanism for anodic exfoliation of MoS_2 in an aqueous Na_2SO_4 solution[259]. The $\dot{OH}$ and $\dot{O}$ radicals are created by oxidation of water or SO_4 anions and intercalate into MoS_2 layers when a positive voltage is applied to the bulk MoS_2 electrodes (Figure 11A). As a result of the oxidation of the radicals and anions, O_2 and/or SO_2 gas is produced, which considerably extends the interlayer distance of MoS_2 and accumulates enough to separate MoS_2 flakes from the bulk MoS_2 crystals. However, because the electrooxidation reaction takes place on the surface of the bulk material electrode, the products are oxidized quickly, which affects the quality and degree of the exfoliated MoS_2.

Parvez et al.[260] demonstrated efficient electrochemical exfoliation of graphite using ammonium sulfate ($(NH_4)_2SO_4$), sodium sulfate (Na_2SO_4), and potassium sulfate (K_2SO_4). They reported that ~85% of the exfoliated nanosheets were less than or three layers thick. The suggested mechanism of exfoliation for this system was as follows: Applying a bias voltage results in a reduction of water at the cathode, creating hydroxyl ions (OH^-) that act as a strong nucleophile in the electrolyte. The nucleophilic attack of graphite by OH^- ions initially occurs at the edge sites and grain boundaries, which leads to depolarization and expansion of the graphite layers, thereby facilitating the intercalation of sulfate ions (SO_4^{2-}) within the graphitic layers. During this stage, water molecules may also intercalate with the SO_4^{2-} anions. Reduction of SO_4^{2-} anions and self-oxidation of water produce gaseous species such as SO_2 and O_2, as evidenced by the vigorous gas evolution during the electrochemical process, which separates the 2D layers. There have also been

numerous other reports on the electrochemical exfoliation of graphene using ions of H_2SO_4, Bu_4NBF, and other electrolytes with good yields[121,261–266].

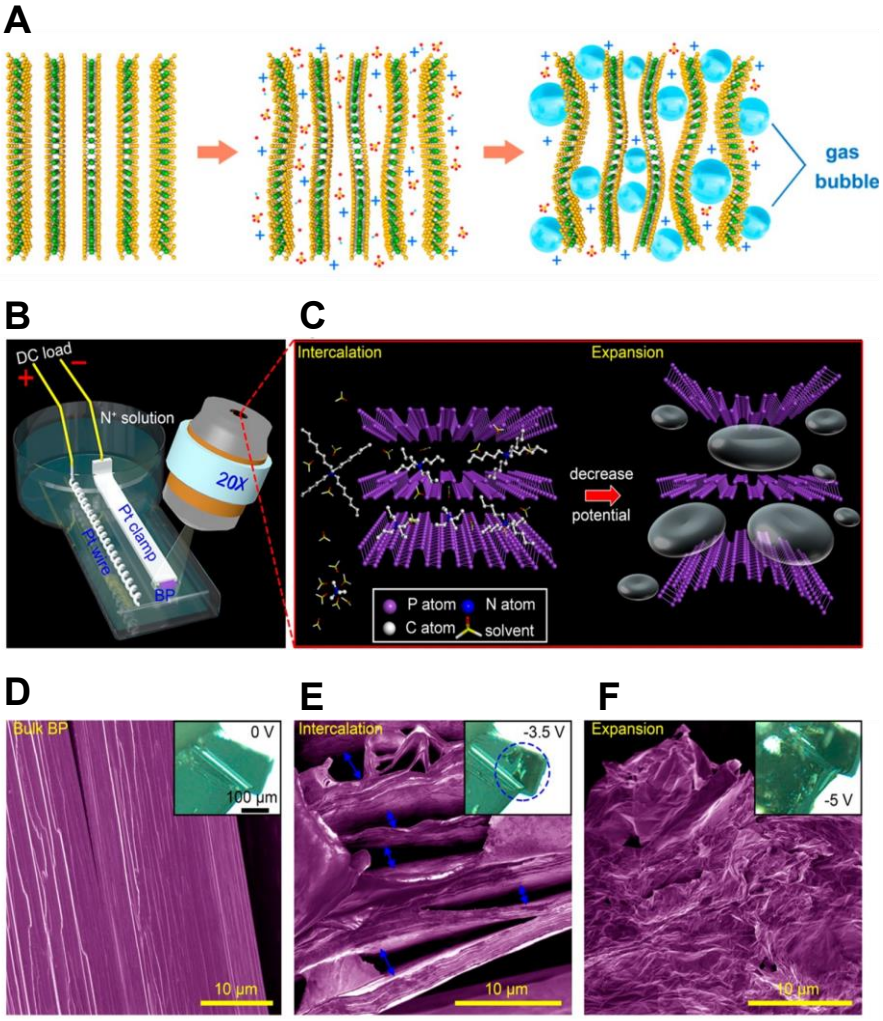

Figure 11. A) Schematic illustration of ion intercalation and exfoliation of 2D sheets in the electrochemical method[259]. B) Schematic of a micro electrochemical cell under a microscope, C) Illustration of intercalation and expansion of a black phosphorous cathode in organic DMSO electrolyte, D) False color SEM image of black phosphorous before expansion, E) after applying a voltage of -3.5 V (double arrow shows expansion gap) and F) -5V[267]. B-F) Reproduced with permission from ***Chem. Mater.*** 2018, 30, 8, 2742–2749. Copyright 2018 Royal Society of Chemistry

Unlike other exfoliation strategies, no analytical models exist of the electrochemical process as a whole. However, the physical and chemical mechanisms at play during the process are known to some degree and the general process can be broken down into three main steps: (i) electrochemical generation of ions in the electrolyte, (ii) interlayer diffusion and intercalation of these ions in the bulk material, and (iii) electrochemical reaction turning the ions into gases within the material, thus separating the layers.

Steps i and iii are electrochemical reactions, and therefore their thermodynamics follows the Nerst equation[268]. Considering a simple reduction reaction $Ox + ze^- \rightarrow Red$, the half-cell reduction

potential (E_{red}), taking as a reference the standard potential (E^0_{red}), can be computed from the universal gas constant (R), the temperature (T), the number of electrons transferred (z), the Faraday constant (F), and the chemical activity of the involved species (a), as shown in Equation 3.6.1, where activity is generally replaced by concentration. The same can be written for an oxidation process, as well as the full cell. Although the effective potentials can be altered by surface effects such as electrocatalysis at the electrode, this modeling can provide estimates for the necessary potential to induce the reduction or oxidation of specific species, as well as to point out any parallel electrochemical reactions that might happen[268].

$$E_{red} = E^0_{red} - \frac{RT}{zF} \ln \frac{a_{Red}}{a_{Ox}} \tag{3.6.1}$$

The kinetics of these electrochemical reactions can be modeled with the Butler-Volmer equation[269]. The electrode current density (j) depends on the exchange current density (j_0), the cathodic and anodic charge transfer coefficients (α), the activation overpotential ($\eta = E - E_{eq}$), and other previously mentioned variables, as shown in Equation 3.6.2. It allows the prediction of the expected current for a given applied potential, or vice-versa, depending on which variable is being controlled. As the current defines the speed of exfoliation, while the potential constrains the electrochemical reactions taking place, being able to predict both can help optimize the synthesis of 2D materials[269].

$$\frac{j}{j_0} = \exp\left[\frac{\alpha_{an} z F \eta}{RT}\right] - \exp\left[\frac{\alpha_{cat} z F \eta}{RT}\right] \tag{3.6.2}$$

Step ii, in its turn, is a process of interlayer diffusion, and its nature depends on the interlayer distance and the ion. For large enough distances, the process can be treated as free diffusion, while for short distances it is a case of Knudsen diffusion, since it happens in a length that is comparable to the mean free path of the particles[270]. The mechanism may vary from system to system, considering that ionic intercalation may be facilitated by modification of layer edges, leading to some degree of separation before formation of gas[268].

In the case of Knudsen diffusion of a species A, the self-diffusion coefficient (D_{AA}) depends on the path length (λ) and the molar mass of the species (M_A), as shown in Equation 3.6.3[270]. This model can estimate diffusibility of ions between layers, although the effective rate of mass transport can be modified by surface effects such as adsorption[270].

$$D_{AA} = \frac{\lambda}{3} \sqrt{\frac{8RT}{\pi M_A}} \tag{3.6.3}$$

Comparing the rate of electrochemical reactions with the rate of interlayer diffusion may help optimize the exfoliation process, as the goal is to produce gas between the layers of the bulk material, not at its surface, as well as to avoid exaggerated voltages and currents that damage the 2D material. However, to our knowledge no unified mathematical approach has been made in that sense.

Similarly, to other fluid-phase strategies, electrochemical exfoliation can be studied with DFT and MD simulations by estimating the energetic changes of the material due to intercalation with other

species (in this case, ions). For instance, DFT calculations showed that sulfate anions are the most efficient for graphene production, demonstrating a mechanism in which their intercalation causes a higher repulsive binding energy between layers (Figure 12A)[271]. Lee et al.[272] performed MD simulations of graphite in different electrolytes that are relevant for battery applications, where exfoliation is not wanted. They unveiled a sliding displacement mechanism for exfoliation and estimated which solvent provides higher and lower energy barriers (Figure 12B). FEM has also been used to investigate electrochemical exfoliation. Muhsan et al.[273] studied the continuum diffusion of sulfate anions within graphite, estimating that the resulting stresses on the graphene layers are high enough to break van der Waals bonds (Figure 12C), and Si et al.[274] used a cohesive zone model to study the bending and delamination of MoS_2 (Figure 12D).

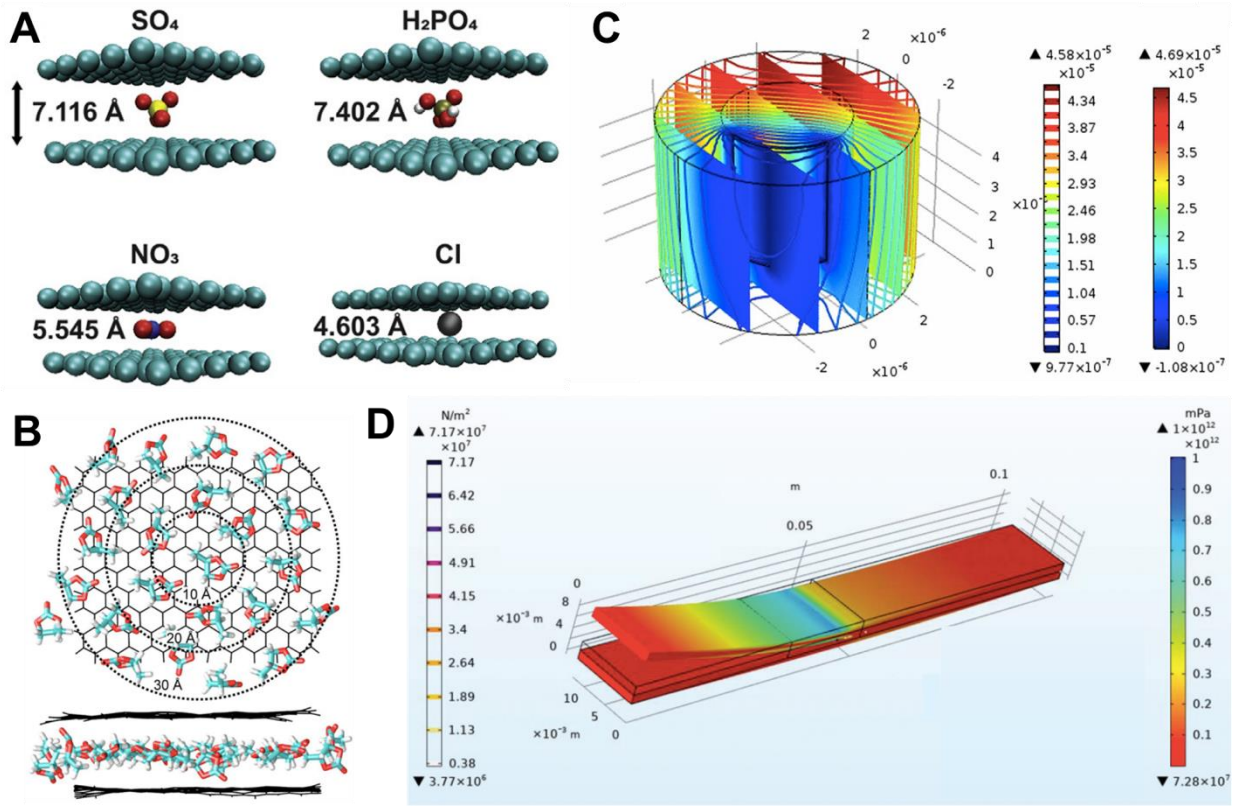

Figure 12. Simulation methods for investigating electrochemical exfoliation. A) DFT-calculated interlayer distances and binding energies for different ion-graphene structures[271]. B) MD snapshot of solvent-intercalated graphene[272]. C) Continuum diffusion simulation of the concentration of sulfate anions within graphite electrode[273]. D) Von Mises stress distribution computed with FEM during exfoliation of nanosheets[274]. A) Reproduced with permission from ***Carbon,*** Volume 167, 2020, Pages 816-825. Copyrights 2020 Elsevier Ltd. B) Reproduced with permission from ***Phys. Chem. C*** 2015, 119, 33, 19415–19422. Copyright 2015 American Chemical Society.

The oxidation of 2D materials during the electrochemical process results in altered materials that can be unsuitable for certain applications, so efforts have been directed toward nonoxidative exfoliation. For example, Cooper et al.[275] reported a nonoxidative exfoliation approach of graphite via the intercalation of tetraalkylammonium cations into pristine graphite. Na^+/dimethyl sulfoxide complexes were used as intercalation agents in a graphite cathode[276] producing exfoliated

graphene flakes of 3.1 nm thickness on average (~7 layers). The resulting film fabricated from exfoliated graphene showed a high electrical conductivity of 380 Sm^{-1}. Many other 2D materials have also been electrochemically exfoliated, including a wide range of TMDs from MoS_2 to WS_2, TiS_2, TaS_2, ZrS_2, $MoTe_2$, $NbSe_2$, and Bi_2Te_3[277,278]. Li et al.[267] demonstrated ultrafast cathodic exfoliation of phosphorene with a reported yield of ~80% (Figure 11B-F). Phosphorene nanoparticles have also recently been reported to be exfoliated using bipolar electrodes[279]. A series of back-gated FETs were fabricated from few-layer black phosphorous synthesized by cathodic exfoliation which demonstrated high mean hole mobility up to ~100 $cm^2 V^{-1} s^{-1}$ with a high on/off ratio (~10^4 on average). Similarly, Liu et al.[280] exfoliated 5-50 µm lateral sized MoS_2 in a Na_2SO_4 electrolyte to produce a back-gated FET of exfoliated MoS_2 nanosheets exhibiting carrier mobility of 1.2 $cm^2 V^{-1} s^{-1}$ and a very high on/off ratio (~10^6).

Unlike mechanical exfoliation processes, one can control the number of exfoliated layers using the electrochemical approach. Huang et al.[281] demonstrated the exfoliation of few-layer phosphorene using the cationic intercalation method and manipulated the layer number by changing the applied potential to the electrode. A negative potential of -2.1 V was required to initiate the intercalation of cations into the bulk BP. When a negative potential of -5 V was applied, the exfoliated flakes were ~0.8 nm (~2-3 layers) thick, while changing the applied potential to -10 V and -15 V led to increasing thicknesses of 2.5-3.7 nm and 2.9-3.3 nm thick flakes, respectively. Similarly, controlled exfoliation of graphene by regulating the intercalating potential was reported by Murat et al.[282] where increasing the intercalating potential led to larger and thinner graphene sheets. Although exfoliation using DC power is the most popular input for electrochemical exfoliation of layered materials, there have also been reports using AC currents. Yang et al.[283] reported exfoliating high-quality graphene nanosheets (~1-3 layer) with a high yield (~75%) by AC applied potential. A moderate potential of ±10 V was applied, and the current frequencies varied from 0.05 Hz to 0.25 Hz. The best quality graphene (I_D/I_G=0.15) was obtained when the potential was ±12 V at frequency = 0.1 Hz, and the lateral size of the flakes varied from 1 to 5 µm.

The inherent size, exceptional electrical properties, and mechanical robustness exhibited by exfoliated 2D materials make them premium candidates for integration with energy storage applications. Specifically, the ability to synthesize 2D materials with relatively high yield, extremely high surface area-to-volume ratio, and control over the number of layers make electrochemically exfoliated 2D materials highly favorable for use in energy storage and discharge. In particular, supercapacitors and high-efficiency batteries have demonstrated considerable performance improvements compared to conventional storage devices when prepared using exfoliated 2D materials.

Supercapacitors, also called ultracapacitors, are a type of electronic energy storage device typically characterized capacitance values several orders of magnitude higher than conventional electrolytic capacitors. Conventional capacitors comprise two layers of conductive materials separated by a dielectric medium. In supercapacitors, high capacitance is achieved through increased surface area conductive electrodes coated with a porous material, typically activated carbon, immersed in electrolyte solution[284] and are capable of storing >100 times the energy per unit volume as electrolytic capacitors at high current for short durations[285]. 2D materials are ideal for integration into supercapacitors as the electrode material on either side of a conducting spacer (Figure 13A). Supercapacitors based on exfoliated 2D materials have demonstrated extremely high power

densities and long capacitance retention lifecycles which can be attributed to the high surface area-to-volume ratio and electrical conductivity they exhibit[33]. The fabrication of 2D material-based supercapacitors requires scalability, high crystallinity for low sheet resistance[286], and ease of processability for transferring and forming 2D materials as electrode materials (Figure 13B)[287]. Electrochemical exfoliation offers advantages, as it is a scalable production method capable of producing highly crystalline and solution-processable 2D materials at a competitive production cost[35,288,289]. Additionally, two other notable benefits of 2D materials are their inherent size and flexibility, which makes them suitable for developing micro-supercapacitors, and flexible supercapacitors.

Some of the most notable examples of supercapacitors produced by the exfoliation of 2D materials take advantage of tuning material properties, such as phase and thickness, during the exfoliation process to produce high specific capacitances from various materials. For example, monolayer *1T* MoS_2 produced by chemical exfoliation exhibits a two-order of magnitude increase in specific capacitance compared to bulk MoS_2 (366.9 F g^{-1} compared to 3.15 F g^{-1} for bulk *2H* MoS_2[290]). Additionally, Acerce et al.[291] prepared supercapacitor electrodes of exfoliated *1T* MoS_2 by performing ion intercalation (H^+, Li^+, Na^+, and K^+) during the electrochemical exfoliation process to control the phase and reported specific capacitance values in the range of ∼400 to ∼700 F g^{-1} with retention greater than 93% over 5000 cycles. Similarly, Khanra et al.[292] modified graphene during electrochemical exfoliation using 9-anthracene carboxylate ions (ACA) as the electrolyte solution. ACA-functionalized graphene sheets were used to prepare an electrode that demonstrated a specific capacitance of 577 F g^{-1} with 83% retention after 1000 cycles.

In addition to this functionalization, exfoliation of 2D materials in a solution can also offer opportunities for scalable production; Liu et al.[293] developed an inkjet-printable solution by electrochemical exfoliation of graphene with an electrochemically active polymer and used a commercial printer to produce flexible micro-supercapacitors with an areal capacitance of 5.4 mF cm^{-2} and capacitance retention of 98.5% after 1000 bending cycles at a radius of 5 mm. These micro-supercapacitors can be connected in arrays of several hundred units to reliably charge and deliver 12 V across repeated charging (Figure 13 C-E). However, the capacitances reported for 2D material-based supercapacitors remain relatively low compared to their theoretical maximums. For example, graphene has a theoretical capacitance of 550 F g^{-1} but typical pure graphene supercapacitors exhibit values of ∼200 F g^{-1} which corresponds to less than half of what is expected theoretically[294]. This is due to inherent imperfections during synthesis, characterization, and device development[295] so improving the electrochemical performance of 2D materials to deliver supercapacitors with even higher energy and power density and cycle life remains an ongoing area of critical focus.

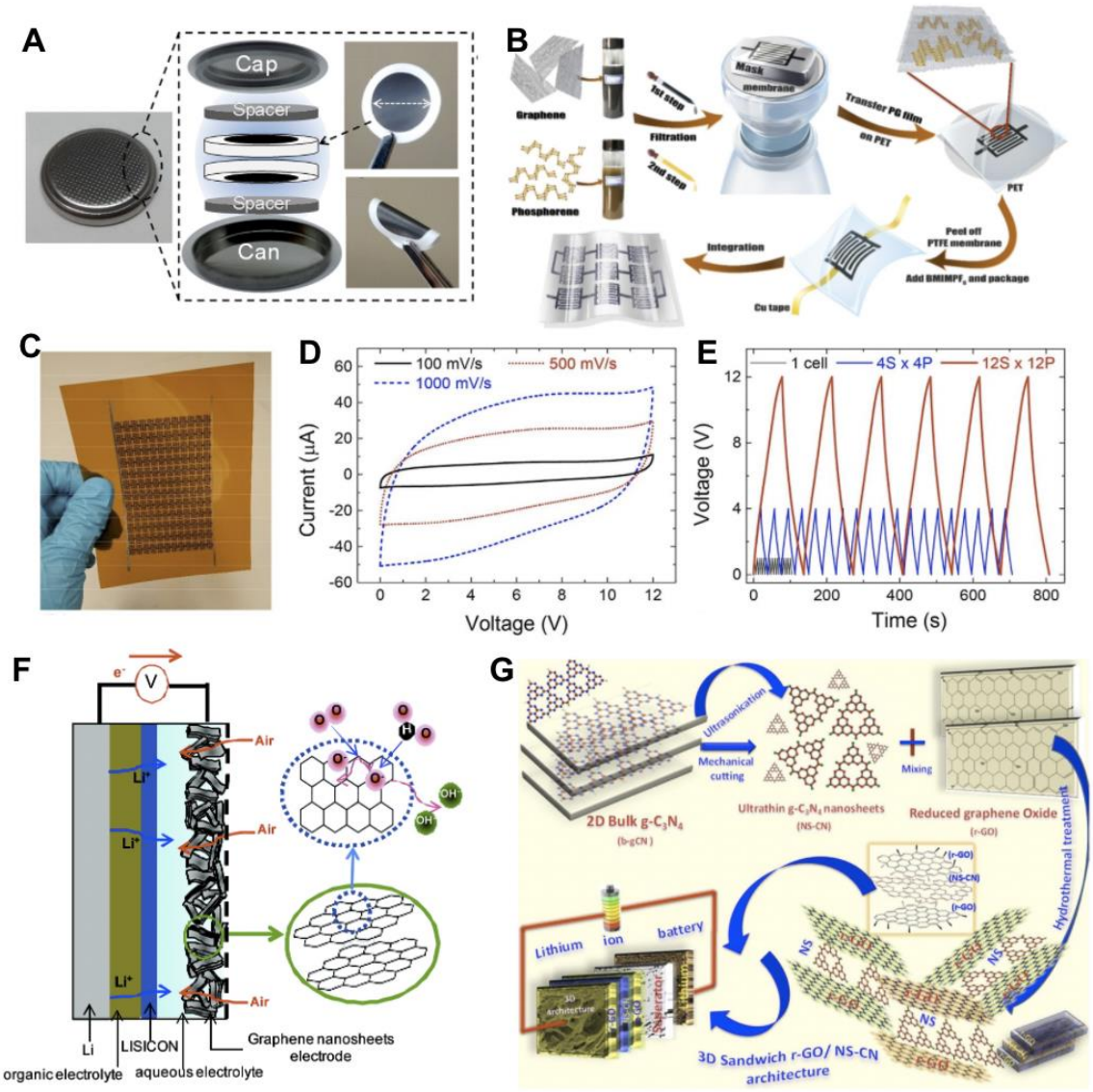

Figure 13. Energy storage and discharge with exfoliated 2D materials. A) Photograph of assembled symmetrical coin cell (CR2032). Exploded view schematically shows the internal construction. Stainless steel spacers are inserted to ensure good electrical contact directly between the active material and the outer electrode. The PVDF membranes themselves act as ion transporting spacers[296]. B) Mask-assisted fabrication of micro-supercapacitors through 2D material inks of graphene and phosphorene in sequence[287]. C-E) Large-scale integration of fully printed MSCs on Kapton [297] {C) Photographs of a 12S × 12P MSC array on Kapton. D) CV profiles of the 12S × 12P MSC array at different scan rates with a voltage window of 12 V. E) GCD curves of the MSC array at a current of 10 μA}. F) Structure of a graphene nanosheet electrode for a high-efficiency LIB[298] G) Workflow schematic of ultrasonication for the production of r-GO/CN composite LIBs[299]. A) Reproduced with permission from ***ACS Appl. Mater. Interfaces*** 2015, 7, 31, 17388–17398. Copyright 2015 American Chemical Society. B) Reproduced with permission from ***ACS Nano*** 2017, 11, 7, 7284–7292. Copyright 2017 American Chemical Society. C-E) Reproduced with permission from ***ACS Nano*** 2017, 11, 8, 8249–8256. Copyright 2017 American Chemical Society. F) Reproduced with permission ***ACS Nano*** 2011, 5, 4, 3020–3026. Copyright 2011 American Chemical Society. G) Reproduced with permission from ***Electrochimica Act*** 2017, Volume 237, Pages 69-77. Copyright 2017 Elsevier Ltd.

Another application of interest for 2D materials within energy storage is high-efficiency batteries which are characterized by high energy density and significant energy retention rates after repeated cycling. Lithium-ion batteries (LIBs) are the most common energy storage device available and induce current between the anode, typically a porous carbon, and cathode, typically a metal oxide, through an electrolyte. Due to their excellent electrochemical performance, high surface area, and stable chemical structure, exfoliated 2D materials have been successfully used as electrode materials, both for the cathode and anode, to develop high-efficiency batteries[300]. The highly crystalline and thin structure of exfoliated 2D materials allows for efficient and reversible conversion reactions with electrolyte ions such as Li^+ as both sides of the 2D material sheet are accessible to ions, leading to enhanced storage capabilities (Figure 13F)[298]. As such, many of the experimental values for 2D material systems are orders of magnitude greater than standard battery materials. Electrochemical exfoliation offers advantages in the synthesis of 2D materials for high-efficiency batteries including that they are solution-processable[35,301], which is common practice in scalable LIB manufacturing[302], and inexpensive compared to bottom-up methods such as CVD[35]. Additionally, sonication-assisted liquid exfoliation is highly suitable for producing 2D material-based LIB electrodes because it can provide high yield and processability[303]. An example of the workflow by ultrasonication for the exfoliation of C_3N_4 and reduced-GO LIBs is shown in Figure 13G[299].

The production of high-efficiency LIBs has been demonstrated for a wide variety of 2D materials to produce remarkably high specific capacities. For example, Lian et al.[304] produced electrothermally exfoliated few-layer graphene anodes with specific capacities as high as 936 mAh g^{-1} and 91% capacity retention after 40 cycles. This high performance was attributed to the high specific surface area resulting from the porous, defective, and few-layer structures that are produced by electrothermal exfoliation. Beyond graphene, many other electrochemically exfoliated 2D materials show significant promise as electrode materials, with recent examples including MoS_2[305], covalent organic frameworks[306], MoS_2/WS_2[307], and V_2O_5[308], GeS[309], and TiO[310] exfoliated nanosheets. In combination with electrochemical exfoliation, ultrasonication can enhance yield and production of 2D materials for electrode development. For example, MoS_2/polyethylene oxide (PEO) composite anodes were prepared by Xiao et al.[311] through hydrolysis and ultrasonication, which achieved discharge capabilities above 1000 mAh g^{-1}, significantly higher than conventional LIB capacities which are limited to a theoretical maximum of ~370 mAh g^{-1} [312]. The high capacity achieved with the addition of 5% PEO was attributed to the increasing MoS_2 interlayer spacing by PEO intercalation during exfoliation, thereby increasing lithium-ion transfer compared to conventional exfoliated or CVD-grown MoS_2. The interlayer spacing of MoS_2 has also been enhanced through a process in which MoS_2 was exfoliated through a combination of a chemical and thermal process, then annealed to form a multilayer hybridized structure containing mesoporous carbon. This structure benefits from the synergy of the two phases to produce a specific capacity of 1113 mAh g^{-1} with 92% retention over 500 cycles[313]. DFT calculations attributed this enhancement to the efficient Li^+ intercalation at the interface. However, it should be noted that issues remain with the adoption of 2D materials as electrodes, including the structural reliability of these ultrathin materials[314]. Despite these challenges, their demonstrated potential makes them ideal candidates for future energy storage devices.

Electrochemical exfoliation is the most controllable technique, which allows for precise tuning of the desired 2D material properties based on the applied voltage during electrochemical exfoliation. This synthesis technique uniquely suits applications requiring low throughput but high thickness control, such as energy storage applications. Additionally, the intercalation of ions during electrochemical exfoliation increases the interlayer thickness, making 2D materials produced by this method well suited for energy storage devices.

The five exfoliation techniques covered in the prior sections represent the most prominent methods for exfoliating 2D materials. Examples of 2D materials exfoliated by these methods, as well as the prominent advantages and disadvantages of each technique are summarized in Table 1 below.

Table 1. Summary of Exfoliation Techniques

Technique	**Materials & Sizes**	**Advantages**	**Disadvantages**
Micro-Mechanical Cleavage	<u>Materials</u> Graphene[1,41,315]; *h*BN[56,97]; MoS_2[316]; WS_2[101]; WSe_2[100] <u>Sheet Sizes</u> Few-layer to cm thick[41,317] 10-100 nm graphite crystallites[318] Between a few and ten atomic layers[97] Micron lateral dimensions on the HOPG surface[315] Atomically thin boron nitride (BN) nanosheets[56]	- Simple and low-cost exfoliation technique[41,317] - High-quality single-crystalline mono- and few-layer BN nanosheets[56] - Strong conductance modulation[318] - Integrating with etching, any desired shape is achievable through controlled etching time and other parameters[315] - The quality of the electron transport properties in the sample does not degraded after micromechanical extraction from the bulk[318]	- Small scale production, no method for large-scale continuous monolayers[1,41,319] - Not an easy process for BNNS[56] - Difficult to control flake lateral size and thickness[320] - Adhesive may leave residues[321] - The exfoliation efficiency depends on the interfacial adhesion between the substrate and 2D materials[96]
Ball Milling	<u>Materials</u> Graphene [123] *h*BN[126,128,322–324] Sandwiched MoS2/reduced graphene oxide (rGO) [125] Layer-by-layered SnS_2/graphene (LL-SnS2/G) hybrid nanosheets[124] MoS_2[121,122] <u>Layer Size</u>	- Highly scalable[121,122,124,119,123,126] -Capable of producing high quality boron nitride (BN) nanosheets in high yield and efficiency[126,128] - High (~98%) yield[323] - Thermostable highly concentrated suspension (90 mg/mL) of *h*BN[322] - β-cyclodextrin assisted ball milling produces BNNS what are covalently grafted with hydroxyl and well dispersed in water and other solvents[324] - Under low-energy milling, nanosheets experience tearing rather than vertical impact	- Very difficult to get high yield of monolayer[119,130] - In high-energy ball milling, strong collisions or vertical impacts can fracture particles and destroy crystallinity[126] - Other chemical species can remain on the 2D nanosheets which compromises the pristine nature of the nanosheets[324] - Optimization of parameters are required for higher efficiency and production yield. Milling parameters including milling

	0.5–1.5 micrometer in diameter and a few nanometers thick [126, 127] Few-layered nanosheets with reduced size[125] *h*BN nanosheets were 0.5 to 2.3 nm thick (1 to 5 layers) [128, 322,323] One to few-layer thickness [121,122]	resulting in no major destructions of the crystal structure[126] - Relative high crystallinity and chemical purity[127] - Milling agent reduces ball impacts and milling contamination[126] - High yield and dispersibility[119] - Applicable to any layered materials for producing nanosheets[126]	speed, ball-to-powder ratio, milling ball size and milling agent[127]
Ultrasonication	<u>Materials</u> Graphene [163,164,172,178,325–327] *h*BN [146,163,328,329] MoS_2, $MoSe_2$, $MoTe_2$, TaS_2,$TaSe_2$, $NiTe_2$, $NbSe_2$, Bi_2Te_3[163] WS_2[330–332] <u>Sheet Size</u> Few nm to hundreds μm laterally and mono-to few-layer nanosheets[163] Average thickness of exfoliated *h*BN were ~3 nm (10 layers)[329] A few μm lateral dimension and 5 layer thickness[164] The lateral size in the range of 0.5–2 μm[326] Few-layer flakes had lateral dimensions of ~1 μm[178] Average flake thickness was 2.9 nm (~8 layers)[328]	- Versatile and up scalable[163,164,172,178,325–327] - Low-cost[326] -Exfoliated BNNS are readily dispersible in number of organic solvents[329] - Low defect concentration and high-quality graphene flakes[164, 172, 178] - Potential to deposit graphene in a variety of environments and on different substrates not available using other methods[327] - Simplicity, easily achievable using equipment available in all chemistry lab, not influenced by air or water[327] - Graphene dispersion is stable for more than 6 months[326] - 72.5% yield was reported[328]	- Further research needed for controlling the distribution of flake thickness and lateral size[178,327] - Uncontrollable in the number of layers[327] - Relatively low yield of single-layer graphene sheets[326] - Requires long lasting sonication treatments[331] - Possibility of having chemical residues from organic solvents on the flakes[333] - Irregularities in lateral flake size[334] - Energy required to exfoliate graphene is balanced by the solvent–graphene interaction for solvents whose surface energies match that of graphene[164,325] - Solvents degrade if long-time sonication or high-intensity of sonication[326] - Presence of residual surfactant in films may obstruct electrical properties[178]

Shear Exfoliation	<u>Materials</u> Graphene [200,230,233–235] *h*BN[200,235,335,336] MoS_2[200,235] WS_2 [236,337] Phosphorene[338] <u>Layer Size:</u> Mono and few layer graphene (0.3 to 15 nm thick) with lateral sizes from 500 nm to 1.5 µm[200, 230] 54% of graphene flakes were folded; lateral size of the flakes were 200-1000 nm and thickness were 0.3-5.4 nm[233] *h*BN average flake thickness was 10 nm[336] and 2 nm (7 layers)[335] Lateral size of the exfoliated MoS_2 flakes were 50 to 750 nm and the flakes were 1 to 10 layers thick[234]	- A mature, scalable and widely accessible technology[200] - Exfoliated flakes can be unoxidized and free of basal-plane defects[200,229,230] - The production of high-quality graphene at a higher yield than a process using sonication[230] - A higher range of production volume, from hundreds of milliliters up to hundreds of liters and beyond[200,233] - Concentration decays very weakly as the volume was increased resulting in a production rate that increased with volume, which is critical for scale-up[233] - Tunable 'soft energy' source is required compared to ball milling and high shear sonication[235] - The maximum production rate is much higher than for standard sonication-based exfoliation methods[233] - Sophisticated surfactants are not required to stabilize the exfoliated graphene[233]	- Requires a minimum (threshold) shear rate to be applied[200,233] - Several assistance mechanisms are required to help this process. i.e. Taylor–Couette flow[230], Turbulence-assisted[233], Vortex fluidic exfoliation[235], temperature assistance[236], these additional steps add complexity into the process. - This process is not ideal to obtain high volume of monolayers[22,200,229,231] -Exfoliated nanosheets are quite small in lateral size compared to mechanical cleavage[204,338,339] -Surfactants are often used to stabilize the dispersion of 2D materials into solution which can leave its residue on the 2D sheets[204,340] - Sometimes, organic solvents like NMP and DMF are used in the exfoliation process. These organic solvents are very hard to wash off after the exfoliation process. As a result, organic residues may be present on the 2D sheets[230]
Electrochemical	<u>Materials</u> MoS_2[277,280] Graphene[121,260,262–266,275,276] Phosphorene[267,281] Black Phosphorus Nanoparticles[279] WS_2,TiS_2, TaS_2, ZrS_2[278] Arsene[341] Sb_2Te_3[342] ReS_2[343]	- This process is capable to mass produce 2D materials[263,277] - Graphene produced by this method have acceptable quality[261,275] - Excellent conductivity (graphene sheet resistance is ~210 ohm/sq)[264] - High efficient large-scale synthesis of graphene [263,266] with low defect content (I_D/I_G below 0.1)[261,263,266,276]	- The exfoliation process is complicated[277] - Additional sonication is needed if HOPG is used for graphene exfoliation causing dispersion[275] - Additional steps, i.e. organic radical-assistance, are required for controlling defect formation[261] - Wide distribution of thickness in exfoliated layered materials[265,275,279]

	NbS_2[344] <u>Layer Size</u> Monolayer or a few layer Nanosheet with lateral size up to 20 μm[277] Monolayer[263,275] or a few layer graphene sheets[263,275,276] Few layer phosphorene[267] Black phosphorus NP of 40-200 nm[279] Large graphene sheets of 5-30 μm can be produced[261, 264] Few-layer MoS_2 nanosheets with a lateral size of 50 μm[280]	- Preserve the intrinsic structure for both graphene [264] and MoS_2 [277,280] - Single stage method[264,275] - No requirement for ultrasonication or secondary processing if a solvent based route is used[275] - Efficient graphene is produced when combined with shear exfoliation[266] - Combined with electrochemical functionalization, electrochemical exfoliation can lead to potential composite design at large scale [266] - Ultrafast expansion of high-yield Black Phosphorus due to cathodic intercalation and decomposition of solvated cations[279] - Electrochemical exfoliation in organic solution makes the process ecofriendly[260] - Simple and scalable process for transitional metal dichalcogenides[280]	- Exfoliated nanosheets can be damaged by oxidation during exfoliation process[276] - Can involves the use of high boiling point organic solvents, ionic electrolytes, and other chemicals which may leave residues on the exfoliated nanosheets[261,267,275,341,344] - Cationic diameter plays as a key factor in successful electrochemical exfoliation[275] - Structural damages like scrolling, wrinkle and fracture are visible[345]

3.7 Non-van der Waals Exfoliation

The library of two-dimensional materials is typically limited to the class of van-der Waals crystals such as MoS_2 (Figure 14A), despite the vast majority of technically viable materials in industrial scale applications belonging to the class of non-van der Waals materials such as iron disulfide (FeS_2) (Figure 14B). The effect of confinement in one dimension on non-van der Waals 2D materials is only recently being explored which is a result of the difficulty in fabricating these materials at atomic thicknesses with large lateral size or area. The main difference between van der Waals and non-van der Waals materials is how their layers are bonded together. In the case of the former, layers are held together by weak vav der Waals interactions in the (001) direction while for the latter, constituent atomic layers are held by much stronger bonds (metallic, covalent, or ionic). Recent advancement of cleaving non-van der Waals bulk materials to their ultra-thin counter parts through the state-of-the-art liquid phase exfoliation approach has led to renewed research interest among scientific community[346]. The existence of cleaving/parting planes in certain directions of non-van der Waals materials, where the bonding strength is relatively weak compared to other crystallographic directions of the bulk crystal, facilitate smooth and preferential exfoliation along that plane when subjected to a high enough magnitude of shear force (Figure 14C).

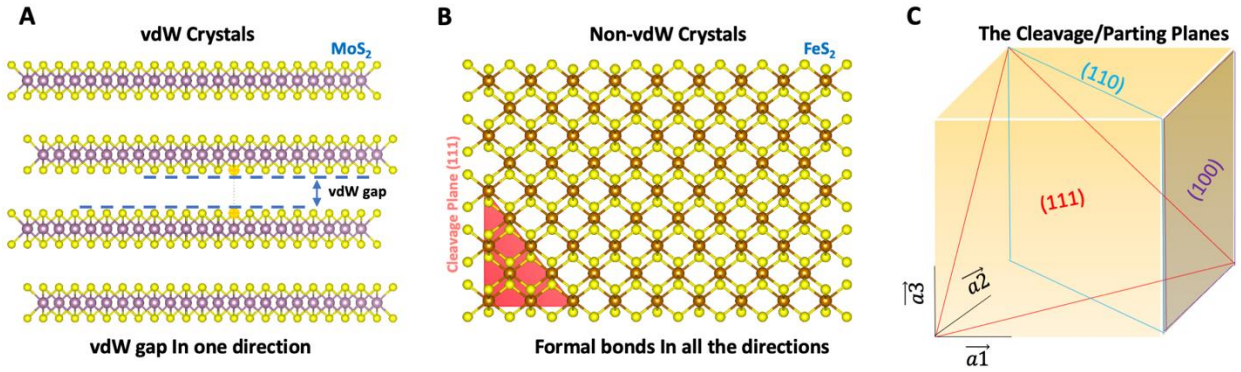

Figure 14. Non-van der Waals 2D material exfoliation. A) MoS_2 van der Waals crystal structure and B) FeS_2 non-van der Waals crystal structure highlighting the difference in bonding configuration between weakly bonded van der Waals layers and strong covalently bonded layers. C) The concept of preferential cleavage and parting planes in crystals can be 100, 110, or 111, and their combinations due to relative weakness in the bonding configuration along that plane which permits exfoliation.

The preparation of non-van der Waals 2D materials is by no means a trivial approach. Unlike their van der Waals counterparts, non-van der Waals materials have a significant tendency to satisfy the surface dangling bonds that are created in the exfoliation process.[347] Given the thermodynamic stability of typical layered van der Waals 2D materials, there exist multiple routes to overcome the weak van der Waals forces and synthesize 2D forms via effective exfoliation techniques as discussed in the preceding sections. However, in order to synthesize non-van der Waals 2D materials, one must develop strategies that depart from the thermodynamic equilibrium. Due to strong three-dimensional covalent/ionic bonding, it is highly unlikely to obtain non-van der Waals 2D materials through top-down approaches such as conventional mechanical exfoliation. However, taking advantage of the cleavage planes along which intrinsic isotropic covalent/ionic crystals tend to be unstable due to very high broken bond density, Balan *et.al,*[348] demonstrated that

even covalent/ionic crystals can be exfoliated to atomic thickness by conventional liquid phase exfoliation in suitable organic solvents.

It is demonstrated that non-van der Waals exfoliation leads to thin layers with different sizes and crystallographic orientations, the characteristics of which are dependent on the crystalline structure of the bulk material and also on the exfoliation energy required to delaminate the layers along a given plane. The exfoliation energy value is an important parameter to guide experimentalists in predicting whether a non-van der Waals material can be easily exfoliated or not while the crystallographic structure of the bulk material can provide insights into the structural characteristics of the thin layers that could be obtained from the exfoliation process. Based on this information, the appropriate exfoliation process to be used can also be determined. The estimated exfoliation energy for layered and non-layered materials have been obtained mainly from *ab-initio* simulations using DFT.[78] During the exfoliation process, the bulk material will experience shear stresses which will induce dislocations and/or create sub-grain boundaries, thereby weakening the bonds among the layers and easing the peeling off process. These dislocations and defects will occur more frequently along the slipping planes of the crystalline structure, which are those with the highest atomic density. Due to this, it is expected that the exfoliation energy will be smaller for layers with the orientation of the slipping planes, which could suggest the preferential orientation found for the exfoliated thin layers. Moreover, besides the exfoliation energy, the crystal structure of the bulk material can provide helpful information of what could be obtained after the exfoliation process.

The exfoliation energies required to exfoliate non-van der Waals materials are significantly higher than those for van der Waals materials. The breaking of formal bonds demands over an order of magnitude more energy than required to overcome the van der Waals interactions in layered materials. However, a fine balance must be struck to ensure that the in-plane structure remains intact and without significant defects introduced during the process. In addition, the dangling bonds which are created at the surface can lead to reagglomeration, oxidation, and structural reorganization during exfoliation which creates a process with significant complexity compared to conventional exfoliation processes. Nonetheless, due to the presence of parting/cleavage planes and the rich verity of oxides, sulfides, and nitrides, naturally existing earth ores and minerals such as Cr_2S_3, Al_2O_3, $FeCr_2O_4$, TiO_2, and many other non-vdW materials have been successfully exfoliated to atomic thicknesses. These exfoliated non-vdW 2D materials are being explored for 2D magnetism, low friction, electro and photocatalysis, piezoelectricity and various optoelectronic properties.[346,349–351]

3.8 Other Notable Exfoliation Techniques

Apart from the five well-studied exfoliation processes previously mentioned, there are reports of other interesting and unique methods to exfoliate layered materials. Some emerging methods that present potential but have not been widely explored and adopted have been included here for discussion. Tang et al.[352] used the interaction between polymer chains and different surfaces of MoS_2 (edge and basal plane surfaces) by a functionalized atomic force microscope cantilever to initiate polymer-based exfoliation of thin layers of MoS_2 by creating shear forces with the AFM tip (Figure 15A). Another interesting technique uses plasma-assisted exfoliation of GO by Wang et al.[353] using a magnetically enhanced dielectric barrier discharge system to produce the plasma.

This was employed to exfoliate N-doped graphene from polyaniline-modified GO to fabricate high-performance solid-state flexible supercapacitors. MXenes are an interesting unique class of 2D material which are synthesized by selective etching (chemical exfoliation) of MAX phases, in which the A atoms are attacked by an acid, leaving a 2D MX structure behind[354]. This has been widely employed for various MXene materials, such as $Ti_3C_2T_x$ and Nb_2CT_x, and has unlocked a new 2D material class since the first synthesis of a stable MXene in 2011[355]. Finally, a novel and fast method (~10 mins) to exfoliate ultrathin 2D materials, including C_3N_4, graphene, *h*BN, and BP, using liquid nitrogen and microwave treatment, was demonstrated by Zhu et al.[356] The bulk material is first soaked in liquid N_2 and then exposed to pulsed microwaves (~700 W) to produce 2D materials of <5 nm thickness (Figure 15B). Liquid N_2 pre-treatment weakens the van der Waals force between the layers of 2D materials before the microwaves add energy to overcome the bonds. While these techniques are indeed non-standard, they employ the same mechanical, ultrasonic, or electrochemical approaches of the more common methods to accomplish similar outcomes through a unique methodology.

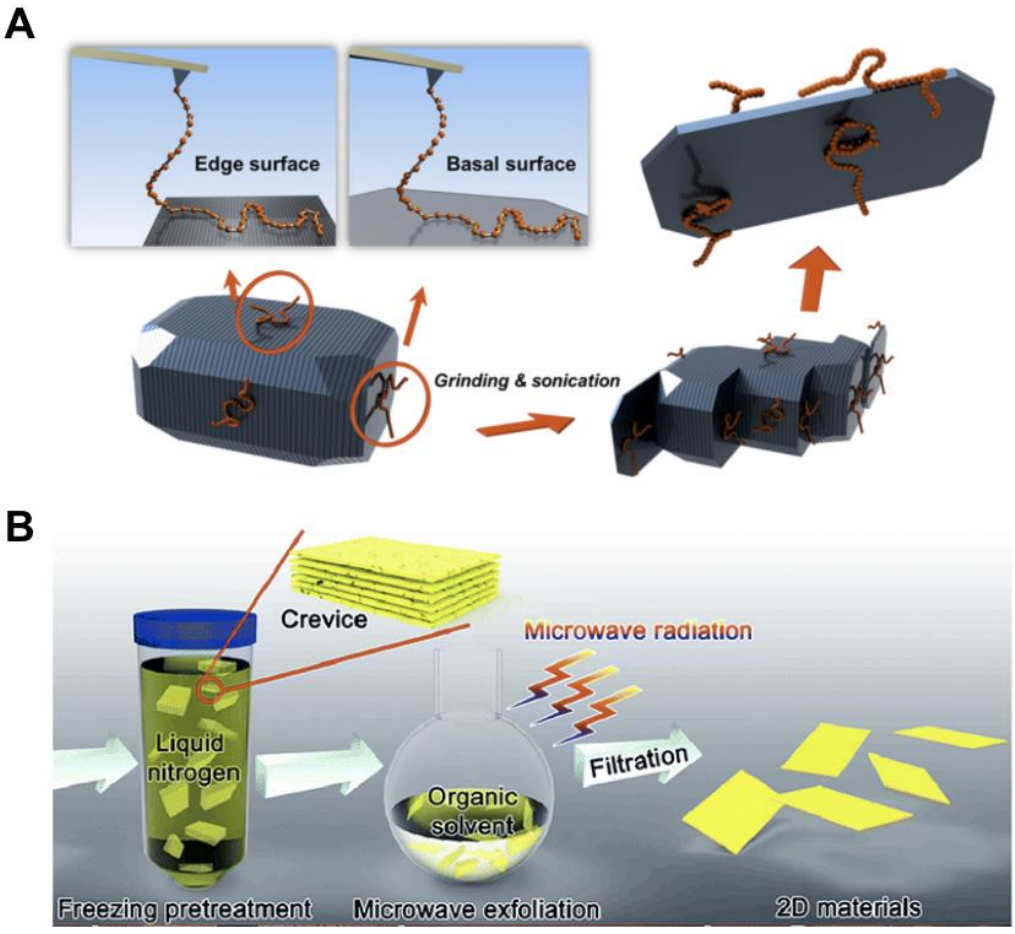

Figure 15. Other exfoliation processes. A) Schematic for the exfoliation of bulk MoS_2 in a single layer material using polymer-poly(vinyl benzyl trimethyl ammonium chloride) (polymer C1)[352] B) Liquid nitrogen and microwave treatment for the preparation of exfoliated C_3N_4, graphene, hBN, and BP[356]. A)

4. Outlook & Conclusion

Given the disruptive potential offered by the remarkable properties of 2D materials, the study of 2D materials is currently a highly active field of research. Developing cost-effective, scalable, and high-throughput methods to produce quality 2D crystals remains a significant focus to scale the fundamental nanoscale properties of these materials to macroscopic applications. Given the enormous amount of research dedicated to the field, and as the applications mentioned in this review begin to penetrate commercial markets, the required improvements to enable mass production will also come to fruition. Table S1 (Supplementary Information) presents a summary of some of the major applications of exfoliated 2D materials used in energy & storage, mechanics & design, polymer composite, and cement composite applications.

While the remarkable properties of two-dimensional materials quickly became evident, these materials' scalable production and use in commercial products have remained a predominant focus throughout the past two decades. While top-down approaches can produce consistent material thicknesses, their scalability for bulk quantities of 2D materials remains limited. Exfoliation processes offer promise for batch-scale processes with a variety of defect densities and throughput scalabilities depending on the technique employed, which are appropriate for several different applications, as discussed in the present article.

The five predominant exfoliation processes – micromechanical exfoliation, ball milling, ultrasonication, shear exfoliation, and electrochemical exfoliation – all produce wide varieties of 2D materials, sizes, thicknesses, defect densities, and scalabilities. Therefore, selecting the appropriate exfoliation process becomes critical for the end application. In this article, we have identified the significant challenges and opportunities associated with the predominant exfoliation processes and we have provided a comprehensive review of the governing mechanisms and computational methods that have been used to simulate exfoliation. Furthermore, some of the major applications of exfoliated 2D materials have been highlighted including energy storage, FETs, lubricants, and composite materials for mechanical, electrical, and thermal enhancements.

In addition to developing and improving mass-scale production methods, it is also vital to enhance low-scale production methods used in laboratories for research purposes. Given that many 2D materials are still in the research and development stage and that new 2D materials are being synthesized, it is important to improve laboratory-scale production methods so that they are more efficient, reliable, and quick. Whether it is the development of devices to automate certain stages of the exfoliation process or the formal establishment of standard best practices, improvements in exfoliation-based production methods will enable the next generation of devices and composite materials to revolutionize many industries. Furthermore, there are still major gaps in the theoretical investigation of exfoliation methods, specifically, in the analytical modeling of electrochemical exfoliation.

Throughout this review, we have covered many areas of promise for exfoliated 2D materials but have also captured only a select portion of the extensive literature on the topic of exfoliated 2D materials. For further reading, the authors suggest the reviews of specific exfoliation processes by

Huo et al.[36] for liquid exfoliation, Yi and Shen[92] for mechanical exfoliation and ball milling of graphene, or Ciesielski and Samori[327] for ultrasonication exfoliation.

Notes
The authors have no conflicts of interest to disclose.

Acknowledgements
The authors wish to acknowledge the support of the University of Toronto Centre for 2D Materials. The authors also wish to acknowledge the funding support of the Natural Science and Engineering Research Council of Canada, The Canada Foundation of Innovation, and The University of Toronto.

Authorship
[#]M.A.I., P.S., and B.K. contributed equally. All authors contributed to the writing and editing of the manuscript.

Supplementary Information
Supplementary information for this manuscript is available online and includes Supplementary Table S1 – Applications of Exfoliated 2D Materials.

References:

1. Novoselov, K. S. *et al.* Two-dimensional atomic crystals. *Proc Natl Acad Sci U S A* **102**, 10451–10453 (2005).
2. Peng, Q., Ji, W. & De, S. Mechanical properties of the hexagonal boron nitride monolayer: Ab initio study. *Computational Materials Science* **56**, 11–17 (2012).
3. Bertolazzi, S., Brivio, J. & Kis, A. Stretching and breaking of ultrathin MoS2. *ACS Nano* **5**, 9703–9709 (2011).
4. Lee, C., Wei, X., Kysar, J. W. & Hone, J. Measurement of the Elastic Properties and Intrinsic Strength of Monolayer Graphene. *Science (1979)* **321**, 385–388 (2008).
5. Bolotin, K. I. *et al.* Ultrahigh electron mobility in suspended graphene. *Solid State Communications* **146**, 351–355 (2008).
6. Xu, Y. *et al.* Holey graphene frameworks for highly efficient capacitive energy storage. *Nature Communications* **5**, (2014).
7. Gusynin, V. P. & Sharapov, S. G. Unconventional integer quantum hall effect in graphene. *Physical Review Letters* **95**, 2–5 (2005).
8. Losurdo, M., Giangregorio, M. M., Capezzuto, P. & Bruno, G. Graphene CVD growth on copper and nickel: Role of hydrogen in kinetics and structure. *Physical Chemistry Chemical Physics* **13**, 20836–20843 (2011).
9. Wang, Y. *et al.* Electrochemical Delamination of CVD-Grown Graphene Film: Toward the Recyclable Use of Copper Catalyst. *ACS Nano* **5**, 9927–9933 (2011).
10. Suk, J. W. *et al.* Transfer of CVD-grown monolayer graphene onto arbitrary substrates. *ACS Nano* **5**, 6916–6924 (2011).
11. Muñoz, R. & Gómez-Aleixandre, C. Review of CVD synthesis of graphene. *Chemical Vapor Deposition* **19**, 297–322 (2013).
12. Azpeitia, J. *et al.* High-quality PVD graphene growth by fullerene decomposition on Cu foils. *Carbon N Y* **119**, 535–543 (2017).

13. Narula, U. & Tan, C. M. Engineering a PVD-Based Graphene Synthesis Method. *IEEE Transactions on Nanotechnology* **16**, 784–789 (2017).
14. Narula, U., Tan, C. M. & Lai, C. S. Growth mechanism for low temperature PVD graphene synthesis on copper using amorphous carbon. *Scientific Reports* **7**, 1–13 (2017).
15. Jeon, C. H. *et al.* Material properties of graphene/aluminum metal matrix composites fabricated by friction stir processing. *International Journal of Precision Engineering and Manufacturing* **15**, 1235–1239 (2014).
16. Fan, H. *et al.* Fabrication, mechanical properties, and biocompatibility of graphene-reinforced chitosan composites. *Biomacromolecules* **11**, 2345–2351 (2010).
17. Chatterjee, S. *et al.* Mechanical reinforcement and thermal conductivity in expanded graphene nanoplatelets reinforced epoxy composites. *Chemical Physics Letters* **531**, 6–10 (2012).
18. Spear, J. C., Ewers, B. W. & Batteas, J. D. 2D-nanomaterials for controlling friction and wear at interfaces. *Nano Today* **10**, 301–314 (2015).
19. Zhang, W. *et al.* Soluble, exfoliated two-dimensional nanosheets as excellent aqueous lubricants. *ACS Applied Materials and Interfaces* **8**, 32440–32449 (2016).
20. Secor, E. B., Prabhumirashi, P. L., Puntambekar, K., Geier, M. L. & Hersam, M. C. Inkjet printing of high conductivity, flexible graphene patterns. *Journal of Physical Chemistry Letters* **4**, 1347–1351 (2013).
21. Grande, L. *et al.* Graphene for energy harvesting/storage devices and printed electronics. *Particuology* **10**, 1–8 (2012).
22. Karagiannidis, P. G. *et al.* Microfluidization of Graphite and Formulation of Graphene-Based Conductive Inks. *ACS Nano* **11**, 2742–2755 (2017).
23. Yang, E. *et al.* 2D materials-based membranes for hydrogen purification: Current status and future prospects. *International Journal of Hydrogen Energy* **46**, 11389–11410 (2021).
24. Dervin, S., Dionysiou, D. D. & Pillai, S. C. 2D nanostructures for water purification: Graphene and beyond. *Nanoscale* vol. 8 15115–15131 (2016).
25. Raza, A., Hassan, J. Z., Mahmood, A., Nabgan, W. & Ikram, M. Recent advances in membrane-enabled water desalination by 2D frameworks: Graphene and beyond. *Desalination* vol. 531 (2022).
26. Zhang, H., Fan, T., Chen, W., Li, Y. & Wang, B. Recent advances of two-dimensional materials in smart drug delivery nano-systems. *Bioactive Materials* vol. 5 1071–1086 (2020).
27. Kurapati, R., Kostarelos, K., Prato, M. & Bianco, A. Biomedical Uses for 2D Materials Beyond Graphene: Current Advances and Challenges Ahead. *Advanced Materials* vol. 28 6052–6074 (2016).
28. Bollella, P. *et al.* Beyond graphene: Electrochemical sensors and biosensors for biomarkers detection. *Biosensors and Bioelectronics* vol. 89 152–166 (2017).
29. Zhang, Y. *et al.* A graphene-oxide-based thin coating on the separator: An efficient barrier towards high-stable lithium-sulfur batteries. *2D Materials* **2**, (2015).
30. Moon, I. K. *et al.* 2D graphene oxide nanosheets as an adhesive over-coating layer for flexible transparent conductive electrodes. *Scientific Reports* **3**, 1–7 (2013).
31. Han, Y., Ge, Y., Chao, Y., Wang, C. & Wallace, G. G. Recent progress in 2D materials for flexible supercapacitors. *Journal of Energy Chemistry* **27**, 57–72 (2018).
32. Zhang, X., Hou, L., Ciesielski, A. & Samorì, P. 2D Materials Beyond Graphene for High-Performance Energy Storage Applications. *Advanced Energy Materials* **6**, (2016).

33. Palaniselvam, T. & Baek, J. B. Graphene based 2D-materials for supercapacitors. *2D Materials* **2**, (2015).
34. Acik, M. & Chabal, Y. J. A Review on Reducing Graphene Oxide for Band Gap Engineering. *Journal of Materials Science Research* **2**, (2012).
35. Cai, X., Luo, Y., Liu, B. & Cheng, H. M. Preparation of 2D material dispersions and their applications. *Chemical Society Reviews* **47**, 6224–6266 (2018).
36. Huo, C., Yan, Z., Song, X. & Zeng, H. 2D materials via liquid exfoliation: a review on fabrication and applications. *Science Bulletin* **60**, 1994–2008 (2015).
37. Bissett, M. A., Konabe, S., Okada, S., Tsuji, M. & Ago, H. Enhanced chemical reactivity of graphene induced by mechanical strain. *ACS Nano* **7**, 10335–10343 (2013).
38. Liu, K. & Wu, J. Mechanical properties of two-dimensional materials and heterostructures. *Journal of Materials Research* **31**, 832–844 (2016).
39. Nicolosi, V., Chhowalla, M., Kanatzidis, M. G., Strano, M. S. & Coleman, J. N. Liquid exfoliation of layered materials. *Science (1979)* **340**, 72–75 (2013).
40. Eckmann, A. *et al.* Probing the nature of defects in graphene by Raman spectroscopy. *Nano Letters* **12**, 3925–3930 (2012).
41. Novoselov, K. S. *et al.* Electric field effect in atomically thin carbon films. *Science (1979)* **306**, 666–669 (2004).
42. Geim, A. K. & Novoselov, K. S. The rise of graphene. *Nature Materials* **6**, 183–191 (2007).
43. Morozov, S. V. *et al.* Giant intrinsic carrier mobilities in graphene and its bilayer. *Physical Review Letters* **100**, 11–14 (2008).
44. Lin, Y. M. *et al.* 100-GHz transistors from wafer-scale epitaxial graphene. *Science (1979)* **327**, 662 (2010).
45. Frank, I. W., Tanenbaum, D. M., Van Der Zande, A. M. & McEuen, P. L. Mechanical properties of suspended graphene sheets. *Journal of Vacuum Science and Technology B: Microelectronics and Nanometer Structures* **25**, 2558–2561 (2007).
46. Faccio, R., Denis, P. A., Pardo, H., Goyenola, C. & Mombrú, Á. W. Mechanical properties of graphene nanoribbons. *Journal of Physics Condensed Matter* **21**, (2009).
47. Scarpa, F., Adhikari, S. & Srikantha Phani, A. Effective elastic mechanical properties of single layer graphene sheets. *Nanotechnology* **20**, (2009).
48. Haastrup, S. *et al.* The Computational 2D Materials Database: High-throughput modeling and discovery of atomically thin crystals. *2D Materials* **5**, (2018).
49. Paine, R. T. & Narula, C. K. Synthetic Routes to Boron Nitride. *Chemical Reviews* **90**, 73–91 (1990).
50. Sinclair, W. & Simmons, H. Microstructure and thermal shock behaviour of BN composites. *Journal of Materials Science Letters* **6**, 627–629 (1987).
51. Pan, C., Kou, K., Zhang, Y., Li, Z. & Wu, G. Enhanced through-plane thermal conductivity of PTFE composites with hybrid fillers of hexagonal boron nitride platelets and aluminum nitride particles. *Composites Part B: Engineering* **153**, 1–8 (2018).
52. Kovalčíková, A., Balko, J., Balázsi, C., Hvizdoš, P. & Dusza, J. Influence of hBN content on mechanical and tribological properties of Si3N4/BN ceramic composites. *J Eur Ceram Soc* **34**, 3319–3328 (2014).
53. Jiang, H. X. & Lin, J. Y. Hexagonal boron nitride for deep ultraviolet photonic devices. *Semiconductor Science and Technology* **29**, (2014).

54. Shi, K., Bao, F. & He, S. Enhanced Near-Field Thermal Radiation Based on Multilayer Graphene-hBN Heterostructures. *ACS Photonics* **4**, 971–978 (2017).
55. Roy, S. *et al.* Structure, Properties and Applications of Two-Dimensional Hexagonal Boron Nitride. *Advanced Materials* vol. 33 (2021).
56. Falin, A. *et al.* Mechanical properties of atomically thin boron nitride and the role of interlayer interactions. *Nature Communications* **8**, 1–9 (2017).
57. Novoselov, K. S. *et al.* A roadmap for graphene. *Nature* **490**, 192–200 (2012).
58. Bernardi, M., Palummo, M. & Grossman, J. C. Extraordinary sunlight absorption and one nanometer thick photovoltaics using two-dimensional monolayer materials. *Nano Letters* **13**, 3664–3670 (2013).
59. Luo, S. *et al.* Photoresponse properties of large-area MoS2 atomic layer synthesized by vapor phase deposition. *Journal of Applied Physics* **116**, (2014).
60. Sundaram, R. S. *et al.* Electroluminescence in single layer MoS2. *Nano Letters* **13**, 1416–1421 (2013).
61. Ghatak, S., Pal, A. N. & Ghosh, A. Nature of electronic states in atomically thin MoS2 field-effect transistors. *ACS Nano* **5**, 7707–7712 (2011).
62. Jariwala, D. *et al.* Band-like transport in high mobility unencapsulated single-layer MoS 2 transistors. *Applied Physics Letters* **102**, 2–6 (2013).
63. Radisavljevic, B., Radenovic, A., Brivio, J., Giacometti, V. & Kis, A. Single-layer MoS2 transistors. *Nature Nanotechnology* **6**, 147–150 (2011).
64. Late, D. J., Liu, B., Matte, H. S. S. R., Dravid, V. P. & Rao, C. N. R. Hysteresis in single-layer MoS2 field effect transistors. *ACS Nano* **6**, 5635–5641 (2012).
65. Pakdel, A., Bando, Y. & Golberg, D. Nano boron nitride flatland. *Chemical Society Reviews* **43**, 934–959 (2014).
66. Luo, M., Hao, S. Y. & Ling, Y. T. Ab initio study of electronic and magnetic properties in Ni-doped WS2 monolayer. *AIP Advances* **6**, (2016).
67. Qian, X., Gu, Z. & Chen, Y. Two-dimensional black phosphorus nanosheets for theranostic nanomedicine. *Materials Horizons* **4**, 800–816 (2017).
68. Jiang, H. Electronic band structures of molybdenum and tungsten dichalcogenides by the GW approach. *Journal of Physical Chemistry C* **116**, 7664–7671 (2012).
69. Roy, S. & Bermel, P. Electronic and optical properties of ultra-thin 2D tungsten disulfide for photovoltaic applications. *Solar Energy Materials and Solar Cells* **174**, 370–379 (2018).
70. Wang, X. *et al.* Machine Learning Enabled Prediction of Mechanical Properties of Tungsten Disulfide Monolayer. *ACS Omega* **4**, 10121–10128 (2019).
71. Island, J. O., Steele, G. A., Van Der Zant, H. S. J. & Castellanos-Gomez, A. Environmental instability of few-layer black phosphorus. *2D Materials* **2**, (2015).
72. Castellanos-Gomez, A. Black Phosphorus: Narrow Gap, Wide Applications. *Journal of Physical Chemistry Letters* **6**, 4280–4291 (2015).
73. Mannix, A. J., Kiraly, B., Hersam, M. C. & Guisinger, N. P. Synthesis and chemistry of elemental 2D materials. *Nature Reviews Chemistry* **1**, 1–15 (2017).
74. Mas-Ballesté, R., Gómez-Navarro, C., Gómez-Herrero, J. & Zamora, F. 2D materials: To graphene and beyond. *Nanoscale* **3**, 20–30 (2011).
75. Israelachvili, J. N. *Intermolecular and Surface Forces*. (Elsevier, 2011).

76. Cutini, M., Maschio, L. & Ugliengo, P. Exfoliation Energy of Layered Materials by DFT-D: Beware of Dispersion! *Journal of Chemical Theory and Computation* **16**, 5244–5252 (2020).
77. Yadav, S. *et al.* Interfacial Interactions and Tribological Behavior of Metal-Oxide/2D-Material Contacts. *Tribology Letters* **69**, 1–11 (2021).
78. Jung, J. H., Park, C. H. & Ihm, J. A Rigorous Method of Calculating Exfoliation Energies from First Principles. *Nano Letters* **18**, 2759–2765 (2018).
79. Rasuli, R. & Iraji Zad, A. Density functional theory prediction for oxidation and exfoliation of graphite to graphene. *Applied Surface Science* **256**, 7596–7599 (2010).
80. Bastos, C. M. O., Besse, R., Da Silva, J. L. F. & Sipahi, G. M. Ab initio investigation of structural stability and exfoliation energies in transition metal dichalcogenides based on Ti-, V-, and Mo-group elements. *Physical Review Materials* **3**, 1–10 (2019).
81. Chahal, S. Borophene via Micromechanical Exfoliation. *Advanced Materials* **33**, 34 (2021).
82. Sansone, G., Maschio, L., Usvyat, D., Schütz, M. & Karttunen, A. Toward an Accurate Estimate of the Exfoliation Energy of Black Phosphorus: A Periodic Quantum Chemical Approach. *Journal of Physical Chemistry Letters* **7**, 131–136 (2016).
83. Kabengele, T. & Johnson, E. R. Theoretical modeling of structural superlubricity in rotated bilayer graphene, hexagonal boron nitride, molybdenum disulfide, and blue phosphorene. *Nanoscale* **13**, 14399–14407 (2021).
84. Hu, T. *et al.* Interlayer coupling in two-dimensional titanium carbide MXenes. *Physical Chemistry Chemical Physics* **18**, 20256–20260 (2016).
85. Schusteritsch, G., Uhrin, M. & Pickard, C. J. Single-Layered Hittorf's Phosphorus: A Wide-Bandgap High Mobility 2D Material. *Nano Letters* **16**, 2975–2980 (2016).
86. Demingos, P. G. & Muniz, A. R. Prediction of φ-P and σ-P: Two New Strain-Interconvertible Phosphorene Allotropes. *Journal of Physical Chemistry C* **124**, 21207–21214 (2020).
87. Wan, Z. & Wang, Q. De. Machine Learning Prediction of the Exfoliation Energies of Two-Dimension Materials via Data-Driven Approach. *Journal of Physical Chemistry Letters* **12**, 11470–11475 (2021).
88. Jun, Z. *et al.* computational database of two- dimensional materials from top- down and bottom-up approaches. 1–10 (2019) doi:10.1038/s41597-019-0097-3.
89. Siriwardane, E. M. D., Joshi, R. P., Kumar, N. & Çaklr, D. Revealing the Formation Energy-Exfoliation Energy-Structure Correlation of MAB Phases Using Machine Learning and DFT. *ACS Applied Materials and Interfaces* **12**, 29424–29431 (2020).
90. Jain, A. The Materials Project: A materials genome approach to accelerating materials innovation. *APL Materials* **1**, 011002 (2013).
91. Saito, Y. *et al.* Deep-learning-based quality filtering of mechanically exfoliated 2D crystals. *npj Computational Materials* **5**, 1–6 (2019).
92. Yi, M. & Shen, Z. A review on mechanical exfoliation for the scalable production of graphene. *Journal of Materials Chemistry A* **3**, 11700–11715 (2015).
93. Huang, Y. *et al.* Reliable Exfoliation of Large-Area High-Quality Flakes of Graphene and Other Two-Dimensional Materials. *ACS Nano* **9**, 10612–10620 (2015).
94. Ng, L. W. T. *et al. Printing of graphene and related 2D materials: Technology, formulation and applications*. *Printing of Graphene and Related 2D Materials: Technology, Formulation and Applications* (2018). doi:10.1007/978-3-319-91572-2.

95. Li, H. *et al.* Rapid and reliable thickness identification of two-dimensional nanosheets using optical microscopy. *ACS Nano* **7**, 10344–10353 (2013).
96. Huang, Y. *et al.* Universal mechanical exfoliation of large-area 2D crystals. *Nature Communications* **11**, (2020).
97. PaciÍ, D., Meyer, J. C., Girit, Ç. & Zettl, A. The two-dimensional phase of boron nitride: Few-atomic-layer sheets and suspended membranes. *Applied Physics Letters* **92**, 1–4 (2008).
98. Lin, Y. & Connell, J. W. Advances in 2D boron nitride nanostructures: Nanosheets, nanoribbons, nanomeshes, and hybrids with graphene. *Nanoscale* **4**, 6908–6939 (2012).
99. Häkkinen, H. The gold-sulfur interface at the nanoscale. *Nature Chemistry* **4**, 443–455 (2012).
100. Fang, H. *et al.* High-performance single layered WSe 2 p-FETs with chemically doped contacts. *Nano Letters* **12**, 3788–3792 (2012).
101. Braga, D., Gutiérrez Lezama, I., Berger, H. & Morpurgo, A. F. Quantitative determination of the band gap of WS 2 with ambipolar ionic liquid-gated transistors. *Nano Letters* **12**, 5218–5223 (2012).
102. Dicamillo, K., Krylyuk, S., Shi, W., Davydov, A. & Paranjape, M. Automated mechanical exfoliation of MoS2 and MoTe2 layers for two-dimensional materials applications. *IEEE Transactions on Nanotechnology* **18**, 144–148 (2019).
103. Sinclair, R. C., Suter, J. L. & Coveney, P. V. Micromechanical exfoliation of graphene on the atomistic scale. *Physical Chemistry Chemical Physics* **21**, 5716–5722 (2019).
104. Yang, B. & Vijayanand, N. Multiscale fracture in peeling of highly oriented pyrolytic graphite. *Key Engineering Materials* **560**, 71–86 (2013).
105. Ting, T. C. T. *Anisotropic Elasticity: Theory and Applications*. (Oxford University Press, 1996).
106. Yang, B., Barsoum, M. W. & Rethinam, R. M. Nanoscale continuum calculation of basal dislocation core structures in graphite. *Philosophical Magazine* **91**, 1441–1463 (2011).
107. Jayasena, B. & Melkote, S. N. A molecular dynamics study of PDMS stamp-based graphene exfoliation. *Journal of Micro and Nano-Manufacturing* **6**, 4–8 (2018).
108. Jayasena, B., Reddy, C. D. & Subbiah, S. Separation, folding and shearing of graphene layers during wedge-based mechanical exfoliation. *Nanotechnology* **24**, (2013).
109. Khomenko, A. V. & Prodanov, N. V. Molecular dynamics of cleavage and flake formation during the interaction of a graphite surface with a rigid nanoasperity. *Carbon N Y* **48**, 1234–1243 (2010).
110. Castellanos-Gomez, A. *et al.* Elastic properties of freely suspended MoS2 nanosheets. *Advanced Materials* **24**, 772–775 (2012).
111. Cao, C., Daly, M., Singh, C. V., Sun, Y. & Filleter, T. High strength measurement of monolayer graphene oxide. *Carbon N Y* **81**, 497–504 (2015).
112. Gupta, A., Sakthivel, T. & Seal, S. Recent development in 2D materials beyond graphene. *Progress in Materials Science* **73**, 44–126 (2015).
113. Cui, T. *et al.* Fatigue of graphene. *Nature Materials* **19**, 405–411 (2020).
114. Jae-Hwang, L., E., L. P., Jun, L. & L., T. E. Dynamic mechanical behavior of multilayer graphene via supersonic projectile penetration. *Science (1979)* **346**, 1092–1096 (2014).
115. Kaushik, N. *et al.* Reversible hysteresis inversion in MoS2 field effect transistors. *npj 2D Materials and Applications* **1**, (2017).

116. Lemme, M. C., Member, S., Echtermeyer, T. J., Baus, M. & Kurz, H. A Graphene Field-Effect Device. **28**, 282–284 (2007).
117. Banszerus, L. *et al.* Ultrahigh-mobility graphene devices from chemical vapor deposition on reusable copper. *Science Advances* **1**, 1–7 (2015).
118. Chen, B. *et al.* How good can CVD-grown monolayer graphene be? *Nanoscale* **6**, 15255–15261 (2014).
119. Lee, D. *et al.* Scalable exfoliation process for highly soluble boron nitride nanoplatelets by hydroxide-assisted ball milling. *Nano Letters* **15**, 1238–1244 (2015).
120. Mohanta, Z., Atreya, H. S. & Srivastava, C. Correlation between defect density in mechanically milled graphite and total oxygen content of graphene oxide produced from oxidizing the milled graphite. *Scientific Reports* 1–6 (2018) doi:10.1038/s41598-018-34109-z.
121. Ambrosi, A. & Pumera, M. Electrochemically Exfoliated Graphene and Graphene Oxide for Energy Storage and Electrochemistry Applications. *Chemistry - A European Journal* **22**, 153–159 (2016).
122. Ambrosi, A., Chia, X., Sofer, Z. & Pumera, M. Enhancement of electrochemical and catalytic properties of MoS2 through ball-milling. *Electrochemistry Communications* **54**, 36–40 (2015).
123. Bellani, S. *et al.* Scalable Production of Graphene Inks via Wet-Jet Milling Exfoliation for Screen-Printed Micro-Supercapacitors. *Advanced Functional Materials* **29**, 1–14 (2019).
124. Xia, J. *et al.* Layer-by-layered SnS2/graphene hybrid nanosheets via ball-milling as promising anode materials for lithium ion batteries. *Electrochimica Acta* **269**, 452–461 (2018).
125. Ji, H. *et al.* Directly scalable preparation of sandwiched MoS 2 /graphene nanocomposites via ball-milling with excellent electrochemical energy storage performance. *Electrochimica Acta* **299**, 143–151 (2019).
126. Li, L. H. *et al.* Large-scale mechanical peeling of boron nitride nanosheets by low-energy ball milling. *Journal of Materials Chemistry* **21**, 11862–11866 (2011).
127. Deepika, A. *et al.* High-efficient production of boron nitride nanosheets via an optimized ball milling process for lubrication in oil. *Scientific Reports* **4**, 2–7 (2014).
128. Yu, C. *et al.* One-Step in Situ Ball Milling Synthesis of Polymer-Functionalized Few-Layered Boron Nitride and Its Application in High Thermally Conductive Cellulose Composites. *ACS Applied Nano Materials* **1**, 4875–4883 (2018).
129. Khossossi, N. Recent progress of defect chemistry on 2D materials for advanced battery anodes. *Chemistry (Easton)* **15**, 3390 (2020).
130. Lin, C. *et al.* A new method for few-layer graphene preparation via plasma-assisted ball milling. *Journal of Alloys and Compounds* **728**, 578–584 (2017).
131. Tavares, L. M. A review of advanced ball mill modelling. *KONA Powder and Particle Journal* **2017**, 106–124 (2017).
132. Burgio, N., Iasonna, A., Magini, M., Martelli, S. & Padella, F. Mechanical alloying of the Fe-Zr system. Correlation between input energy and end products. *Il Nuovo Cimento D* **13**, 459–476 (1991).
133. Ghayour, H., Abdellahi, M. & Bahmanpour, M. Optimization of the high energy ball-milling: Modeling and parametric study. *Powder Technology* **291**, 7–13 (2016).
134. Martinez-Garcia, A. *et al.* Effect of ball to powder ratio on the mechanosynthesis of Re2C and its compressibility. *Journal of Alloys and Compounds* **810**, 151867 (2019).

135. Fourmont, A., Le Gallet, S., Politano, O., Desgranges, C. & Baras, F. Effects of planetary ball milling on AlCoCrFeNi high entropy alloys prepared by Spark Plasma Sintering: Experiments and molecular dynamics study. *Journal of Alloys and Compounds* **820**, 153448 (2020).
136. Hara, K. O., Yamasue, E., Okumura, H. & Ishihara, K. N. Molecular dynamics study of the milling-induced allotropic transformation in cobalt. *Philosophical Magazine* **92**, 2117–2129 (2012).
137. Arao, Y. *et al.* Mass production of low-boiling point solvent- And water-soluble graphene by simple salt-assisted ball milling. *Nanoscale Advances* **1**, 4955–4964 (2019).
138. Liu, L. *et al.* Ammonia borane assisted solid exfoliation of graphite fluoride for facile preparation of fluorinated graphene nanosheets. *Carbon N Y* **81**, 702–709 (2015).
139. Meiyazhagan, A. K. *et al.* Gas-Phase Fluorination of Hexagonal Boron Nitride. *Advanced Materials* **33**, 1–11 (2021).
140. Compton, O. C. & Nguyen, S. T. Graphene oxide, highly reduced graphene oxide, and graphene: Versatile building blocks for carbon-based materials. *Small* vol. 6 711–723 (2010).
141. Liu, Y., Wu, H. & Chen, G. Enhanced mechanical properties of nanocomposites at low graphene content based on in situ ball milling. *Polymer Composites* **37**, 1190–1197 (2016).
142. Khan, U., May, P., O'Neill, A. & Coleman, J. N. Development of stiff, strong, yet tough composites by the addition of solvent exfoliated graphene to polyurethane. *Carbon N Y* **48**, 4035–4041 (2010).
143. Debelak, B. & Lafdi, K. Use of exfoliated graphite filler to enhance polymer physical properties. *Carbon N Y* **45**, 1727–1734 (2007).
144. Wang, X., Xing, W., Feng, X., Song, L. & Hu, Y. MoS2/Polymer Nanocomposites: Preparation, Properties, and Applications. *Polymer Reviews* **57**, 440–466 (2017).
145. Shen, J. *et al.* Surface Tension Components Based Selection of Cosolvents for Efficient Liquid Phase Exfoliation of 2D Materials. *Small* **12**, 2741–2749 (2016).
146. Khan, U. *et al.* Polymer reinforcement using liquid-exfoliated boron nitride nanosheets. *Nanoscale* **5**, 581–587 (2013).
147. May, P., Khan, U., O'Neill, A. & Coleman, J. N. Approaching the theoretical limit for reinforcing polymers with graphene. *Journal of Materials Chemistry* **22**, 1278–1282 (2012).
148. Kim, J. *et al.* Strength dependence of epoxy composites on the average filler size of non-oxidized graphene flake. *Carbon N Y* **113**, 379–386 (2017).
149. Nie, X. *et al.* Exfoliation of hexagonal boron nitride assisted with hierarchical ionic fragments by ball-milling for achieving high thermally conductive polymer nanocomposite. *Polymer Composites* **43**, 946–954 (2022).
150. Kim, H. S., Bae, H. S., Yu, J. & Kim, S. Y. Thermal conductivity of polymer composites with the geometrical characteristics of graphene nanoplatelets. *Nature Publishing Group* 1–9 (2016) doi:10.1038/srep26825.
151. Jan, R. *et al.* Flexible, thin films of graphene-polymer composites for EMI shielding. *Materials Research Express* **4**, (2017).
152. Zhang, H. *et al.* Synergistic effect of carbon nanotube and graphene nanoplates on the mechanical, electrical and electromagnetic interference shielding properties of polymer

composites and polymer composite foams. *Chemical Engineering Journal* **353**, 381–393 (2018).
153. Wang, H. *et al.* Electrical and mechanical properties of antistatic PVC films containing multi-layer graphene. *Composites Part B: Engineering* **79**, 444–450 (2015).
154. Boland, C. S. *et al.* Sensitive, high-strain, high-rate bodily motion sensors based on graphene-rubber composites. *ACS Nano* **8**, 8819–8830 (2014).
155. Eswaraiah, V., Balasubramaniam, K. & Ramaprabhu, S. One-pot synthesis of conducting graphene-polymer composites and their strain sensing application. *Nanoscale* **4**, 1258–1262 (2012).
156. Wang, J., Wu, Z., Hu, K., Chen, X. & Yin, H. High conductivity graphene-like MoS2/polyaniline nanocomposites and its application in supercapacitor. *Journal of Alloys and Compounds* **619**, 38–43 (2015).
157. Xu, B. H., Lin, B. Z., Sun, D. Y. & Ding, C. Preparation and electrical conductivity of polyethers/WS2 layered nanocomposites. *Electrochimica Acta* **52**, 3028–3034 (2007).
158. Fu, Y., He, Z., Mo, D. & Lu, S. Thermal conductivity enhancement of epoxy adhesive using graphene sheets as additives. *International Journal of Thermal Sciences* **86**, 276–283 (2014).
159. Teng, C. *et al.* Thermal conductivity and structure of non-covalent functionalized graphene / epoxy composites. *Carbon N Y* **49**, 5107–5116 (2011).
160. Hamidinejad, S. M., Chu, R. K. M., Zhao, B., Park, C. B. & Filleter, T. Enhanced Thermal Conductivity of Graphene Nanoplatelet-Polymer Nanocomposites Fabricated via Supercritical Fluid-Assisted in Situ Exfoliation. *ACS Applied Materials and Interfaces* **10**, 1225–1236 (2018).
161. Sullivan, E. M., Oh, Y. J., Gerhardt, R. A., Wang, B. & Kalaitzidou, K. Understanding the effect of polymer crystallinity on the electrical conductivity of exfoliated graphite nanoplatelet/polylactic acid composite films. *Journal of Polymer Research* **21**, 1–9 (2014).
162. Najafi, F. *et al.* Toughening of graphene-based polymer nanocomposites via tuning chemical functionalization. *Composites Science and Technology* **194**, (2020).
163. Coleman, J. N. *et al.* Two-dimensional nanosheets produced by liquid exfoliation of layered materials. *Science (1979)* **331**, 568–571 (2011).
164. Hernandez, Y. *et al.* High-yield production of graphene by liquid-phase exfoliation of graphite. *Nature Nanotechnology* **3**, 563–568 (2008).
165. Amiri, A., Naraghi, M., Ahmadi, G., Soleymaniha, M. & Shanbedi, M. A review on liquid-phase exfoliation for scalable production of pure graphene, wrinkled, crumpled and functionalized graphene and challenges. *FlatChem* **8**, 40–71 (2018).
166. Fu, B. *et al.* Solution-processed two-dimensional materials for ultrafast fiber lasers (invited). *Nanophotonics* **9**, 2169–2189 (2020).
167. Tyurnina, A. v. *et al.* Ultrasonic exfoliation of graphene in water: A key parameter study. *Carbon N Y* **168**, 737–747 (2020).
168. Kim, J. *et al.* Direct exfoliation and dispersion of two-dimensional materials in pure water via temperature control. *Nature Communications 2015 6:1* **6**, 1–9 (2015).
169. Gu, X. *et al.* Method of ultrasound-assisted liquid-phase exfoliation to prepare graphene. *Ultrasonics Sonochemistry* **58**, (2019).

170. Hernandez, Y., Lotya, M., Rickard, D., Bergin, S. D. & Coleman, J. N. Measurement of Multicomponent Solubility Parameters for Graphene Facilitates Solvent Discovery. *Langmuir* **26**, 3208–3213 (2010).
171. Hamilton, C. E., Lomeda, J. R., Sun, Z., Tour, J. M. & Barron, A. R. High-Yield Organic Dispersions of Unfunctionalized Graphene. doi:10.1021/nl9016623.
172. Arifutzzaman, A. Effect of Exfoliated Graphene Defects on Thermal Conductivity of Water Based Graphene Nanofluids. **13**, 4871–4877 (2018).
173. Notley, S. M. Highly concentrated aqueous suspensions of graphene through ultrasonic exfoliation with continuous surfactant addition. *Langmuir* **28**, 14110–14113 (2012).
174. Smith, R. J. *et al.* Large-scale exfoliation of inorganic layered compounds in aqueous surfactant solutions. *Advanced Materials* **23**, 3944–3948 (2011).
175. Gurvitz, S. *et al.* Production of graphene by exfoliation of graphite in a volatile organic solvent. *Nanotechnology* **22**, 365601–365607 (2011).
176. O'neill, A., Khan, U., Nirmalraj, P. N., Boland, J. & Coleman, J. N. Graphene Dispersion and Exfoliation in Low Boiling Point Solvents. *J. Phys. Chem. C* **115**, 5422–5428 (2011).
177. Guardia, L. *et al.* High-throughput production of pristine graphene in an aqueous dispersion assisted by non-ionic surfactants. *Carbon N Y* **49**, 1653–1662 (2011).
178. Lotya, M. *et al.* Liquid phase production of graphene by exfoliation of graphite in surfactant/water solutions. *J Am Chem Soc* **131**, 3611–3620 (2009).
179. Bang, G. S. *et al.* Effective liquid-phase exfoliation and sodium ion battery application of MoS2 nanosheets. *ACS Applied Materials and Interfaces* **6**, 7084–7089 (2014).
180. Wu, J. Y., Zhang, X. Y., Ma, X. D., Qiu, Y. P. & Zhang, T. High quantum-yield luminescent MoS2 quantum dots with variable light emission created via direct ultrasonic exfoliation of MoS2 nanosheets. *RSC Advances* **5**, 95178–95182 (2015).
181. May, P., Khan, U., Hughes, J. M. & Coleman, J. N. Role of Solubility Parameters in Understanding the Steric Stabilization of Exfoliated Two-Dimensional Nanosheets by Adsorbed Polymers. *The Journal of Physical Chemistry C* **116**, 11393–11400 (2012).
182. Bourlinos, A. B. *et al.* Aqueous-phase exfoliation of graphite in the presence of polyvinylpyrrolidone for the production of water-soluble graphenes. *Solid State Communications* **149**, 2172–2176 (2009).
183. Liang, Y. T. & Hersam, M. C. Highly Concentrated Graphene Solutions via Polymer Enhanced Solvent Exfoliation and Iterative Solvent Exchange. *J Am Chem Soc* **132**, 17661–17663 (2010).
184. Lee, D. W., Kim, T. & Lee, M. An amphiphilic pyrene sheet for selective functionalization of graphene. *Chemical Communications* **47**, 8259–8261 (2011).
185. Niu, L. *et al.* Production of Two-Dimensional Nanomaterials via Liquid-Based Direct Exfoliation. *Small* **12**, 272–293 (2016).
186. Yang, H. *et al.* A simple method for graphene production based on exfoliation of graphite in water using 1-pyrenesulfonic acid sodium salt. *Carbon N Y* **53**, 357–365 (2013).
187. Pu, N. W., Wang, C. A., Sung, Y., Liu, Y. M. & Ger, M. der. Production of few-layer graphene by supercritical CO2 exfoliation of graphite. *Materials Letters* **63**, 1987–1989 (2009).
188. Wang, W., Wang, Y., Gao, Y. & Zhao, Y. Control of number of graphene layers using ultrasound in supercritical CO2 and their application in lithium-ion batteries. *Journal of Supercritical Fluids* **85**, 95–101 (2014).

189. Varinot, C., Hiltgun, S., Pons, M. N. & Dodds, J. Identification of the fragmentation mechanisms in wet-phase fine grinding in a stirred bead mill. *Chemical Engineering Science* **52**, 3605–3612 (1997).
190. Hennart, S. L. A., Wildeboer, W. J., van Hee, P. & Meesters, G. M. H. Identification of the grinding mechanisms and their origin in a stirred ball mill using population balances. *Chemical Engineering Science* **64**, 4123–4130 (2009).
191. Kapur, P. C. & Agrawal, P. K. Approximate solutions to the discretized batch grinding equation. *Chemical Engineering Science* **25**, 1111–1113 (1970).
192. Li, C., Lin, J., Shen, L. & Bao, N. Quantitative analysis and kinetic modeling of ultrasound-assisted exfoliation and breakage process of graphite oxide. *Chemical Engineering Science* **213**, 115414 (2020).
193. Shih, C. J. *et al.* Bi- and trilayer graphene solutions. *Nature Nanotechnology* **6**, 439–445 (2011).
194. Yi, M., Shen, Z., Zhang, X. & Ma, S. Vessel diameter and liquid height dependent sonication-assisted production of few-layer graphene. *Journal of Materials Science* **47**, 8234–8244 (2012).
195. Pupysheva, O. v., Farajian, A. A., Knick, C. R., Zhamu, A. & Jang, B. Z. Modeling direct exfoliation of nanoscale graphene platelets. *Journal of Physical Chemistry C* **114**, 21083–21087 (2010).
196. Sresht, V., Pádua, A. A. H. & Blankschtein, D. Liquid-Phase Exfoliation of Phosphorene: Design Rules from Molecular Dynamics Simulations. *ACS Nano* **9**, 8255–8268 (2015).
197. Mukhopadhyay, T. K. & Datta, A. Deciphering the role of solvents in the liquid phase exfoliation of hexagonal boron nitride: A molecular dynamics simulation study. *Journal of Physical Chemistry C* **121**, 811–822 (2017).
198. Sresht, V. *et al.* Quantitative Modeling of MoS2-Solvent Interfaces: Predicting Contact Angles and Exfoliation Performance using Molecular Dynamics. *Journal of Physical Chemistry C* **121**, 9022–9031 (2017).
199. Purkait, T., Ahammed, R., de Sarkar, A. & Dey, R. S. The role of exfoliating solvents for control synthesis of few-layer graphene-like nanosheets in energy storage applications: Theoretical and experimental investigation. *Applied Surface Science* **509**, 145375 (2020).
200. Paton, K. R. *et al.* Scalable production of large quantities of defect-free few-layer graphene by shear exfoliation in liquids. *Nature Materials* **13**, 624–630 (2014).
201. Trigueiro, P. C. *et al.* Enhanced thermal conductivity and mechanical properties of hybrid MoS 2 / h-BN polyurethane nanocomposites. **46560**, 10–13 (2018).
202. Howe, R. C. T. *et al.* Surfactant-aided exfoliation of molybdenum disulfide for ultrafast pulse generation through edge-state saturable absorption. *Physica Status Solidi (B) Basic Research* **253**, 911–917 (2016).
203. Quinn, M. D. J., Ho, N. H. & Notley, S. M. Aqueous dispersions of exfoliated molybdenum disulfide for use in visible-light photocatalysis. *ACS Applied Materials and Interfaces* **5**, 12751–12756 (2013).
204. Varrla, E. *et al.* Large-scale production of size-controlled MoS2 nanosheets by shear exfoliation. *Chemistry of Materials* **27**, 1129–1139 (2015).
205. Brent, J. R. *et al.* Production of few-layer phosphorene by liquid exfoliation of black phosphorus. *Chemical Communications* **50**, 13338–13341 (2014).
206. Liang, L. *et al.* Vacancy associates-rich ultrathin nanosheets for high performance and flexible nonvolatile memory device. *J Am Chem Soc* **137**, 3102–3108 (2015).

207. Baig, Z. *et al.* Investigation of tip sonication effects on structural quality of graphene nanoplatelets (GNPs) for superior solvent dispersion. *Ultrasonics Sonochemistry* **45**, 133–149 (2018).
208. Tyurnina, A. v. *et al.* Environment friendly dual-frequency ultrasonic exfoliation of few-layer graphene. *Carbon N Y* **185**, 536–545 (2021).
209. Morton, J. A. *et al.* New insights into sono-exfoliation mechanisms of graphite: In situ high-speed imaging studies and acoustic measurements. *Materials Today* **49**, 10–22 (2021).
210. Liang, S. *et al.* In-situ exfoliated graphene for high-performance water-based lubricants. *Carbon N Y* **96**, 1181–1190 (2016).
211. Wang, Y., Du, Y., Deng, J. & Wang, Z. Friction reduction of water based lubricant with highly dispersed functional MoS2 nanosheets. *Colloids and Surfaces A: Physicochemical and Engineering Aspects* **562**, 321–328 (2019).
212. Xiao, H. & Liu, S. 2D nanomaterials as lubricant additive: A review. *Materials and Design* **135**, 319–332 (2017).
213. Zhang, S., Ma, T., Erdemir, A. & Li, Q. Tribology of two-dimensional materials: From mechanisms to modulating strategies. *Materials Today* **26**, 67–86 (2019).
214. Rajendhran, N., Palanisamy, S., Periyasamy, P. & Venkatachalam, R. Enhancing of the tribological characteristics of the lubricant oils using Ni-promoted MoS2 nanosheets as nano-additives. *Tribology International* **118**, 314–328 (2018).
215. Zhang, X. *et al.* Synthesis of Ultrathin WS2 Nanosheets and Their Tribological Properties as Lubricant Additives. *Nanoscale Research Letters* **11**, (2016).
216. Sharma, V., Joshi, R., Pant, H. & Sharma, V. K. Improvement in frictional behaviour of SAE 15W-40 lubricant with the addition of graphite particles. *Materials Today: Proceedings* **25**, 719–723 (2019).
217. Cho, D. H., Kim, J. S., Kwon, S. H., Lee, C. & Lee, Y. Z. Evaluation of hexagonal boron nitride nano-sheets as a lubricant additive in water. *Wear* **302**, 981–986 (2013).
218. Khaledialidusti, R., Mahdavi, E. & Barnoush, A. Stabilization of 2D graphene, functionalized graphene, and Ti2CO2 (MXene) in super-critical CO2: A molecular dynamics study. *Physical Chemistry Chemical Physics* **21**, 12968–12976 (2019).
219. Wang, L. F., Ma, T. B., Hu, Y. Z., Wang, H. & Shao, T. M. Ab initio study of the friction mechanism of fluorographene and graphane. *Journal of Physical Chemistry C* **117**, 12520–12525 (2013).
220. Arif, T., Yadav, S., Colas, G., Singh, C. V. & Filleter, T. Understanding the Independent and Interdependent Role of Water and Oxidation on the Tribology of Ultrathin Molybdenum Disulfide (MoS2). *Advanced Materials Interfaces* **6**, 1–9 (2019).
221. Gupta, M. K., Bijwe, J. & Padhan, M. Role of size of hexagonal boron nitride particles on tribo-performance of nano and micro oils. *Lubrication Science* **30**, 441–456 (2018).
222. Sahoo, R. R. & Biswas, S. K. Deformation and friction of MoS2 particles in liquid suspensions used to lubricate sliding contact. *Thin Solid Films* **518**, 5995–6005 (2010).
223. Wengeler, R. & Nirschl, H. Turbulent hydrodynamic stress induced dispersion and fragmentation of nanoscale agglomerates. *Journal of Colloid and Interface Science* **306**, 262–273 (2007).
224. Narayan, R. & Kim, S. O. Surfactant mediated liquid phase exfoliation of graphene. *Nano Convergence* vol. 2 (2015).

225. Wang, Q. B., Yin, J. Z., Xu, Q. Q. & Zhi, J. T. Insightful Understanding of Shear-Assisted Supercritical CO2 Exfoliation for Fabricating Graphene Nanosheets through the Combination of Kinetics and Process Parameters. *Industrial and Engineering Chemistry Research* **59**, 10967–10975 (2020).
226. Liu, L., Shen, Z., Yi, M., Zhang, X. & Ma, S. A green, rapid and size-controlled production of high-quality graphene sheets by hydrodynamic forces. *RSC Advances* **4**, 36464–36470 (2014).
227. Botto, L. Toward Nanomechanical Models of Liquid-Phase Exfoliation of Layered 2D Nanomaterials: Analysis of a π − peel Model. *Frontiers in Materials* **6**, (2019).
228. Salussolia, G., Barbieri, E., Pugno, N. M. & Botto, L. Micromechanics of liquid-phase exfoliation of a layered 2D material: A hydrodynamic peeling model. *Journal of the Mechanics and Physics of Solids* **134**, 103764 (2020).
229. Paton, K. R., Anderson, J., Pollard, A. J. & Sainsbury, T. Production of few-layer graphene by microfluidization. *Materials Research Express* **4**, (2017).
230. Tran, T. S., Park, S. J., Yoo, S. S., Lee, T. R. & Kim, T. Y. High shear-induced exfoliation of graphite into high quality graphene by Taylor-Couette flow. *RSC Advances* **6**, 12003–12008 (2016).
231. Rizvi, R. *et al.* High-Throughput Continuous Production of Shear-Exfoliated 2D Layered Materials using Compressible Flows. *Advanced Materials* **30**, 1–11 (2018).
232. del Rio Castillo, A. E. *et al.* High-yield production of 2D crystals by wet-jet milling. *Materials Horizons* **5**, 890–904 (2018).
233. Varrla, E. *et al.* Turbulence-assisted shear exfoliation of graphene using household detergent and a kitchen blender. *Nanoscale* **6**, 11810–11819 (2014).
234. Yin, X. *et al.* Preparation of Two-Dimensional Molybdenum Disulfide Nanosheets by High-Gravity Technology. *Industrial and Engineering Chemistry Research* **56**, 4736–4742 (2017).
235. Chen, X., Dobson, J. F. & Raston, C. L. Vortex fluidic exfoliation of graphite and boron nitride. *Chemical Communications* **48**, 3703–3705 (2012).
236. Pal, S., Tadi, K. K., Sudeep, P. M., Radhakrishnan, S. & Narayanan, T. N. Temperature assisted shear exfoliation of layered crystals for the large-scale synthesis of catalytically active luminescent quantum dots. *Materials Chemistry Frontiers* **1**, 319–325 (2017).
237. S., N. K. *et al.* Electric Field Effect in Atomically Thin Carbon Films. *Science (1979)* **306**, 666–669 (2004).
238. Cong, H.-P., Ren, X.-C., Wang, P. & Yu, S.-H. Flexible graphene–polyaniline composite paper for high-performance supercapacitor. *Energy & Environmental Science* **6**, 1185 (2013).
239. Qureshi, T. S. & Panesar, D. K. A comparison of graphene oxide, reduced graphene oxide and pure graphene: early age properties of cement composites. in *2nd RILEM Spring Convention & International Conference on Sustainable Materials, Systems and Structures* (2019).
240. Qureshi, T. S. & Panesar, D. K. Nano reinforced cement paste composite with functionalized graphene and pristine graphene nanoplatelets. *Composites Part B: Engineering* 108063 (2020) doi:10.1016/J.COMPOSITESB.2020.108063.
241. An, J., McInnis, M., Chung, W. & Nam, B. Feasibility of Using Graphene Oxide Nanoflake (GONF) as Additive of Cement Composite. *Applied Sciences* **8**, 419 (2018).

242. Qureshi, T. S., Panesar, D. K. & Peterson, K. Thin section microscopy and DVS study to determine the influence of graphene materials on the microstructure of cement based composite. in *17th Euroseminar on Microscopy Applied to Building Materials* 134–140 (2019).
243. Qureshi, T. S. & Panesar, D. K. A review: the effect of graphene oxide on the properties of cement-based composites. in *CSCE Annual Conference* 642–1 to 642–10 (2017).
244. Li, X. *et al.* Dispersion of graphene oxide agglomerates in cement paste and its effects on electrical resistivity and flexural strength. *Cement and Concrete Composites* **92**, 145–154 (2018).
245. Long, W.-J., Zheng, D., Duan, H., Han, N. & Xing, F. Performance enhancement and environmental impact of cement composites containing graphene oxide with recycled fine aggregates. *Journal of Cleaner Production* **194**, 193–202 (2018).
246. Li, X. *et al.* Effects of graphene oxide agglomerates on workability, hydration, microstructure and compressive strength of cement paste. *Construction and Building Materials* **145**, 402–410 (2017).
247. Qureshi, T. S., Panesar, D. K., Sidhureddy, B., Chen, A. & Wood, P. C. Nano-cement composite with graphene oxide produced from epigenetic graphite deposit. *Composites Part B: Engineering* **159**, 248–258 (2019).
248. Stephens, C., Brown, L. & Sanchez, F. Quantification of the re-agglomeration of carbon nanofiber aqueous dispersion in cement pastes and effect on the early age flexural response. *Carbon N Y* **107**, 482–500 (2016).
249. Zhao, L. *et al.* An intensive review on the role of graphene oxide in cement-based materials. *Construction and Building Materials* **241**, 117939 (2020).
250. Lu, Z. *et al.* Steric stabilization of graphene oxide in alkaline cementitious solutions: Mechanical enhancement of cement composite. *Materials & Design* **127**, 154–161 (2017).
251. Long, W.-J., Wei, J.-J., Xing, F. & Khayat, K. H. Enhanced dynamic mechanical properties of cement paste modified with graphene oxide nanosheets and its reinforcing mechanism. *Cement and Concrete Composites* **93**, 127–139 (2018).
252. Zhao, L. *et al.* Mechanical behavior and toughening mechanism of polycarboxylate superplasticizer modified graphene oxide reinforced cement composites. *Composites Part B: Engineering* **113**, 308–316 (2017).
253. Pan, Z. *et al.* Mechanical properties and microstructure of a graphene oxide–cement composite. *Cement and Concrete Composites* **58**, 140–147 (2015).
254. Chen, Z. S., Zhou, X., Wang, X. & Guo, P. Mechanical behavior of multilayer GO carbon-fiber cement composites. *Construction and Building Materials* **159**, 205–212 (2018).
255. Li, X. *et al.* Incorporation of graphene oxide and silica fume into cement paste: A study of dispersion and compressive strength. *Construction and Building Materials* **123**, 327–335 (2016).
256. Yang, H., Monasterio, M., Cui, H. & Han, N. Experimental study of the effects of graphene oxide on microstructure and properties of cement paste composite. *Composites Part A: Applied Science and Manufacturing* **102**, 263–272 (2017).
257. Zhou, Y., Xiong, C., Peng, Z., Huang, J. & Chang, H. Molecular dynamics simulation of the interfacial interaction mechanism between functional groups on graphene-based two-dimensional matrix and calcium silicate hydrate. *Construction and Building Materials* **284**, 122804 (2021).

258. Hou, D., Lu, Z., Li, X., Ma, H. & Li, Z. Reactive molecular dynamics and experimental study of graphene-cement composites: Structure, dynamics and reinforcement mechanisms. *Carbon N Y* **115**, 188–208 (2017).
259. Fang, Y. *et al.* Janus electrochemical exfoliation of two-dimensional materials. *Journal of Materials Chemistry A* **7**, 25691–25711 (2019).
260. Parvez, K. *et al.* Exfoliation of graphite into graphene in aqueous solutions of inorganic salts. *J Am Chem Soc* **136**, 6083–6091 (2014).
261. Yang, S. *et al.* Organic Radical-Assisted Electrochemical Exfoliation for the Scalable Production of High-Quality Graphene. *J Am Chem Soc* **137**, 13927–13932 (2015).
262. Zhong, Y. L. & Swager, T. M. Enhanced electrochemical expansion of graphite for in situ electrochemical functionalization. *J Am Chem Soc* **134**, 17896–17899 (2012).
263. Wang, G. *et al.* Highly efficient and large-scale synthesis of graphene by electrolytic exfoliation. *Carbon N Y* **47**, 3242–3246 (2009).
264. Su, C. Y. *et al.* High-quality thin graphene films from fast electrochemical exfoliation. *ACS Nano* **5**, 2332–2339 (2011).
265. Jeon, I., Yoon, B., He, M. & Swager, T. M. Hyperstage Graphite: Electrochemical Synthesis and Spontaneous Reactive Exfoliation. *Advanced Materials* **30**, 1–7 (2018).
266. Bjerglund, E. T. *et al.* Efficient graphene production by combined bipolar electrochemical intercalation and high-shear exfoliation. *ACS Omega* **2**, 6492–6499 (2017).
267. Li, J. *et al.* Ultrafast Electrochemical Expansion of Black Phosphorus toward High-Yield Synthesis of Few-Layer Phosphorene. *Chemistry of Materials* **30**, 2742–2749 (2018).
268. Yang, Y. *et al.* Electrochemical exfoliation of graphene-like two-dimensional nanomaterials. *Nanoscale* **11**, 16–33 (2019).
269. Dickinson, E. J. F. & Wain, A. J. The Butler-Volmer equation in electrochemical theory: Origins, value, and practical application. *Journal of Electroanalytical Chemistry* **872**, 114145 (2020).
270. Ruthven, D. M., DeSisto, W. J. & Higgins, S. Diffusion in a mesoporous silica membrane: Validity of the Knudsen diffusion model. *Chemical Engineering Science* **64**, 3201–3203 (2009).
271. Lee, H., Choi, J. Il, Park, J., Jang, S. S. & Lee, S. W. Role of anions on electrochemical exfoliation of graphite into graphene in aqueous acids. *Carbon N Y* **167**, 816–825 (2020).
272. Lee, O. S. & Carignano, M. A. Exfoliation of Electrolyte-Intercalated Graphene: Molecular Dynamics Simulation Study. *Journal of Physical Chemistry C* **119**, 19415–19422 (2015).
273. Muhsan, A. A. & Lafdi, K. Numerical study of the electrochemical exfoliation of graphite. *SN Applied Sciences* **1**, 1–8 (2019).
274. Si, J. *et al.* Electrochemical exfoliation of ultrathin ternary molybdenum sulfoselenide nanosheets to boost the energy-efficient hydrogen evolution reaction. *Nanoscale* **11**, 16200–16207 (2019).
275. Cooper, A. J., Wilson, N. R., Kinloch, I. A. & Dryfe, R. A. W. Single stage electrochemical exfoliation method for the production of few-layer graphene via intercalation of tetraalkylammonium cations. *Carbon N Y* **66**, 340–350 (2014).
276. Zhou, M. *et al.* Few-layer graphene obtained by electrochemical exfoliation of graphite cathode. *Chemical Physics Letters* **572**, 61–65 (2013).
277. You, X., Liu, N., Lee, C. J. & Pak, J. J. An electrochemical route to MoS2 nanosheets for device applications. *Materials Letters* **121**, 31–35 (2014).

278. Zeng, Z. *et al.* Single-layer semiconducting nanosheets: High-yield preparation and device fabrication. *Angewandte Chemie - International Edition* **50**, 11093–11097 (2011).
279. Mayorga-Martinez, C. C., Mohamad Latiff, N., Eng, A. Y. S., Sofer, Z. & Pumera, M. Black Phosphorus Nanoparticle Labels for Immunoassays via Hydrogen Evolution Reaction Mediation. *Analytical Chemistry* **88**, 10074–10079 (2016).
280. Liu, N. *et al.* Large-area atomically thin MoS2 nanosheets prepared using electrochemical exfoliation. *ACS Nano* **8**, 6902–6910 (2014).
281. Huang, Z. *et al.* Layer-Tunable Phosphorene Modulated by the Cation Insertion Rate as a Sodium-Storage Anode. *Advanced Materials* **29**, 1–7 (2017).
282. Alanyalioğlu, M., Segura, J. J., Oró-Sol, J. & Casañ-Pastor, N. The synthesis of graphene sheets with controlled thickness and order using surfactant-assisted electrochemical processes. *Carbon N Y* **50**, 142–152 (2012).
283. Yang, S. *et al.* Ultrafast Delamination of Graphite into High-Quality Graphene Using Alternating Currents. *Angewandte Chemie - International Edition* **56**, 6669–6675 (2017).
284. Liu, C., Li, F., Lai-Peng, M. & Cheng, H. M. Advanced materials for energy storage. *Advanced Materials* **22**, 28–62 (2010).
285. Häggström, F. & Delsing, J. IoT Energy Storage - A Forecast. *Energy Harvesting and Systems* **5**, 43–51 (2018).
286. Saito, Y., Nojima, T. & Iwasa, Y. Highly crystalline 2D superconductors. *Nature Reviews Materials* **2**, 1–18 (2016).
287. Xiao, H. *et al.* One-Step Device Fabrication of Phosphorene and Graphene Interdigital Micro-Supercapacitors with High Energy Density. *ACS Nano* **11**, 7284–7292 (2017).
288. Han, J. H., Kwak, M., Kim, Y. & Cheon, J. Recent Advances in the Solution-Based Preparation of Two-Dimensional Layered Transition Metal Chalcogenide Nanostructures. *Chemical Reviews* **118**, 6151–6188 (2018).
289. Bu, F. *et al.* Recent developments of advanced micro-supercapacitors: design, fabrication and applications. *npj Flexible Electronics* **4**, (2020).
290. Jiang, L. *et al.* Optimizing hybridization of 1T and 2H phases in MoS2 monolayers to improve capacitances of supercapacitors. *Materials Research Letters* **3**, 177–183 (2015).
291. Acerce, M., Voiry, D. & Chhowalla, M. Metallic 1T phase MoS2 nanosheets as supercapacitor electrode materials. *Nature Nanotechnology* **10**, 313–318 (2015).
292. Khanra, P., Kuila, T., Bae, S. H., Kim, N. H. & Lee, J. H. Electrochemically exfoliated graphene using 9-anthracene carboxylic acid for supercapacitor application. *Journal of Materials Chemistry* **22**, 24403–24410 (2012).
293. Liu, Z. *et al.* Ultraflexible In-Plane Micro-Supercapacitors by Direct Printing of Solution-Processable Electrochemically Exfoliated Graphene. *Advanced Materials* **28**, 2217–2222 (2016).
294. Cossutta, M. *et al.* A comparative life cycle assessment of graphene and activated carbon in a supercapacitor application. *Journal of Cleaner Production* **242**, 118468 (2020).
295. Chen, K., Song, S., Liu, F. & Xue, D. Structural design of graphene for use in electrochemical energy storage devices. *Chemical Society Reviews* **44**, 6230–6257 (2015).
296. Bissett, M. A., Kinloch, I. A. & Dryfe, R. A. W. Characterization of MoS2-Graphene Composites for High-Performance Coin Cell Supercapacitors. *ACS Applied Materials and Interfaces* **7**, 17388–17398 (2015).
297. Li, J. *et al.* Scalable Fabrication and Integration of Graphene Microsupercapacitors through Full Inkjet Printing. *ACS Nano* **11**, 8249–8256 (2017).

298. Yoo, E. & Zhou, H. Li-air rechargeable battery based on metal-free graphene nanosheet catalysts. *ACS Nano* **5**, 3020–3026 (2011).
299. M Subramaniyam, C. *et al.* 2D Layered Graphitic Carbon Nitride Sandwiched with Reduced Graphene Oxide as Nanoarchitectured Anode for Highly Stable Lithium-ion Battery. *Electrochimica Acta* **237**, 69–77 (2017).
300. Ye, C. *et al.* Unveiling the Advances of 2D Materials for Li/Na-S Batteries Experimentally and Theoretically. *Matter* **2**, 323–344 (2020).
301. Tung, V. C., Allen, M. J., Yang, Y. & Kaner, R. B. High-throughput solution processing of large-scale graphene. *Nature Nanotechnology* **4**, 25–29 (2009).
302. Li, J., Daniel, C. & Wood, D. Materials processing for lithium-ion batteries. *Journal of Power Sources* **196**, 2452–2460 (2011).
303. Zheng, J. *et al.* High yield exfoliation of two-dimensional chalcogenides using sodium naphthalenide. *Nature Communications* **5**, 1–7 (2014).
304. Lian, P. *et al.* Large reversible capacity of high quality graphene sheets as an anode material for lithium-ion batteries. *Electrochimica Acta* **55**, 3909–3914 (2010).
305. Yoo, H. D. *et al.* Intercalation Pseudocapacitance of Exfoliated Molybdenum Disulfide for Ultrafast Energy Storage. *ChemNanoMat* **2**, 688–691 (2016).
306. Chen, X. *et al.* High-Lithium-Affinity Chemically Exfoliated 2D Covalent Organic Frameworks. *Advanced Materials* **31**, 1–8 (2019).
307. Zhao, H. *et al.* Preparation of MoS2/WS2 nanosheets by liquid phase exfoliation with assistance of epigallocatechin gallate and study as an additive for high-performance lithium-sulfur batteries. *Journal of Colloid and Interface Science* **552**, 554–562 (2019).
308. Zhang, C. (John) J. *et al.* Liquid exfoliation of interlayer spacing-tunable 2D vanadium oxide nanosheets: High capacity and rate handling Li-ion battery cathodes. *Nano Energy* **39**, 151–161 (2017).
309. Boland, J. B. *et al.* Liquid phase exfoliation of GeS nanosheets in ambient conditions for lithium ion battery applications. *2D Materials* **7**, (2020).
310. Patil, S. B. *et al.* Exfoliated 2D Lepidocrocite Titanium Oxide Nanosheets for High Sulfur Content Cathodes with Highly Stable Li-S Battery Performance. *ACS Energy Letters* **3**, 412–419 (2018).
311. Xiao, J. *et al.* Exfoliated MoS2 nanocomposite as an anode material for lithium ion batteries. *Chemistry of Materials* **22**, 4522–4524 (2010).
312. Shao, G. *et al.* Polymer-Derived SiOC Integrated with a Graphene Aerogel As a Highly Stable Li-Ion Battery Anode. *ACS Applied Materials & Interfaces* **12**, 46045–46056 (2020).
313. Jiang, H. *et al.* 2D Monolayer MoS 2 -Carbon Interoverlapped Superstructure: Engineering Ideal Atomic Interface for Lithium Ion Storage. *Advanced Materials* **27**, 3687–3695 (2015).
314. Mendoza-Sánchez, B. & Gogotsi, Y. Synthesis of Two-Dimensional Materials for Capacitive Energy Storage. *Advanced Materials* **28**, 6104–6135 (2016).
315. Lu, X., Yu, M., Huang, H. & Ruoff, R. S. Tailoring Graphite - Nanotechnology. **10**, 269–272 (1999).
316. Splendiani, A. *et al.* Emerging photoluminescence in monolayer MoS 2. *Nano Letters* **10**, 1271–1275 (2010).
317. Novoselov, K. S. *et al.* Two-dimensional gas of massless Dirac fermions in graphene. *Nature* **438**, 197–200 (2005).

318. Zhang, Y., Small, J. P., Pontius, W. V. & Kim, P. Fabrication and electric-field-dependent transport measurements of mesoscopic graphite devices. *Applied Physics Letters* **86**, 1–3 (2005).
319. Radisavljevic, B., Whitwick, M. B. & Kis, A. Integrated circuits and logic operations based on single-layer MoS 2. *ACS Nano* **5**, 9934–9938 (2011).
320. Yang, J., Shen, X., Wang, C., Chai, Y. & Yao, H. Deciphering mechanical properties of 2D materials from the size distribution of exfoliated fragments. *Extreme Mech Lett* **29**, 100473 (2019).
321. Yang, H., Qin, S., Peng, G., Zheng, X. & Zhang, X. Ultraviolet-Ozone Treatment for Effectively Removing Adhesive Residue on Graphene. *Nano* **11**, (2016).
322. Cao, C. *et al.* Scalable exfoliation and gradable separation of boric-acid-functionalized boron nitride nanosheets. *2D Materials* **6**, (2019).
323. Ding, J. H., Zhao, H. R. & Yu, H. bin. High-yield synthesis of extremely high concentrated and few-layered boron nitride nanosheet dispersions. *2D Materials* **5**, (2018).
324. Ji, D., Wang, Z., Zhu, Y. & Yu, H. One-step environmentally friendly exfoliation and functionalization of hexagonal boron nitride by β-cyclodextrin-assisted ball milling. *Ceramics International* **46**, 21084–21089 (2020).
325. Bergin, S. D. *et al.* Towards solutions of single-walled carbon nanotubes in common solvents. *Advanced Materials* **20**, 1876–1881 (2008).
326. Wang, Y. Z., Chen, T., Gao, X. F., Liu, H. H. & Zhang, X. X. Liquid phase exfoliation of graphite into few-layer graphene by sonication and microfluidization. *Materials Express* **7**, 491–499 (2017).
327. Ciesielski, A. & Samorì, P. Graphene via sonication assisted liquid-phase exfoliation. *Chemical Society Reviews* **43**, 381–398 (2014).
328. Chen, Y., Kang, Q., Jiang, P. & Huang, X. Rapid, high-efficient and scalable exfoliation of high-quality boron nitride nanosheets and their application in lithium-sulfur batteries. *Nano Research* **12**, 1–8 (2020).
329. Wang, Y., Shi, Z. & Yin, J. Boron nitride nanosheets: Large-scale exfoliation in methanesulfonic acid and their composites with polybenzimidazole. *Journal of Materials Chemistry* **21**, 11371–11377 (2011).
330. Han, G. Q. *et al.* WS2 nanosheets based on liquid exfoliation as effective electrocatalysts for hydrogen evolution reaction. *Materials Chemistry and Physics* **167**, 271–277 (2015).
331. Jha, R. K. & Guha, P. K. Liquid exfoliated pristine WS2 nanosheets for ultrasensitive and highly stable chemiresistive humidity sensors. *Nanotechnology* **27**, (2016).
332. Xu, D. *et al.* High Yield Exfoliation of WS2 Crystals into 1-2 Layer Semiconducting Nanosheets and Efficient Photocatalytic Hydrogen Evolution from WS2/CdS Nanorod Composites. *ACS Applied Materials and Interfaces* **10**, 2810–2818 (2018).
333. Zhang, X. *et al.* Dispersion of graphene in ethanol using a simple solvent exchange method. *Chemical Communications* **46**, 7539–7541 (2010).
334. Hanlon, D. *et al.* Production of molybdenum trioxide nanosheets by liquid exfoliation and their application in high-performance supercapacitors. *Chemistry of Materials* **26**, 1751–1763 (2014).
335. Shi, X. *et al.* Few-Layer Hydroxyl-Functionalized Boron Nitride Nanosheets for Nanoscale Thermal Management. *ACS Applied Nano Materials* **3**, 2310–2321 (2020).

336. Tian, X. *et al.* Shear-Assisted Production of Few-Layer Boron Nitride Nanosheets by Supercritical CO2 Exfoliation and Its Use for Thermally Conductive Epoxy Composites. *Scientific Reports* **7**, 1–9 (2017).
337. Chen, H. *et al.* Facile one-step exfoliation of large-size 2D materials via simply shearing in triethanolamine. *Materials Letters* **199**, 124–127 (2017).
338. Xu, F. *et al.* Scalable shear-exfoliation of high-quality phosphorene nanoflakes with reliable electrochemical cycleability in nano batteries. *2D Materials* **3**, (2016).
339. Biccai, S. *et al.* Exfoliation of 2D materials by high shear mixing. *2D Materials* **6**, (2019).
340. Arao, Y., Mizuno, Y., Araki, K. & Kubouchi, M. Mass production of high-aspect-ratio few-layer-graphene by high-speed laminar flow. *Carbon N Y* **102**, 330–338 (2016).
341. Kovalska, E., Antonatos, N., Luxa, J. & Sofer, Z. "Top-down" Arsenene Production by Low-Potential Electrochemical Exfoliation. *Inorganic Chemistry* **59**, 11259–11265 (2020).
342. Marzo, A. M. L., Gusmão, R., Sofer, Z. & Pumera, M. Towards Antimonene and 2D Antimony Telluride through Electrochemical Exfoliation. *Chemistry - A European Journal* **26**, 6583–6590 (2020).
343. Yu, W. *et al.* Domain Engineering in ReS2 by Coupling Strain during Electrochemical Exfoliation. *Advanced Functional Materials* **30**, 1–8 (2020).
344. Si, J. *et al.* Scalable Production of Few-Layer Niobium Disulfide Nanosheets via Electrochemical Exfoliation for Energy-Efficient Hydrogen Evolution Reaction. *ACS Applied Materials and Interfaces* **11**, 13205–13213 (2019).
345. Chhowalla, M. *et al.* The chemistry of two-dimensional layered transition metal dichalcogenide nanosheets. *Nature Chemistry* vol. 5 263–275 (2013).
346. Balan, A. P. *et al.* Exfoliation of a non-van der Waals material from iron ore hematite. *Nature Nanotechnology* **13**, 602-+ (2018).
347. Zhang, K., Feng, Y., Wang, F., Yang, Z. & Wang, J. Two dimensional hexagonal boron nitride (2D-hBN): Synthesis, properties and applications. *Journal of Materials Chemistry C* (2017) doi:10.1039/c7tc04300g.
348. Puthirath Balan, A. *et al.* Exfoliation of a non-van der Waals material from iron ore hematite. *Nature Nanotechnology* **13**, 602–609 (2018).
349. Puthirath, A. B. *et al.* Scale-Enhanced Magnetism in Exfoliated Atomically Thin Magnetite Sheets. *Small* **16**, (2020).
350. Puthirath, A. B. *et al.* Apparent Ferromagnetism in Exfoliated Ultrathin Pyrite Sheets. *The Journal of Physical Chemistry C* **125**, 18927–18935 (2021).
351. Serles, P. *et al.* Friction of magnetene, a non-van der Waals 2D material. *Sci. Adv* **7**, 2041 (2021).
352. Tang, Y. *et al.* Single-Molecule MoS2-Polymer Interaction and Efficient Aqueous Exfoliation of MoS2 into Single Layer. *Journal of Physical Chemistry C* **122**, 8262–8269 (2018).
353. Wang, K., Zheng, B., Shrestha, M., Schuelke, T. & Fan, Q. H. Magnetically enhanced plasma exfoliation of polyaniline-modified graphene for flexible solid-state supercapacitors. *Energy Storage Materials* **14**, 230–237 (2018).
354. Serles, P. *et al.* Friction of Ti3C2Tx MXenes. *Nano Letters* **22**, 3356–3363 (2022).
355. Naguib, M. *et al.* Two-dimensional nanocrystals produced by exfoliation of Ti 3AlC 2. *Advanced Materials* **23**, 4248–4253 (2011).

356. Zhu, X. *et al.* Rapid synthesis of ultrathin 2D materials through liquid-nitrogen and microwave treatments. *Journal of Materials Chemistry A* **7**, 5209–5213 (2019).